Domain Antibody Fragment Phage Display as a Biomarker Discovery Tool for Traumatic Brain Injury

by

Briana Isabella Martinez

A Dissertation Presented in Partial Fulfillment
of the Requirements for the Degree
Doctor of Philosophy

Approved April 2020 by the
Graduate Supervisory Committee:

Sarah Stabenfeldt, Chair
Jeff Kleim
Jonathan Lifshitz
Michael Sierks

ARIZONA STATE UNIVERSITY

May 2020

ABSTRACT

Traumatic brain injury (TBI) affects an estimated 1.7 million people in the United States each year and is a leading cause of death and disability for children and young adults in industrialized countries. Unfortunately, the molecular and cellular mechanisms of injury progression have yet to be fully elucidated. Consequently, this complexity impacts the development of accurate diagnosis and treatment options. Biomarkers, objective signatures of injury, can inform and facilitate development of sensitive and specific theranostic devices. Discovery techniques that take advantage of mining the temporal complexity of TBI are critical for the identification of high specificity biomarkers.

Domain antibody fragment (dAb) phage display, a powerful screening technique to uncover protein-protein interactions, has been applied to biomarker discovery in various cancers and more recently, neurological conditions such as Alzheimer's Disease and stroke. The small size of dAbs (12-15 kDa) and ability to screen against brain vasculature make them ideal for interacting with the neural milieu in vivo. Despite these characteristics, implementation of dAb phage display to elucidate temporal mechanisms of TBI has yet to reach its full potential.

My dissertation employs a unique target identification pipeline that entails in vivo dAb phage display and next generation sequencing (NGS) analysis to screen for temporal biomarkers of TBI. Using a mouse model of controlled cortical impact (CCI) injury, targeting motifs were designed based on the heavy complementarity determining region (HCDR3) structure of dAbs with preferential binding to acute (1 day) and subacute (7 days) post-injury timepoints. Bioreactivity for these two constructs was validated via

immunohistochemistry. Further, immunoprecipitation-mass spectrometry analysis identified temporally distinct candidate biological targets in brain tissue lysate.

The pipeline of phage display followed by NGS analysis demonstrated a unique approach to discover motifs that are sensitive to the heterogeneous and diverse pathology caused by neural injury. This strategy successfully achieves 1) target motif identification for TBI at distinct timepoints and 2) characterization of their spatiotemporal specificity.

DEDICATION

This dissertation is dedicated to Grandma: I don’t think you would have expected me to be a scientist, but I think you would have been proud anyway.

ACKNOWLEDGMENTS

I am thankful to my advisor, Sarah Stabenfeldt, for taking a chance on me and helping me to become an independent scientist. I would also like to thank my committee, Jeff Kleim, Jonny Lifshitz, and Mike Sierks for their patience and guidance.

Thank you to the Shanshan Yang of the Biodesign Genomics Core and Tim Karr of the Mass Spectrometry Core for being patient with me as I learned sequencing analysis and the many intricacies of proteomics analysis.

Thank you to Chris Diehnelt and Nick Stephanopoulos for your expertise in antibody mimetics and great contribution of the HCDR3 cyclic peptides used in this dissertation project. I couldn't have done this without you.

Thank you to the various mentees I've had throughout the years for their help and enthusiasm with this project! Specifically, I'd like to thank Gergey Mousa, Kiera Fleck, and Nathan Borgogni for all of their help with phage biopanning and immunohistochemistry.

Thank you to my fellow graduate students who made me feel like I belonged to be here, your kindness and understanding is why I persisted.

Thank you to the SOLS Graduate Programs Office for your assistance in navigating the more administrative difficulties of graduate student life. I would like to thank Amanda Witten for her artistic expertise and design for all the schematics I use in my presentations and documents.

And thank you to the ARCS Foundation, Graduate College, and the Graduate and Professional Student Association for their funding assistance.

TABLE OF CONTENTS

Page

LIST OF TABLES v

LIST OF FIGURES vi

CHAPTER

1 INTRODUCTION 1

1.1 Omics-based Approaches 4

1.2 Phage-facilitated Discovery 10

1.3 Imaging 13

1.4 Machine Learning and Statistical Modeling 16

1.5 Conclusion 19

1.6 Goals of This Dissertation 20

1.7 Figures 21

2 IN VIVO PHAGE DISPLAY AS BIOMARKER DISCOVERY TOOL FOR THE COMPLEX NEURAL MICROENVIRONMENT 24

2.1 Background 24

2.2 Materials 28

2.3 Procedure 30

2.4 Discussion/Conclusion 39

2.5 Figures 41

3 PHAGE DISPLAY FACILITATED DEVELOPMENT OF HCDR3 CONSTRUCTS WITH TEMPORAL SPECIFICITY TO ACUTE AND SUBACUTE TRAUMATIC BRAIN INJURY 43

CHAPTER Page

3.1 Introduction....43

3.2 Materials and Methods 46

3.3 Results 52

3.4 Discussion....57

3.5 Figures 62

4 CONCLUSION 78

4.1 Summary of Findings....78

4.2 Future Work....82

REFERENCES 87

APPENDIX

A ANIMAL SUBJECTS 106

B DOMAIN ANTIBODY FRAGMENT BIOREACTIVITY 108

C CHRONIC INJURY-TARGETING HCDR3 CONSTRUCTS 112

D INDIRECT IMMUNOPRECIPITATION 114

LIST OF TABLES

Table		Page
1.1	Advantages and Disadvantages of Biomarker Discovery Approaches	23
2.1	DAb Sequencing Primers for MiSeq 2 x 300 Module	42
3.1	DAb Sequencing Primers for MiSeq 2 x 300 Module	72
3.2	Phage Accumulation in Ipsilateral and Contralateral Hemispheres	73
3.3	Percentage of HCDR3s Meeting Selection Criteria	74
3.4	Selected HCDR3s	74
3.5	HCDR3 Control Constructs	74
3.6	A2 Isolated Proteins Determined by Mass Spectrometry	75
3.7	SA1 Ssolated Proteins Determined by Mass Spectrometry	76
3.8	Candidate Proteins Isolated by HCDR3 Constructs	77

LIST OF FIGURES

Figure Page

1.1 TBI Pathophysiology 21

1.2 Phage Display Biopanning Process 22

2.1 DAb Phage Display-Next Generation Sequencing Pipeline 41

3.1 In Vivo Phage Display Biopanning 62

3.2 Hemisphere Distribution of Phage 63

3.3 Sequence Population Diversity 64

3.4 Frequency Distribution of Recovered HCDR3s Within Injury Libraries 65

3.5 Reads Per Million (RPMs) of Sequences Increased After Biopanning 66

3.6 Analysis of HCDR3 Temporal Specificity 67

3.7 HCDR3 Constructs Show Selectivity to Injured Neural Tissue 68

3.8 Control Constructs Show No Detectable Bioreactivity on Injured Neural Tissue 69

3.9 Biological Process Categorization of Identified Proteins 70

3.10 Pathway Categorization of Identified Proteins 71

CHAPTER 1

INTRODUCTION

Current trends in biomarker discovery and analysis tools for traumatic brain injury

B.I. Martinez, S.E. Stabenfeldt

Traumatic brain injury (TBI) affects an estimated 1.7 million people in the United States each year and is the leading cause of death in young adults and children in industrialized countries [1–4]. Individuals with TBI are likely to develop cognitive and sensorimotor impairments, such as decreased processing time, memory loss, and difficulties using fine motor coordination [5–7]. Furthermore, individuals with TBI are more likely to acquire neurodegenerative diseases such as Alzheimer's Disease (AD) and Parkinson's Disease (PD) later in their lifetime [8–10]. In the United States alone, the direct (hospital treatments) and indirect (loss of productivity, lost wages) costs of TBI in 2010 were estimated at $76.5 billion [11]. Thus, TBI is of major public and economic concern.

TBI should be viewed as not a single pathophysiological event, but a cascade that involves two separate injury phases (Figure 1.1). The initial insult triggers the primary injury process, which results in tissue deformation, necrosis, and shearing of neurons, axons, and glial cells [12]. The mechanical force disrupts the blood-brain barrier (BBB), typically reaching maximum permeability within a few hours of the initial insult [13, 14]. Glutamate released from damaged nerves then trigger a secondary injury cascade, which causes edema, increase of pro-inflammatory cytokines, and ischemia [12, 15]. This secondary cascade persists for weeks to months after the initial insult, causing an accumulation of cell damage and death [16, 17]. This heterogeneous environment varies

on a case by case basis dependent upon anatomical site of the injury, injury phenotype (e .g., closed head trauma vs. penetrating brain injury), severity, and age of patient at time of injury [18–20].

Since the complexities of the injury microenvironment are still not fully elucidated, this heterogeneous pathology is a primary barrier to developing sensitive diagnostic tools. The Glasgow Coma Scale (GCS), a commonly used survey in emergency room settings, diagnoses TBI with a battery of observations such as patient's eye and motor response to stimuli. Despite being a hallmark of TBI diagnosis, the GCS has been found to be a poor predictor of patient outcome and is not appropriate for patients with prior neurological conditions [18, 21, 22]. Similarly, traditional computerized tomography (CT) and magnetic resonance imaging (MRI) scans are reliable for visualizing fractures, hematomas, and edema, but may have difficulty capturing more mild characteristics of brain trauma [18, 23]. Diagnostic inaccuracy is detrimental to patient well-being, as patients who are incorrectly diagnosed may receive sub-optimal treatments as their quality of life decreases.

Researchers are now turning to biomarkers, objective molecular signatures of injury, as a platform for developing more sensitive and specific TBI treatment and diagnosis tools. Identification and quantification of biomarker expression provides the basis for producing these technologies. For example, a biosensor targeting TBI biomarkers can potentially work to both diagnose TBI patients and monitor the severity of their disease progression. Further, these tools may provide insight on treatment efficiency by assessing changes in biomarker expression. Several biomarkers for TBI have been identified, mostly located in serum or cerebral spinal fluid after injury,

including indicators of inflammation, necrosis, apoptosis, and astrocytosis [18, 24]. There have been several clinical trials analyzing the reliability of using biomarker expression as an indicator of disease progression [25–27]. While various biomarkers of injury have been identified, such as glial fibrillary acidic protein (GFAP), S100beta, and ubiquitin carboxyl-terminal hydrolase isozyme L1 (UCH-L1), the utility as TBI diagnostic markers in the clinic is debated due to lack of specificity and sensitivity to TBI [28, 29]. These confounding results may be attributed to several factors of polytrauma, including time post-injury, severity, and injury phenotype.

Due to the complex heterogeneity of TBI, biomarker discovery in preclinical models must consider the limitations of each model when characterizing candidate biomarkers. Although no one animal model can recapitulate the full complexity of TBI, they have distinct characteristics that can aid researchers in discovery of biomarkers associated with different aspects of TBI pathology. Focal injury models, such as the controlled cortical impact (CCI) model, produce cavitation, contusion, vasogenic and cytotoxic edema [12, 30]. While focal injury models are clinically relevant to edema in TBI patients, diffuse models share characteristics with TBI experienced by athletes and military personnel [12, 31]. Factors such as high intracranial pressure and progressive gray matter degradation are investigated are often investigated using diffuse injury models, such as the fluid percussion injury (FPI) [12]. Blast-induced injury models in particular are designed to reflect TBI in military conflicts by using compression shock tubes to induce blast waves [12, 32]. This model produces an array of symptoms highly relevant to human blast-induced TBI, such as axonal injury, diffuse edema, and prolonged behavioral deficits [32, 33]. Another subset of models known for their human

relevance are weight-drop models. These injuries are produced by a free-falling weight onto an intact or non-intact skull and specifically mimics the biomechanics of human TBI induced by falls or vehicle accidents [34]. This technique produces a mix of focal and diffuse injury dependent on the model, and results in neural inflammation, contusion, and hemorrhage [35]. Biomarkers investigated with these models can provide unprecedented insight for injury mechanisms and have potential to translate for prognostic and therapeutic use in the clinic.

Biomarker discovery is an ongoing subfield of TBI research due to the critical need of biomarkers for development of clinical tools. Currently novel biomarker discovery methods are emerging to detect markers that may be further characterized and validated for their translational utility, with each approach having distinct advantages and disadvantages (Table 1.1). This chapter will focus on current trends in biomarker discovery tools for TBI, including innovations on established techniques and novel approaches to elucidating the neural injury environment.

1.1 -OMICS-BASED APPROACHES

MicroRNA Transcriptomics

MicroRNAs (miRNAs) are single-stranded RNAs of 17-25 nucleotides in length and are responsible for regulating gene expression at the post-transcriptional level [36]. These miRNAs can be collected from either tissue or serum, and are screened using either deep sequencing or microarray methodologies. This technique is already emerging as a means for elucidating mechanisms of other central nervous system (CNS) disorders, such as AD, PD, and stroke [37–40], demonstrating its sensitivity with complex neural environments and showing promise as a possible avenue for TBI biomarker discovery.

By analyzing miRNA expression in distinct neuropathologies, researchers are able to identify significant changes in gene expression profiles that may contribute to distinct mechanisms of injury, such as temporal injury progression and injury severity [41, 42]. Due to their early expression, miRNAs could be potentially used in point-of-care applications to inform clinicians of the severity of a patient's trauma [43]. Currently, companies are exploring surface plasma resonance and nanoparticle-based approaches to increase detection of miRNAs to develop sensitive point-of-care technology [43–46].

Biomarker discovery through miRNA expression also has immense clinical utility due to the non-invasive nature of analyzing gene expression through plasma samples and ease of analysis due to advances in microarray and high throughput sequencing technology. Studies utilizing this approach have demonstrated the ability to discriminate TBI patients from non-injured controls. A 2018 study conducted by Qin et al. exhibited this capability by identifying miR-319 and miR-328-5p as miRNAs indicative of severe TBI in comparison to mild or moderate TBI in patients [47]. Similarly, Yang et al. found that specific miRNAs identified in previous microarray studies, miR-93, miR-191, and miR-499 had significantly increased expression in patients with severe TBI and poor prognosis [48–50].

Screening for modulated miRNAs in saliva samples is an approach that has demonstrated powerful detection sensitivity while maintaining the non-invasiveness that makes miRNA analysis so beneficial to research in patient populations. In a 2017 case study, Hicks et al. found that 6 specific miRNAs in the saliva of children with TBI were significantly modulated from control samples, with three of those miRNAs associated with neuronal development [51]. Further, they identified miR-320 as a miRNA directly

correlated with reports of attention dysfunction [51], showing utility in providing critically needed age-appropriate biomarkers of injury [52, 53]. Samples taken from concussed athletes also revealed five miRNAs that were significantly upregulated in comparison to non-injured sample expression [54]. When screening for inflammatory proteins in those same samples, analysis revealed no significant difference between groups, suggesting that miRNA analysis may have more sensitivity to certain aspects of the neural injury microenvironment. While promising, it is important to note that miRNA analysis of saliva is relatively new to biomarker discovery literature, and more in-depth research must be done to further test its sensitivity in the clinic.

miRNA expression methods have also shown the same promise in identifying markers of severity as studies conducted in animal models. Balankathiresan at al. found that a blast-induced injury model produced five serum miRNAs were significantly altered in injury groups when compared to control animals at three distinct injury timepoints [55]. Similarly, microarray analysis conducted by Lei et al. revealed hundreds of significantly modulated miRNAs at 6, 24, 48, and 72 hours post injury in rat model of diffuse injury [49]. Several miRNA array studies have revealed similar results, with various injury timepoints yielding tens to hundreds of differentially expressed miRNAs in comparison to sham controls using multiple different injury models [56–58]. Further, microarray analyses have revealed miRNAs to reveal essential information about key cellular pathologies in the injury process. For example, miRNA-21, identified by Redell et al. [56] as an indicator of neural injury, has been characterized as a marker indicative of injury progression in aged brains. Sandhir et al. found that miRNA-21 expression increased significantly in injured adult (5-6 months) mice but decreased in aged (22-24

months) mice [59]. However, this decreased expression lead to an upregulation in miRNA-21 targets such as PTEN and RECK, consequently increasing the probability of poor prognosis [59]. From these findings, we can expect for miRNA array analysis to be tremendously beneficial to not only identifying biomarkers of injury, but biomarkers of distinct temporal injury events that may go undetected otherwise. Similarly, biomarkers of injury severity can also be characterized by analyzing miRNA expression. When using a weight-drop model of mTBI with four varying severities, Sharma et al. found that injured animals had a significant increase in miRNAs in comparison to sham controls, while seeing a steady increase in the number of modulated miRNAs correlating to injury severity [60]. These findings were corroborated by a 2017 study that used the same model and severity scale, but also identified the modulated miRNA's targets, such as calcium signaling pathways [61].

Neuroproteomics

Neuroproteomics, the study of protein complements of the genome, seeks to analyze protein expression within the CNS to answer questions about disease states and progression [62]. Recently, neuroproteomics approaches have been applied to neurotrauma to identify possible protein biomarkers of TBI, a logical step considering the surge of success with the search for genomic biomarkers [62]. In contrast to genomics analysis, neuroproteomics can elucidate signal transduction events associated with biochemical processes of injury [63] First, the protein complex is fractionated either by electrophoresis or chromatography. Then, the fractionated proteins are identified and quantified by mass spectrometry. Advances in mass spectrometry have provided researchers with the capability to collect an immense amount of data from proteomes,

giving an in-depth look at the global protein environment [62, 64, 65]. Due to the substantial volume of data gathered, neuroproteomics is often coupled with bioinformatics and systems biology to identify proteins of interest and analyze their interactions with other proteins to specific pathways associated with the target condition.

The specificity and sensitivity of neuroproteomics approaches have been successfully demonstrated with animal models of TBI. Boutte et al. used this technique to assess protein expression in CSF and brain tissue within the acute timepoints of a penetrating ballistic-like brain injury (PBBI) rodent model of TBI. In addition to observing significant expression changes of UCH-L1, this method was able to isolate CUL-1, PP2C-alpha, and BM28, proteins associated with neurite outgrowth and cell differentiation, as potential candidate biomarkers of injury, demonstrating the power of utilizing bottom-up discovery techniques with advanced proteomic methodology [66]. A similar study found CRMP-2, dehydrogenase, and synaptotagmin were significantly expressed in cortical tissue samples of rats with focal injury when compared to naïve samples [67]. Using a similar injury model, a study by Thelin et al. found several proteins differentially expressed in correlation with temporal stages of injury. For example, aldolase C showed increased expression at earlier timepoints after injury while hypoxia inducing factor (HIF)-1a and amyloid precursor protein showed increased expression 2-4 weeks post-injury [68]. Other studies assessing the temporal profile of injury have been conducted, revealing several candidate markers that may be influenced by temporal mechanisms of the microinjury environment [69, 70]. While not yet heavily researched, neuroproteomics may also have utility in the clinic due to the relative ease of analyze whole proteomes of biofluid samples. From the CSF and blood of injured patients,

Halford et al. analysis revealed candidate astroglial markers of injury such as aldolase C and astrocytic phosphoprotein [71]. Overall, neuroproteomics takes advantage of the advances in data output and cost of proteome analysis to adequately discover novel candidate biomarkers.

Metabolomics and Lipidomics

An alternative to neuroproteomics is metabolomics, the study of global metabolic profiles in specific conditions and diseases using mass spectrometry or nuclear magnetic resonance spectrometry [72, 73]. This technique is beneficial for biomarker discovery due to the disruption of homeostasis after injury that is reflected in the metabolome [74]. Similar to neuroproteomics, applying a metabolomics perspective when exploring the injury microenvironment can give rise to novel biomarker candidates not well discussed in the literature. For example, analyzing plasma metabolomics of rats with focal injury revealed significant differentially expressed galactose, demonstrating its capability as an early marker of acute TBI [75]. Several studies have used metabolomics in animal models of TBI to report similar findings of novel candidate biomarkers, including ADP and spermidine [76, 77].

Lipidomics, a subset of metabolomics, is emerging as a new approach to biomarker discovery in TBI. The rationale for using lipidomics over neuroproteomics is that lipid expression in blood is reflective of expression in brain tissue and therefore has more clinical utility [78, 79]. Further, CNS tissue has the highest lipid content of any tissue type excluding adipose tissue, and also has a high diversity of different sub-types of lipids [80, 81]. This relatively new approach to injury biomarker research is already demonstrating diagnostic capability in rodent models of TBI. Analyses on the serum

lipidome of rodents with a controlled cortical impact injury revealed that polyunsaturated fatty acids and sphingolipids are significantly upregulated after injury and may serve purpose as a quantifiable TBI biomarkers [79, 82]. In the other direction, analyzing the plasma of injured mice revealed significant decrease of ether phosphatidylethanolamine levels 3 months post-injury in comparison to controls [83]. Utilizing lipidomics approaches to study perioxidative processes of lipids is also informative of possible biomarkers associated with injury-induced oxidation. For example, Bayir et al.'s analysis of rat cortical tissues after focal injury revealed cardiolipin, a mitochondria-specific phospholipid, may be indicative of apoptosis and oxidative stress [84]. A similar study conducted with the same rodent model of injury found increased levels of 8-epi-prostaglandin $F_{2\alpha}$, a marker of oxidative damage, at 6 hours and 24 hours post-injury [85]. Despite overwhelming evidence of the possible utility of applying lipidomics to biomarker discovery research, very few studies with human patients exist in the literature at this time. However, these studies have shown promise in positively identifying lipids that may be associated with TBI and its neuropsychological outcomes, such as posttraumatic stress disorder [86].

1.2 PHAGE-FACILITATED DISCOVERY

Phage display is a powerful screening/selection process that is often utilized in drug discovery research [87, 88]. First described in 1985, phage display has the capabilities of elucidating biological mechanisms by revealing protein-protein interactions [89–91]. Briefly, George P. Smith's 1985 work provides the foundation for modern phage display technology, in which biological motifs (e.g. peptides, DNA, or antibody fragments) are fused to the gene III of filamentous bacteriophage, such as M13

phage. This fusion results in the bacteriophage "displaying" the motif on its surface with the specific sequence encoded in the gene's DNA [89]. Large libraries (diversity of 10^6-10^{11} different ligands) of biological motif-displaying bacteriophages can then be generated to screen against a target antigen or tissue. The target receptors capture binding bacteriophage while unbound phage are washed away. Collecting only target bound bacteriophage followed by subsequent amplification in bacterial hosts creates a new phage library that is biased toward the target antigen or tissue, thereby completing a single screening cycle, also known as "biopanning". Biopanning is repeated several times to enrich for biological motifs that have strong affinity for the target antigen or tissue. Upon completion of biopanning rounds, bacteriophage plasmids are sequenced and analyzed for discovering biological motifs that may bind specifically to the target (Figure 1.2) [92]. This technology has been used in many pathologies to discover novel biomarkers, for example ovarian cancer and atherosclerosis [93, 94].

Ghoshal et al. explored the feasibility of using phage display as a biomarker discovery tool for TBI using the serum of a focal injury model as target for biopanning [95]. Proteomic analysis (protein pull-down and mass spectrometry) of the converged peptide sequence revealed GFAP as the target antigen. Similarly, phage biopanning can be applied to *in vivo* screening applications. Filamentous phage display has successfully screened against brain vasculature and have demonstrated targeted transmigration across the BBB [96, 97], overcoming the primary bottleneck of drug development for neurological conditions [96–99]. The mechanisms behind this transmigration are partially due to the rod-like shape of filamentous phage, which increases their possibility of membrane penetration in contrast to spherical nanomaterials [100, 101]. Therefore, using

this method on an animal model of TBI *in vivo* may yield peptides or proteins with high affinity to the neural injury milieu. An additional advantage of *in vivo* biopanning as opposed to a traditional *in vitro* or *ex vivo* screening methods is that the former embraces the heterogeneous injury pathology as it unfolds in the neural milieu, creating an opportunity for increased biomarker discovery of TBI. Mann et al. capitalized on this concept and performed *in vivo* screening in a rodent model of focal TBI [102]. Through this methodology, a novel short peptide, Cys-Ala-Gln-Lys (CAQK), was identified as a unique targeting motif of acute brain injury. To validate specificity, a liver injury model was analyzed and showed no accumulation of the CAQK peptide [102]. The authors exploited this discovery for targeted therapeutics, which demonstrates this method's feasibility of identifying distinct candidate biomarkers of injury severity and progression.

Despite successful identification of unique ligands of disease and injury in AD and stroke respectively, utilization of phage display for TBI biomarkers has not been thoroughly conducted [103–105]. This slow adoption may be in part due to the difficulty of identifying biomarker candidates from the biopanning process. Traditionally, phage display screening from biopanning involved Sanger sequencing, which only captures genomic analysis of a small fraction of the phage population. This sequence analysis method is consequently prone to selection of false positives and parasitic non-specific clones [106] The advancement of next generation sequencing (NGS) has improved this process, increasing the sequencing space from 100 clones to 10^7 clones and consequentially uncovering more positive biomarker candidates for further validation [106, 107]. Additionally, NGS analysis specifically for phage libraries has evolved to development of user-friendly programs [108–110].

Another possible reason for the slow adoption of phage display to biomarker discovery studies is bioreactivity validation. A common method for mass-producing the selected phage-displayed proteins or peptides is amplification of the bacteriophage displaying the selected sequence for downstream analysis. While this process is fairly straightforward, this method is highly incompatible with *in vivo* screening due to the high diversity of clones. Further, this limits the flexibility of analysis, limiting detection options to anti-phage antibodies. Recombinant protein production is a more viable option for adding custom tags to expand to several different bioreactivity studies, but this method is often cited as the main bottleneck of several screening initiatives due to its complexity and vast number of variables that affect results [111, 112]. Overall, the combination of phage display and NGS for TBI biomarker discovery is promising yet requires more validation to fully achieve its potential.

1.3 IMAGING

Due to its application in hospital settings, especially within the first 48 hours of injury, researchers have made strides in discovering biosignatures that are detectable by imaging modalities. These imaging-based diagnostic approaches inform clinicians on trauma severity and can also aid in evaluating the progression of injury with routine monitoring. Despite its common use and great capability of visualizing severe trauma, such as skull fracture, hematoma, and edema, traditional imaging tests such as CT and MRI may have difficulties detecting subtle aspects of brain injury [113, 114]. Experimental and clinical researchers are now improving sensitivity of these imaging techniques and using them to detect biosignatures of neural injury that are not seen in

control populations, leading them to characterize and validate candidate biomarkers of TBI.

Recent efforts have explored the utility in employing diffusion tensor imaging (DTI) as a tool for analyzing possible biomarkers of injury in patients. In contrast to traditional MRI, DTI provides the ability to spatially map white matter and analyze its diffusivity via fractional anisotropy. This feature shows promise in being more sensitive to detection of axonal injury as opposed to traditional MR techniques alone [115], which is significant due to traumatic axonal injury (TAI) being a key contributor to cognitive dysfunction in TBI populations [115, 116]. Animal studies employing DTI as a discovery and validation technique have shown success in analyzing biomarkers of injury. Mac Donald et al. found promising results when using DTI in conjunction with histological analysis compared to common MRI analysis when imaging rodent focal injury model brains. Their analysis suggested that DTI was able to detect significant changes in axial diffusivity and relative anisotropy, validated by amyloid beta precursor protein histology. Meanwhile, DTI of the same region was not able to detect this axonal injury, only the contusion [117]. Several other studies using both rodent and porcine models have corroborated these results [118–120], further demonstrating both the utility of axonal diffusion as a candidate biomarker and DTI as a possible imaging tool for the validation of this biomarker.

Clinical applications of DTI are also being heavily researched with high levels of optimism. Rangaprakash et al. applied DTI in an effort to differentiate chronic mild TBI patients from non-injured controls, and found a significant loss of integrity of white matter fibers in hippocampal-striatum pathway in injured patients that was not found in

the control population [121]. While the decreased connectivity of the hippocampus after chronic injury is unsurprising given findings of significant neuronal cell death within the injured hippocampus [122, 123], the ability to visualize axonal integrity in the patient population further validates the use of DTI as an applicable biomarker discovery tool. Further, DTI can be used to analyze possible biomarkers of injury indicative of cognitive outcome [124, 125]. For example, one study found significantly higher diffusivity in children with TBI correlated with poor social cognitive skills [126]. This study corroborates findings from a 2013 study demonstrating the link between axonal diffusivity and memory in a rodent model of blast injury [127], suggesting a strong case for analyzing white matter abnormalities as not only a marker of injury severity, but one of cognitive dysfunction. A link between motor outcome in injured patients and white matter diffusivity is also being heavily researched, with many studies finding that significantly lower fractional anisotropy (FA) values in patients may be indicators of motor control affect after injury [128, 129]. FA values taken from DTI scans have also shown promise as a predictor of mortality in clinical studies for individuals with severe TBI, demonstrating that DTI is not only useful for mild injury diagnosis [130].

Single photon emission computed tomography (SPECT) is another imaging modality that has high potential for biomarker discovery applications [131]. Approved by the FDA as a diagnosis tool in PD [132, 133], the capability of SPECT to provide true 3D information is beneficial for detection and validation of biomarkers in the patient population. A study conducted by Kinuya et al. in 2004 found that in comparison to CT and MRI analysis, SPECT revealed frontal hypoperfusion and cerebellar hypoperfusion, abnormalities associated with personality change and vertigo respectively [134]. SPECT

identifying MRI/CT-negative abnormalities is also seen in both acute and chronic imaging of mild TBI, further demonstrating its utility in the clinic [135]. Furthermore, using ^{99m}Tc exametazime in conjunction with SPECT to measure cerebral blood flow (CBF) revealed significantly lower CBF levels in the right temporal lobes of patients with poorer physical health [136]. However promising, candidate biomarkers detected by SPECT appear to lack a strong correlation with cognitive and neuropsychiatric dysfunction, which may affect its clinical utility [136].

1.4 MACHINE LEARNING AND STATISTICAL MODELING

Machine learning involves using advanced algorithms to analyze large sets of data to progressively recognize patterns without being programmed to do so. Machine learning algorithms can be applied to many categories of datasets, from proteomics to imaging data. This approach is well suited for identifying patterns of disease in biomedical data, and as such, has been applied to biomarker research of many diseases including cancers, psychosis, and Huntington's disease [137–140]. For biomarker discovery in TBI, machine learning procedures have focused on gathering large amounts of imaging data from the injured patient population. Combining the advancing imaging technology with powerful statistical modeling algorithms has the potential to reveal in depth analysis on prospective biomarkers with direct utility for clinical use, specifically for analyzing white matter connectivity. This approach is evidenced by Mitra et al.'s application of a Network-Based Statistics (NBS) model to fractional anisotropy data [141]. With NBS's capability of analyzing low contrast-to-noise data, this study revealed sensitivity of 80% when classifying TBI patients [141]. Dynamic functional network connectivity (dFNC) for example is used to analyze global temporal connectivity, but

with a linear support vector machine algorithm to classify the data, researchers have found significant connectivity states between cerebellum and sensorimotor networks that may serve as a possible biomarker for classification of mTBI [142]. Similarly, Hellyer et al. applied pattern classification algorithms to DTI data acquired from TBI patients and then applied the classifiers to patients without DTI scans, successfully predicting severity of cognitive impairment induced by injury [143]. Graphical-model-based multivariate analysis (GAMMA), a machine learning tool to analyze interactions between brain regions [144], and Tract-based spatial statistics (TBSS) were also be applied to DTI data to use fractional anisotropy values as classifiers to detect neuroimaging biomarkers of mTBI [145]. Additionally, GAMMA has revealed significant differences in the cerebellar white matter integrity between injured and non-injured patients that may have utility as a diagnostic maker of acute stage TBI [146], demonstrating the model's utility in TBI applications. Predictive algorithms are also utilized with imaging techniques sparsely used for TBI to improve their capability of detecting neurotrauma. In a recent study by Shi et al., a machine learning algorithm was applied to terahertz (THz) continuous-wave (CW) transmission imaging to develop an automatic classification system for diagnosis of TBI [147]. The spatial and temporal power of THz CW imaging proved to be an excellent data source for predictive modeling, with the analysis revealing up to 87.5% classification accuracy [147]. These data demonstrate the capability of machine learning to use or improve upon established imaging techniques to improve accuracy of candidate biomarker discovery.

Machine learning algorithms are versatile in that they can be applied to non-imaging datasets as well. For example, topological data analysis (TDA), a machine

learning tool that clusters patient data based on outcome metrics, was used by Nielson et al. to predict novel biomarkers associated with several variables indicative of unfavorable outcome post-injury [148]. The TDA algorithm, which showed great promise in an earlier study involving rodent models of TBI and spinal cord injury [149], analyzed TBI patient data in a multidimensional space, with each patient having over 900 measurable variables. From this model, Nielson et al. found that high levels of specific genetic polymorphisms predicted unfavorable recovery after injury and high probability of PTSD [148]. To analyze and predict protein expression in acute injury, Peacock et al. applied a random forest (RF) predictive model to a panel of biomarkers, including NRGN, NSE, and MT3 ,selected by American Congress of Rehabilitation Medicine criteria [150]. By building a model from this panel, researchers were able to observe the diagnostic accuracy of these biomarkers in predicting mTBI, regardless of neuroimaging findings [150]. RF was also applied to injury data acquired by the American National Football League using metrics including corpus callosum fiber strain and cumulative strain damage of the whole brain to identify predictive concussion biomarkers and evaluate their accuracy [151], Functional connectivity data detected through magnetoencephalographic recordings can also be analyzed through machine learning methods, revealing that the model was eventually able to discriminate injured patients against controls with 100% accuracy [152]. Machine learning algorithms are also incredibly useful for evaluating pediatric TBI cases. When analyzing metrics from physical examination findings, Chong et al.'s application of a machine learning algorithm yielded accuracy above 94% for both sensitivity and specificity [153]. This approach demonstrates the utility of using predicative algorithms for pediatric TBI biomarker

discovery and showcases its power in the probability of detecting which biomarkers are indicative of a more aggressive disease progression later in life. Hemodynamics influenced by injury have also been explored as possible biomarkers of TBI, with predictive classification algorithms revealing significant temporal and spatial activity in the prefrontal cortex as possible diagnostic markers of injury [154].

While promising, machine learning algorithms applied to neurotrauma research still have drawbacks. Even though using multivariate analysis is extremely beneficial for analyzing the heterogeneous injury microenvironment, it is critical to consider that larger sample sizes are needed to validate the specificity and sensitivity of the biomarkers selected from these models prior to full utility in clinical applications.

1.5 CONCLUSION

Several biomarkers of TBI have been identified but they carry the disadvantage of either not being sensitive or specific to TBI, which diminishes their clinical utility. Biomarkers have the potential for improving diagnostic accuracy, predicting the severity of injury progression, and conveying information to clinicians about injury progression for individual patients. Advancements in biomarker discovery range from improving upon already established techniques to applying novel methods to elucidate mechanisms of the neural injury environment. Many emerging tools and techniques have shown promise in inching the field towards a better comprehension of TBI and have given rise to multiple novel candidate biomarkers to further characterize. While preclinical discovery has not yet lead directly to clinical translation, the technological strides discussed here are immensely promising. Ultimately, future efforts in biomarker

discovery should continue to rigorously test potential biomarkers and critically inspect their potential clinical utility.

1.6 GOALS OF THIS DISSERTATION

The complexity of TBI lends to the need for characterized temporal biomarkers, which can then be implemented in various biomarker-based theranostic applications. The overarching goal of this dissertation is identification of temporally distinct TBI biomarkers using antibody fragment phage display-facilitated discovery. Specifically, domain antibody (dAb) fragment phage display was applied to a controlled cortical impact (CCI) rodent injury model at 1, 7, and 21 days post-injury. This method will contribute to elucidation of temporal mechanisms of injury pathology while simultaneously informing the development of an unambiguous targeting motif for the discovered antigens.

Development and refinement of a novel candidate biomarker discovery pipeline incorporating antibody fragment phage display, next generation sequencing (NGS) analysis, synthetic antibody development, and proteomic analysis was foundational to the execution of this dissertation. Chapter 2 describes this streamlined methodology in-depth, emphasizing its benefits in the context of interacting with the neural environment *in vivo*. Chapter 3 reports the application of this discovery method to CCI injury model *in vivo*. This study not only validates bioreactivity of the phage-selected antibody constructs to injured tissue using a series of immunohistochemical experiments, but also reveals the identity of the targeted proteins through immunoprecipitation-mass spectrometry analysis. Chapter 4 concludes with careful considerations of the described work and perspective on future directions.

1.7 FIGURES

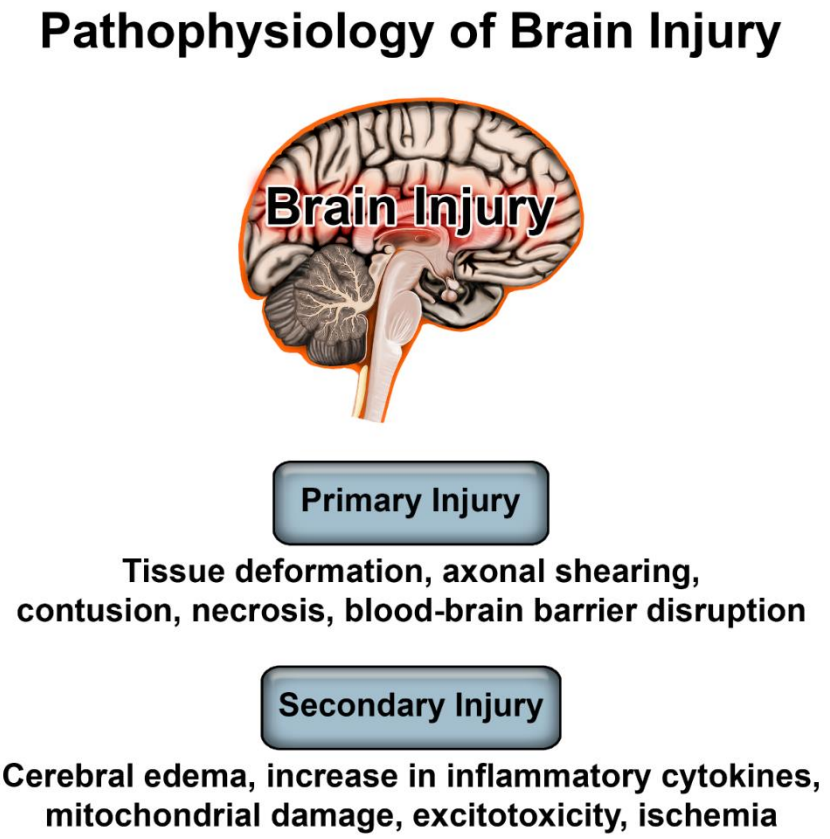

Figure 1.1: TBI pathophysiology. The primary injury, caused by the initial insult, contributes to a secondary injury progression.

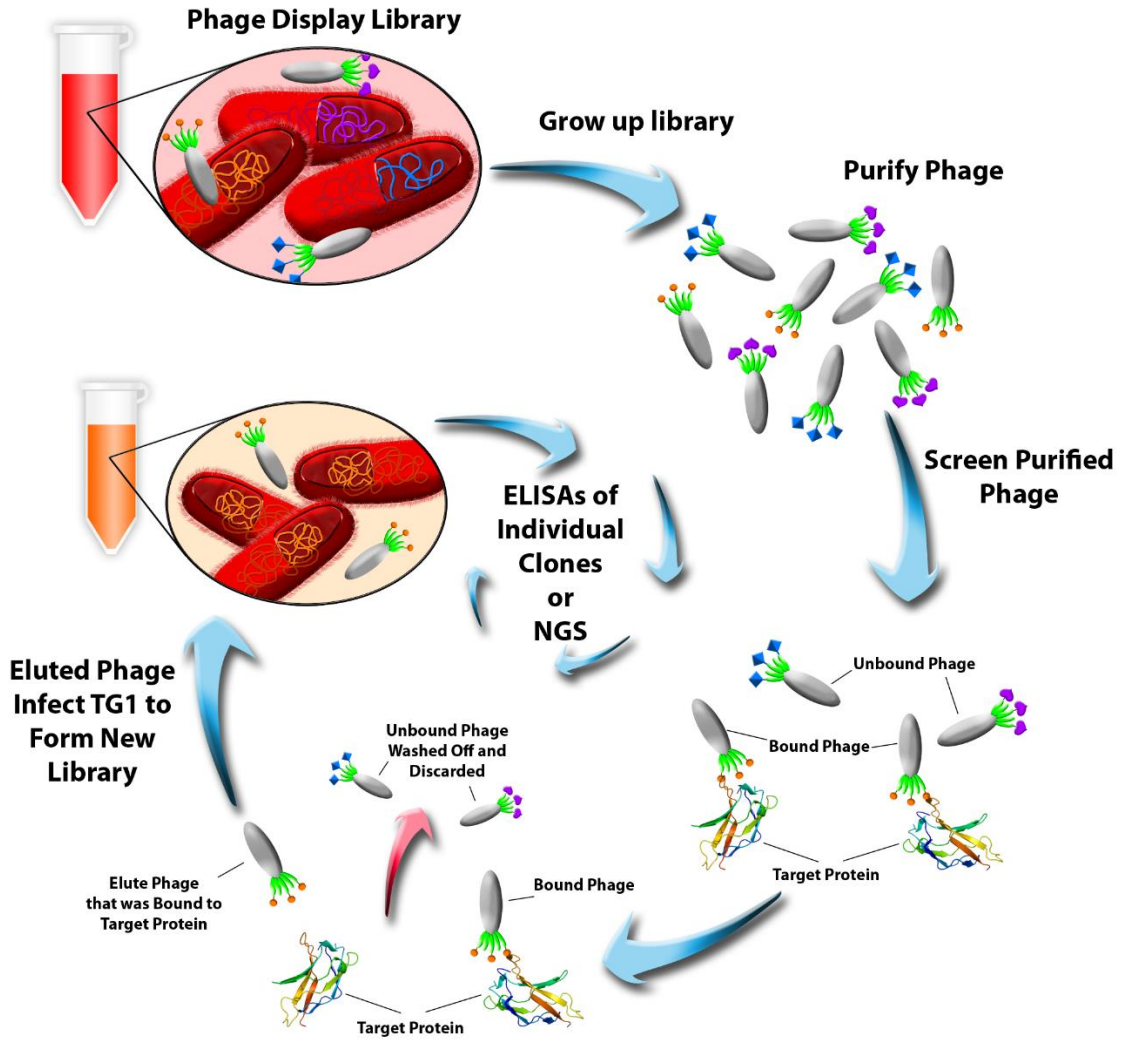

Figure 1.2: Phage display biopanning process. Phage libraries are grown and incubated with target antigens. Bound phage are rescued and amplified to generate a new library, which is used in subsequent biopanning rounds. Generally, phage selected through this process are validated for specificity with sequencing and ELISAs.

Table 1.1: Advantages and disadvantages of biomarker discovery approaches

Discovery Approach	Advantages	Disadvantages
MicroRNA transcriptomics	miRNAs are more abundant in human biofluids than proteins, making them more accessible as biomarkers [43]	miRNA expression may vary due to specific conditions such as fasting, introducing variability in analysis [43]
Neuroproteomics	Elucidate signal transduction events associated with biochemical processes of injury [63]	Large datasets require sophisticated bioinformatics software [17]
Metabolomics/Lipidomics	Metabolites' proximity to CSF and brain and ease of lipid transport make them easily detectable [73,79]	Subject's environment affects metabolome, possibly producing unwanted variation in data [74]
Phage display	Screening can directly take advantage of heterogeneous injury environment [102]	Requires high throughput sequencing to prevent selection of false positive [106]
Diffusion tensor imaging	Sensitive to detection of diffuse axonal injury and white matter microstructure [113]	Prone to partial volume effect, which may produce false positive [127]
Single-photon emission computed tomography	More sensitivity than CT for detecting lesions, capable of detecting cerebral blood flow abnormalities [111, 133]	Less specificity detecting in vivo morphology [133]
Machine learning	Uncovers nonlinear and higher order effects of predictive variables to model complex relationships [139, 151]	High volume of data required for accurate prediction [150]

CHAPTER 2

IN VIVO PHAGE DISPLAY AS A BIOMARKER DISCOVERY TOOL FOR THE COMPLEX NEURAL MICROENVIRONMENT

2.1 BACKGROUND

Biomarkers, biological signatures of injury or disease, are critical for the advancement of modern medicine for neurological conditions [155]. Molecular based biomarkers inform clinicians on disease diagnosis, progression, and treatment efficiency. Additionally, biomarkers can be integrated in efficacy assessment for emerging therapeutic approaches, such as pharmacological interventions. The discovery of markers specific to neurological conditions comes with the challenge of identifying molecules in an incredibly heterogeneous and dynamic biological system. To this end, several approaches are being taken to address the problem of identifying sensitive and specific markers for brain conditions and diseases. Recent advancements in neuroproteomics lend to "shot-gun" analyses of a whole tissue brain samples that has undergone a distinct condition of interest to compare against healthy controls [70, 156–158]. This method entails a large volume of non-specific data, often leading to the selection of false-positives as candidate biomarkers [24]. In contrast, detection of hallmark disease/injury biomarkers has been enabled by novel biosensor development, such as gold nanoparticles and nanotubes, to detect specific changes in the brain such as the expression of nitric oxide or glucose [159, 160]. While the potential of these materials is still being explored, major limitations include low sensitivity and non-specific protein adsorption [161]. Overall, high specificity is a substantial challenge in discovery and validation phases of biomarker development. Combining the high-throughput screening power of

neuroproteomics with the elegance of novel biomaterial-based biosensors is ideal for interacting with complex molecular environments.

Phage display is a directed molecular evolution screening technique to uncover protein-ligand interactions and is commonly used in drug discovery and pharmacological research [89–91]. Biological motifs (e.g. peptides or antibody fragments) are fused to filamentous M13 bacteriophage, resulting in the display of the motif on the bacteriophage surface [89]. Large libraries of these phage-displayed motifs (10^6-10^{11} different ligands) are screened against a target antigen. Bound phage are then collected and amplified in bacterial hosts to form an enriched library biased toward the target antigen. The "biopanning" cycle is repeated to further enrich the population of motifs that have a strong affinity to the target antigen. Bacteriophage plasmids are then sequenced and analyzed for specific peptides or antibodies that are strong candidates for targeting the desired antigen. Thus, this technology is ideal for providing high specificity and affinity of discovered antigen-binding motifs.

Consequently, phage display has the capacity to act as a "first step" to biomarker discovery and can simultaneously set the foundation for screening and validation/characterization. Phage displayed peptides have been applied as a biomarker discovery/validation tool for TBI by screening against serum of a rodent focal injury model, revealing increased expression of glial fibrillary acidic protein (GFAP) [95]. *In vivo* phage display also has the capacity to take advantage of the heterogeneous injury environment by interacting with injury pathology as it develops. For example, Mann et al. utilized *in vivo* peptide phage display biopanning to identify a unique targeting motif, Cys-Ala-Gln-Lys (CAQK), with affinity to versican core protein and hyaluronan and

proteoglycan link protein 4 in an acute penetrating brain injury model [102]. Discoveries such as these demonstrate the ability of phage display to identify unique proteins implicated in injury and disease.

Domain antibody (dAb) phage display is unique from other display methods because of their combined small size (12-15 kDa) and strong affinity. Consisting of only the variable heavy (V_H) domain of a full length antibody, these fragments contain three heavy complementarity determining regions (HCDRs: 1, 2, and 3) to facilitate stability and antigen binding capabilities (Figure 2.1a) [162, 163]. Of the three HCDRs, the HCDR3 is the most diverse in composition and is responsible for antigen binding [164, 165]. dAbs are also highly resistant to aggregation and their small size is thought to improve potential for tissue penetration in comparison to other antibody fragment types [162, 166, 167]. Prior studies have conducted successful phage screens against brain vasculature [168]. Furthermore, researchers have used such dAb phage libraries specifically for screening against diverse targets such as amyloid β fibrils and cerebromicrovascular endothelial cells [98, 169], demonstrating their potential for direct interaction with the neural milieu to identify candidate targeting motifs for biomarkers of several conditions.

In vivo dAb phage display screening for neural targets is advantageous for interacting with the native neural microenvironment *in situ*, but the herculean task of selectively identifying target-specific motifs is a significant obstacle to overcome. Parasitic sequences (i.e. sequences that are non-preferentially enriched through biopanning) are abundant in eluted phage libraries [170]. Sanger sequencing methodology, traditionally employed for phage library analysis, is time intensive and

unable to uncover the diversity and depth of these massive libraries and could potentially lead to selection of parasitic or generally non-specific motifs [171, 172]. Advancement of next generation sequencing (NGS) analysis has been transformative for phage display, as this method is capable of analyzing millions of reads and provides coverage of the full population of phage libraries [107, 171]. The Illumina MiSeq modules are particularly helpful in this regard. At a length of 105-120 amino acid residues, the dAb sequence can be fully analyzed by the MiSeq 2x300 bp module [107]. Sophisticated bioinformatic analysis is then required to identify potential targets of candidate biomarkers. While existing programs are available for analysis of phage libraries, support for antibody fragments often requires both the variable heavy and variable light gene for processing, effectively excluding dAb libraries. In lieu of these pipelines, open source programs such as Bioconductor for R [173] can be customized to direct analysis efforts solely to the HCDR3, which can significantly decrease computational workload. While this will remove HCDR1 and HCDR2 from all subsequent analyses, it has been shown that the HCDR3 alone is sufficient for determining antigen binding [165, 174].

Here, we describe a pipeline for using dAb phage display *in vivo* to uncover biomarkers in the neural milieu. This methods article provides a detailed protocol for phage biopanning and NGS analysis for biomarker discovery (Figure 2.1b). While this protocol is based on a culmination of prior published protocols and manufacturer's instructions [92, 167], the methods have been optimized for screening *in vivo* for mouse models of neurological conditions.

2.2 MATERIALS

In vivo biopanning

- Human domain antibody (dAb) library, E. coli TG1 TR strain (Source BioScience LifeSciences, Nottingham, UK).
- Hyperphage stock (Progen Biotechnik, Heidelberg, Germany)
- 2xYT growth medium
- 20% glucose solution
- 50% glycerol
- Ampicillin stock (1000X): 100 mg/mL ampicillin (Sigma Aldrich, St. Louis, MO) in deionized water. Sterile filter and store in 1 mL aliquots at -20 °C.
- TYE ampicillin glucose agar (TAG) plates. Dissolve 8 g NaCl, 10g bacto-tryptone, and 5 g yeast extract in 600 mL deionized water. Add 15 g of agar and bring final volume to 800 mL with deionized water. Autoclave, then cool to 50°C. Add 1 mL ampicillin solution and 200 mL 20% glucose solution. Pour approximately 20 mL of solution into 100 mm x 15 mm petri dishes. Place lid on dishes, cool for 1 hour, then store at 4°C for up to 4 weeks.
- Kanamycin stock: 50 mg/mL kanamycin (Sigma) dissolved in deionized water. Sterile filter, and store in 1 mL aliquots at -20°C.
- 1X Phosphate Buffered Saline (PBS; pH 7.4).
- 1X Tris Phosphate Buffer (TBS; pH 7.4)
- 1X Phosphate Buffer (PB; pH 7.4)
- Lysis buffer: 1X PBS, 1% Triton X-100, and protease inhibitor cocktail tablet (Thermo Fisher Scientific, Cat. No. A32955).

    - NOTE: do not add protease inhibitor tablet until ready to use
- Trypsin stock: 10 mg/mL trypsin (Sigma) at 10 mg/mL in TBS. Sterile filter and store in 100 µL aliquots at -20°C.
- PBS/EDTA/BSA solution: 4 mg of bovine serum albumin in 40 mL of 1X PBS supplemented with 74.45 mg EDTA. Sterile filter and store at 4°C.
- PEG/NaCl solution: Dissolve 125 g of PEG-6000 and 73 g of NaCl in 500 mL of deionized water. Autoclave, then stir continuously while cooling to room temperature.
- Dounce homogenizer or other means of mechanical tissue disruption
- Protease inhibitor cocktail tablet (Thermo Fisher Scientific, Cat. No. A32955)
- Insulin needle syringes (27.5 gauge or smaller)
- Surgical tools for tissue dissection

Illumina sequencing and sequencing analysis

- QIAprep Miniprep Kit (Qiagen, MD, USA, Cat No. 27104)
- Amplicon PCR forward and reverse Primer (Custom, see Table 2.1))
- 2X KAPA HiFi HotStart ReadyMix (Kapa Biosystems, Cat. No. KK2602)
- 10 mM Tris (pH 8.5)
- Agencourt AMPure XP beads (Beckman Coulter, Cat. No. A63881)
- 80% ethanol
- Illumina compatible barcodes for MiSeq 2 x 300 bp (Illumina, Cat. No. MS-102-3001)
- Magnetic stand (Life Technologies, Cat. No. AM10027)
- 96 well 0.2 mL PCR plate

Recommended tools for sequence analysis

- FASTAptamer Toolkit [109]. Requires Perl or Perl interpreter
- Bioconductor for R [173]
- Galaxy [175]

2.3. PROCEDURE

Phage display biopanning

dAb phage production and purification

1. Grow an overnight culture of 135 mL 2xTY, 13.5 mL 20% glucose (filtered), 300 µL phage stock, and 150 µL ampicillin in one 1 L flask. Let grow in incubator at 37°C, 250 rpm overnight.
2. Use 5 mL of overnight culture to add to 450 mL 2xTY, 45 mL filtered 20% glucose, and 500 µL ampicillin. Place in shaker at 250 rpm and 37°C.
    - Note: Reaching an OD_{600} of 0.5 will take 1.5-2.5 hours.
3. Once appropriate OD is reached, infect the bacteria with hyperphage at a multiplicity of infection of 2. Incubate the culture at 37°C for 15-20 minutes in water bath. Shake for 45 minutes at 250 rpm and 37°C
4. Pellet the bacteria for 10 minutes at 2000 x g at 4°C.
5. Resuspend the pelleted bacteria in 500 mL of 2xTY with 500 µL ampicillin and 500 µL kanamycin.
6. Shake overnight with 250 rpm at 37°C for antibody-phage production
7. The next day, pellet the bacteria with 3200 x g for 20 minutes at 4°C and recover the supernatant.

8. Precipitate the produced phage particles with 1/5 volume of PEG/NaCl for 5 hours in either ice or 4°C storage.
9. Pellet the antibody phage by centrifugation with 10,000xg at 4°C for 1 hour. Discard the supernatant.
10. Resuspend the white phage pellet in PBS/EDTA/BSA (~ 1mL per bottle). Aliquot into 15 mL tube.
11. Remove bacterial debris by two times centrifugation with 10,000 x g for 5 minutes at 4°C.
12. Streak out TG1 bacteria on TYE plates and culture at 37°C overnight. Transfer plates to 4°C storage.
    - NOTE: use within 1 month.
13. Prepare an overnight, starved TG1 culture by inoculating 5 mL of 2xTY with a single TG1 colony pulled from the TG1 plate. Incubate in shaker overnight at 250 rom and 37°C.
14. The next day, prepare 100-fold dilution of overnight-starved bacteria with 10 mL of fresh 2xTY media. Incubate at 250 rpm and 37°C until OD_{600} of 0.5 is reached (about 1.5-2.5 hours). Culture may be stored at 4°C for up to 8 hours until ready to complete the assay.
15. Prepare serial dilution from purified phage sample to achieve the following dilutions: 10^{-5}, 10^{-7}, 10^{-9}, 10^{-11}, 10^{-13} in 1X PBS.
16. Transfer 90 µl of the starved TG1 culture to each tube. Transfer 10 µl of the phage serial dilutions to each tube to achieve an end dilution set of 10^{-6}, 10^{-8}, 10^{-10}, 10^{-12}, 10^{-14}. Include a PBS + TG1 cells control.

17. Incubate inoculated phage TG1 solution in a water bath set at 37°C for 30-45 minutes.
18. During this incubation, place 2-3 TAG plates in the bacterial incubator for 15-30 min (37°C). This step serves to dry any condensation that may have formed on the TAG plate.
19. On the back of the TAG plate, draw two lines to divide the plate into quarters with 3 small circles in each lane.
20. Pipette 10 µL of each dilution onto the TAG plate. Once the solution has absorbed into the TAG plates, seal the plate with a thin layer of parafilm.
21. Place the plate on a stationary shelf in incubator or oven set to 37°C for 9-16 hours. Determine colony forming unit (CFU) concentration for phage sample with the following equation: CFU/mL = (average colony count)/(dilution*0.01 mL).

Injection of Phage/Dissection of tissues

1. The day before procedure, prepare an overnight culture of TG1 (5 mL 2xTY, one colony of TG1).
2. The next day, make a 100-fold TG1 solution with 297 mL 2xTY and 3 mL overnight TG1 culture.
3. Lightly anesthetize mouse and prepare for intravenous injection (i.e. tail vein or retro-orbital injection [176]) of 100 µL phage solution.
4. Allow phage to circulate for 5-10 minutes before humanely euthanizing mouse via pentobarbital solution overdose (150 mg/kg intraperitoneal injection)
5. Perform perfusion with chilled 1X PB using peristaltic pump.
6. Dissect the brain and collect control tissues

7. Weigh tissue samples and homogenize tissue thoroughly with Dounce homogenizer or other means of mechanical disruption and lysis buffer
8. Add 2 mL of trypsin solution to homogenate to elute the phage. Incubate at 30°C for 15 minutes at 50 rpm.
9. Transfer trypsin phage elution to a clean 15 mL centrifuge tube and spin down at 1110 x g for 5 minutes.
10. Transfer supernatant (discard pellet) to 30 mL culture of overnight starved TG1 cells in a 50 mL tube and incubate for 30 minutes at 37°C and 50 rpm.
    a. Dry out 20 TAG plates at this time (4 for each sample)
11. Spin down bacterial culture at 3400 x g for 15 minutes.
12. Discard supernatant, resuspend the TG1 pellet in 1 mL of 2xTY.
13. Evenly distribute 1 mL cell suspension over 4 different plates per sample (~250 µl per plate)
14. Wait until cell solution absorbs into TAG gel. Wrap dish in parafilm
15. Incubate at 37°C overnight.
16. The following day, transfer 3 mL to each TAG plate and use sterile bacterial cell scraper to gently dislodge bacteria. Collect bacteria dense media and transfer into 50 mL polypropylene centrifuge tube
17. Add 15% glycerol by volume to bacteria dense media and place into 1 mL aliquots to 80C freezer. These aliquots will act as stock for production of phage for next round of biopanning.
18. Repeat biopanning steps 1-2 additional times.

Next Generation Sequencing

Amplicon PCR

1. Thaw eluted phage from -80°C (previous step) on ice.
2. Transfer 500 µl into 1.5 mL microcentrifugation tubes.
3. Perform DNA isolation of eluted phage libraries with QIAGEN Spin miniprep kit or similar procedure.
4. Set up the following reaction of DNA, 2x KAPA HiFi HotStart ReadyMix, and primers:
    - Microbial DNA (5 ng/µl) – 2.5 µL
    - Forward Primer – 5 µL
    - Reverse Primer – 5 µL
    - 2x KAPA Hifi HotStart Ready Mix – 12.5 µL
5. Seal plate and perform PCR in a thermal cycler using the following program:
    - 95°C for 3 minutes
    - 25 cycles of:
        i. 95°C for 30 seconds
        ii. 55° for 30 seconds
        iii. 72 °C for 30 seconds
    - 72°C for 5 minutes
    - Hold at 4°C.
6. Bring the AMPure XP beads to room temperature.
7. Centrifuge the PCR plate at 1000 x g at 20 °C for 1 minute to collect condensation and carefully remove seal.

8. Vortex the AMPure beads for 30 seconds or until beads are evenly dispersed.
9. Add 20 µL of AMPure XP beads to each well of the PCR plate. Change tips between columns.
10. Gently pipette entire volume up and down 10 times, then let incubate at room temperature without shaking for 5 minutes.
11. Place the plate on a magnetic stand for 2 minutes or until supernatant has cleared.
12. With the PCR plate on the magnetic stand, remove and discard the supernatant. Change tips between samples.
13. With the PCR plate on the magnetic stand, wash the beads with freshly prepared 80% ethanol by adding 200 µl of freshly prepared 80% ethanol to each sample well. Incubate the plate on the magnetic stand for 30 seconds, then carefully remove and discard the supernatant.
14. With the PCR plate on the magnetic stand, allow the beads to air dry for 10 minutes.
15. Remove the PCR plate from the magnetic stand. Add 52.5 µL of 10 mM Tris pH 8.5 to each well of the PCR plate
16. Gently pipette mix up and down 10 times. Assure that beads are fully resuspended.
17. Incubate at room temperature for 2 minutes. Then, place PCR plate on magnetic stand for 2 minutes
18. Transfer 50 µL of the supernatant from the PCR plate to a new plate. Change tips between samples to avoid cross-contamination.

Index PCR

1. Transfer 5 µL from each well to a new 96-well plate.
2. Set up the following reaction of DNA, Index 1 and Index 2 primers, 2X KAPA HiFi HotStart ReadyMix, and PCR grade water.
    - DNA- 5µl
    - Nextera XT Index Primer 1 (N7xx) – 5 µl
    - Nextera XT Index Primer 2 (S5xx) – 5 µL
    - 2X KAPA HiFi HotStart Ready Mix – 25 µL
    - PCR Grade water – 10 µL
3. Gently pipette up and down to mix. Cover plate with microseal and centrifuge the plate at 1000 x g at 20°C for 1 minute.
4. Perform PCR on a thermal cycler using the following program:
    - 95°C for 3 minutes
    - 8 cycles of:
        i. 95°C for 30 seconds
        ii. 55° for 30 seconds
        iii. 72 °C for 30 seconds
    - 72°C for 5 minutes
    - Hold at 4°C.
5. Centrifuge PCR plate at 280 x g at 20 °C for 1 minute to collect condensation.
6. Vortex the AMPure XP beads for 30 seconds to resuspend.
7. Add 56 µL of AMPure XP beads to each well of the Index PCR plate.

8. Gently pipette mix up and down 10 times if using a 96-well PCR plate and incubate at room temperature without shaking for 5 minutes.
9. Place the plate on a magnetic stand for at least 2 minutes to clear supernatant.
10. With the plate still on the magnetic stand, remove and discard the supernatant.
11. With the plate still on the magnetic stand, wash the beads with freshly prepared 80% ethanol by adding 200 µL of freshly prepared 80% ethanol to each sample well. Incubate the plate on a magnetic stand for 30 seconds and carefully remove and discard the supernatant. Repeat this step one more time.
12. With the PCR plate still on the magnetic stand, allow the beads to air-dry for 10 minutes.
13. Remove the Index PCR plate from the magnetic stand. Add 27.5 µL of 10 mM tris pH 8.5 to each well of the PCR plate.
14. If using a 96-well PCR plate, gently pipette to resuspend beads. Incubate plate at room temperature for 2 minutes.
15. Place the plate on the magnetic stand for 2 minutes or until the supernatant has cleared.
16. Transfer 25 µL of the supernatant from the Index PCR plate to a new PCR plate.
17. Normalize samples by measuring protein A280 (ng/mL) and normalizing to the smallest protein concentration.
18. Samples are then loaded and processed according to Illumina MiSeq procedures

Sequence analysis

When analyzing HCDR3s of recovered libraries from *in vivo* screening experiments, taking a multifaceted approach is paramount. The frequency of these

HCDR3 sequences and their respective enrichment through biopanning rounds are both critical aspects of reflective of their specificity to the target antigen. In this protocol, enrichment is defined as the fold value change in frequency between the first and final biopanning round. However, parsing through hundreds of thousands of sequences is and overwhelming task to select a handful of candidates for further experimentation. We recommend analysis of the z-score of each sequence's expression in the experimental conditions. This reveals sequences that have high preference for the target condition as opposed to control. Calculating a z-score threshold by averaging the scores obtained for each sequence further narrows down candidates. This stringent selection criteria allows for a streamlined identification process for which sequences are 1) enriched through the biopanning process and 2) specific to the desired condition.

1. Upload FASTQ files to Galaxy, and use FLASH (Fast Length Adjustment of Short Reads) [177] to stitch forward and reverse reads together.
2. Convert FASTQ to FASTA file type
    - NOTE: save both types of sequencing file
3. Translate nucleotide sequences to amino acid residues
    - R example code:

      seqdata<-translate(seqdata, GENETIC_CODE, if.fuzzy.codon="X")
4. Extract HCDR3s. HCDR3s are variable in residue length and therefore cannot be identified by calling numerical positions. Identifying the HCDR3s can be achieved by using the subsetting command in R to subset between dAb frameworks 3 and 4
    - R example code:

seqdata_cdr3<- AAStringSet(sub(".*YYC *(.*?) *WGQ.*", "\\1", seqdata))

5. Obtain enrichment data. By using FASTAptamer, use fastaptamer_count to identify the number of total and unique sequences in an HCDR3 file, and then use fastaptamer_enrich to obtain .tsv file of sequences that have been enriched between rounds.
    - NOTE: when comparing enrichment of sequences from different libraries, normalizing by a factor of Reads Per Million (RPMs) is highly recommended.
6. Use Bioconductor for R or similar to generate z-score table of values from sequences. Calculate Z-score threshold value
7. Apply stringent criteria to sequences that meet the Z-score threshold to identify candidate motifs that are positively enriched through biopanning rounds and specific to the desired condition being screened against.
8. After identification of HCDR3, retrieves remaining frameworks and HCDRs of the structure from the translated FASTA file.

2.4 DISCUSSION/ CONCLUSION

This methodology is optimized for interaction with the neural microenvironment *in vivo*, providing an unbiased screening perspective for biomarker discovery. The combination of dAb phage display with NGS analysis substantially decreases the possibility of selecting non-specific motifs by providing sequence coverage of the entire library population and applying stringent selection criteria. Additionally, focusing on the HCDR3 allows for a streamlined and less computationally intensive analysis.

After selection, dAbs may be produced for validation studies. Traditionally, recombinant protein production techniques have been standard for producing antibody

biomotifs discovered through phage display. However, producing and purifying dAbs involves several obstacles including protein stability and degradation of affinity tags [178]. To address these challenges, “synthetic antibodies” may be produced based on the HCDR3 portion of the dAb sequence [179–181]. These constructs have been shown to mimic the same antigen-binding capabilities as full-length antibodies [181]. With a produced dAb or HCDR3 construct based on the selected targeting motif, conducting experiments such as immunohistochemistry, ELISAs, immunoprecipitation-mass spectrometry will identify and characterize the candidate biomarker. Unfortunately, predicting the suitability of a phage-selected dAb for a target antigen is difficult even with stringent sequence selection criteria, due to losing a percentage of antigen-specific dAbs during screening due to misfolding in *E. coli* [107, 182]. Nonetheless, the presented analysis pipeline is optimized to assist in the section of specific biomotifs to identify novel biomarkers.

2.5 FIGURES

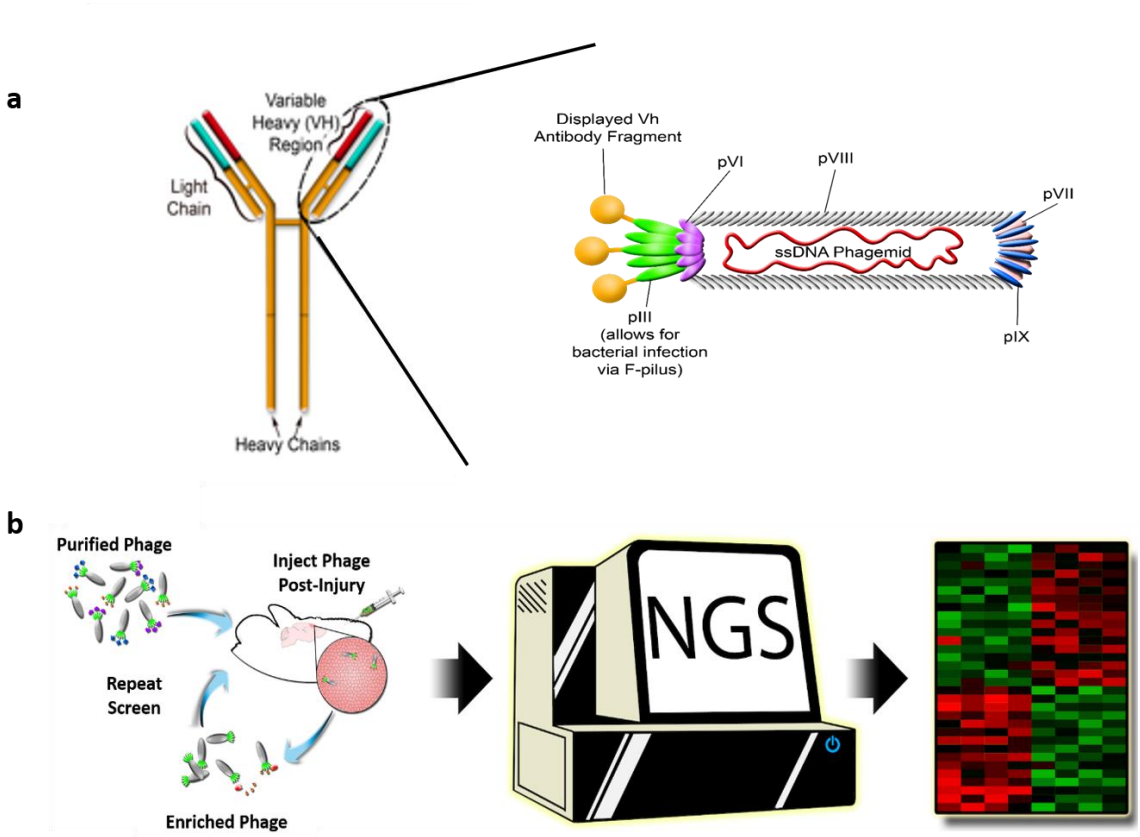

Figure 2.1: dAb phage display-next generation sequencing pipeline. a) Representation of dAb phage structure. The dAb is comprised of the variable heavy ($V_{H)}$ fragment of a full-length antibody. dAbs are fused to filamentous M13 bacteriophage, resulting in the "display" of the dAb on its surface. b) Purified dAb phage are first intravenously injected into the mouse post-injury. After circulation, the mouse is perfused and phage are eluted. Phage eluted from the injured region are then amplified and used in the subsequent screen. After biopanning, next generation sequencing (NGS) is used to uncover the full population of dAb libraries. The libraries are then analyzed for enriched, highly specific HCDR3s.

Table 2.1: dAb sequencing primers for MiSeq 2 x 300 module. Underlined fraction indicates Illumina overhang adapter sequence.

Primer Name	Sequence
dAb For	5’ TCGTCGGCAGCGTCAGATGTGTATAAGAGACAGCAGC TGTTGGAGTCTGGGG 3’
dAb rev	5’ GTCTCGTGGGCTCGGAGATGTGTATAAGAGACAGGAGA CGGTGACCAGGGTTC 3

CHAPTER 3

PHAGE DISPLAY FACILITATED DEVELOPMENT OF HCDR3 CONSTRUCTS WITH TEMPORAL SPECIFICITY TO ACUTE AND SUBACUTE TRAUMATIC BRAIN INJURY

3.1 INTRODUCTION

Traumatic brain injury (TBI) affects an estimated 1.7 million people in the United States each year and is a leading cause of death and disability for children and young adults in industrialized countries [1, 3, 4]. Individuals who experience TBI are more likely to develop cognitive and behavioral deficits, as well as physical conditions such as inhibited motor coordination and balance [5]. These individuals are also more susceptible to acquiring neurodegenerative diseases than the non-injured population [8, 10]. Treatment costs of TBI are estimated at $76.5 billion annually in the United States alone [11], making TBI a great economic burden and public concern.

TBI is characterized not by a singular event, but a cascade of two separate injury phases. The initial insult disrupts the blood-brain barrier (BBB) and causes necrosis, tissue deformation, and cell shearing [12]. This primary injury then catalyzes the secondary injury cascade, leading to an increase of inflammatory cytokines, mitochondrial damage, ischemia, and cell death [12, 15]. This pathology may persist for hours to months after the initial insult, introducing temporal complexity to the injured neural milieu [16]. Unfortunately, the molecular and cellular mechanisms of injury progression are poorly understood and have yet to be fully elucidated. Consequently, this complexity impacts the development of accurate diagnosis and treatment options.

Biomarkers, objective signatures of injury, can inform and facilitate development of sensitive and specific theranostic devices. For example, a quantifiable biomarker can provide insight on the severity of a patient's injury or be utilized to assess treatment efficiency. Biomarkers can also inform the design of targeted therapeutic agents. However, the temporal progression of injury is a bottleneck to the development of sensitive theranostic devices. A marker identified acutely after injury may not carry the same diagnostic or therapeutic value at more chronic timepoints and vice versa. Accordingly, identification and characterization of temporal TBI biomarkers is critical for improving patient care. Molecular-based biomarker discoveries are often facilitated with "top-down" approaches, where known involvement in the condition is paramount to classification as a candidate biomarker. Advances in neuroproteomics have been applied to TBI biomarker discovery to support "bottom-up" approaches [17, 70]. This method takes advantage of the heterogeneous injury environment by fractionating lysate and analyzing global protein expression via mass spectrometry to identify proteins with differential expression after injury. Several studies have successfully analyzed the proteome of rodent brain tissue after experimental TBI to uncover hundreds of differentially expressed proteins that have the potential to be candidate biomarkers of neural injury [70, 183, 184]. However, neuroproteomics approaches often yield a large volume of data, leading to time intensive analysis and difficulties selecting candidates [17, 70].

Phage display, a powerful screening technique to uncover protein-protein interactions, has been applied to biomarker discovery in various cancers and more recently, neurological conditions such as Alzheimer's Disease and stroke [87, 93–95,

185]. This technique utilizes libraries of biological motif-displaying bacteriophages that are then screened against target antigens. Bound bacteriophage are then collected and amplified to use in a subsequent biopanning round. This process is repeated to enrich the population of motifs that have strong affinity to the target antigen. Several display systems can be applied to biomarker discovery, but the domain antibody fragment (dAb) -based display systems in particular hold distinct advantages. Their small size (12-15 kDa) and ability to isolate proteins specific to brain vasculature make them ideal for interacting with the neural milieu in vivo [98, 186]. Despite these characteristics, implementation of dAb phage display to elucidate temporal mechanisms of TBI has yet to reach its full potential.

The difficulty of utilizing dAb displayed systems lies in producing individual candidate dAbs for bioreactivity validation. Recombinant protein production techniques for antibody fragments are time consuming and resource intensive. Purifying dAbs with protein A resin can decrease stability due to the acids required for elution. Similarly, protein A is able to bind to a variety of immunoglobulins and is therefore inconvenient for detection in immunoassays [187]. Designing affinity tags for recombinantly produced dAbs is also an arduous process as these tags tend to deteriorate or completely degrade [178]. To address this, “synthetic antibody”-type constructs are developed using the heavy complementarity determining region 3 (HCDR3) structure of the dAb which facilitates antigen binding [165, 181, 188]. These constructs have been shown to mimic the binding capacities of full-length antibodies at a fraction of the size and can be easily customized via biotinylation for detection in downstream analysis.

Here, we use in vivo phage display biopanning to take advantage of the heterogeneous injury milieu and identify domain antibody fragments (dAbs) that specifically target injured neural tissue at 1 and 7 days post-injury in a mouse model of controlled cortical impact (CCI). HCDR3 constructs were developed based on NGS and bioinformatic analysis dAb phage populations and spatiotemporal specificity was validated via immunohistochemical analysis. Through immunoprecipitation-mass spectrometry (IP-MS) with the HCDR3 constructs, we identified several potential targets associated with metabolic dysfunction and neurodegenerative processes expressed at the acute and subacute timepoint, respectively.

3.2 MATERIALS AND METHODS

Controlled cortical impact

All experiments were approved by the Arizona State University Institutional Animal Care and Use Committee (IACUC).

Eight-weeks-old male and female C57Bl/6 mice (Charles River) were assigned to four experimental groups; acute (sacrificed 1 day post-injury (dpi)), subacute (7 days), chronic (21 days) and sham (craniotomy with no injury, sacrificed 1 day post-procedure). Mice were further divided for each experimental assay: biopanning, immunohistochemistry (IHC), or IP-MS whereby each experimental condition and analysis technique had a range of n = 6-10. Briefly, mice were anesthetized with isoflurane (3% induction, 1.5% maintenance and secured on a stereotaxic frame (Leica Microsystems, Wetzlar, Germany). A 3 mm craniotomy (-1 AP mm bregma, 1.5 lateral to midline) was performed to accommodate a 2 mm diameter, 1 mm deep impact to the frontoparietal cortex at 6 m/s velocity and 100 ms duration. Surgical area was sutured,

then analgesics (0.05mg/kg buprenorphine) and saline were subcutaneously administered. Mice were placed in single housed cages and monitored during recovery.

***In Vivo* Biopanning**

A human dAb library (Source Bioscience, Nottingham, UK) was prepared with hyperphage (Progen, Heidelberg, Germany) as described in the manufacturers protocols [167, 189]. At the 1,7, or 21 dpi), the parent phage library (10^{12}- 10^{14} CFU in 100 µL) was administered via retro-orbital injection. Phage circulated for 10 minutes before animals were euthanized via pentobarbital solution overdose (150 mg/kg intraperitoneal injection). Non-specific phage were cleared by transcardial perfusion with 0.1M phosphate buffer, pH 7.4. The ipsilateral (injured) and contralateral hemisphere of the brain were extracted and dissected, in addition to the heart and spleen. Immediately, tissues were weighed, diced, pooled (n=3/biopanning round), and mechanically homogenized in chilled phosphate buffer with protease inhibitors. Trypsin was added to the homogenate to elute binding phage from tissue. Phage concentration determined by colony forming units (CFU) of tissue elutions were quantified by bacteria titers (TG1 E. coli). Titers were completed after each round to confirm distribution across tissues. Eluted phage were amplified with TG1 E. coli and stored under -80°C conditions. Between biopanning rounds, phage DNA were isolated (QIAprep Spin Miniprep; Qiagen, Valencia, CA) and analyzed for sequence convergence by the DNASU Sequencing Core (Tempe, AZ).

For the second biopanning cycle, the eluted phage from the ipsilateral brain hemisphere were amplified and purified to serve as the phage population for the second biopanning round. Injection, tissue preparation, phage elution, amplification, and storage

were completed as stated previously. A stock library from the manufacturer was amplified without a screening target to serve as a propagation library control to prevent selection of non-specific, parasitic sequences.

Next Generation Sequencing and Analysis

Preparation of phage dAb libraries for deep sequencing was completed following the Illumina Nextera XT amplicon sequencing protocol (Illumina, San Diego, CA). Briefly, amplicons were created with a single PCR step and Illumina-compatible indexes were added to each sample with a second PCR cycle. Phage libraries were sequenced with primers including Illumina-specific barcodes (Table 3.1) via Illumina MiSeq 2 x 300 bp module by the DNASU Next Generation Sequencing Core at ASU Biodesign Institute (Tempe, AZ).

Paired end sequences were stitched with Fast Length Adjustment of Short reads (FLASH) [177], using a minimum and maximum overlap of 10 and 200bp respectively. The heavy complementarity determining region 3 (HCDR3) sequence of each dAb was extracted in Bioconductor for R [173] by subsetting between dAb frameworks 3 and 4. Mutated HCDR3 sequences were excluded from analysis by filtering for sequence length. Raw reads and normalized reads per million (RPMs) were retrieved with the FASTAptamer Toolkit [109]. HCDR3 sequences in injury groups that were enriched through biopanning (i.e. increase of reads from round 1 to round 2) were selected from each library. Enriched sequences were then compared with peripheral tissue (spleen and heart) and propagation control libraries to ensure final selection of HCDR3s that were specific to injured neural tissue libraries. Further, selected sequences were compared against other injury timepoints (i.e., sequences selected from acute injury were compared

with sequences from the subacute injury group) using z-scores to enhance temporal specificity for each sequence selection. Top HCDR3s were selected for antibody-mimetic production and further validation based on the following criteria: 1. frequency, 2. fold enrichment values, and 3. specificity to neural injury at the distinct biopanning timepoints.

dAb production and purification

dAbs were ligated into pET-22b (+) expression plasmid with a C-terminus 6x histidine affinity tag (Genscript, USA) and sequenced to confirm correct dAb sequence. Production was optimized through a Design of Experiments (DoE) 2-level fractional factorial design assessing interactions between IPTG induction concentration, temperature, media, and time post-induction (Appendix B). dAb-A1 was produced in LB media and with growth induced with 0.5 mM IPTG once culture reached OD_{600} of 0.5. Cultures were shaken at 250 RPM for 1 hour at 25°C. dAb-A2 was produced in Terrific Broth with growth induced with 0.1 mM IPTG once culture reached OD_{600} of 0.5. Cultures were shaken at 250 RPM for 3 hours at 25°C. Soluble fractions were purified by fast protein liquid chromatography (FPLC) using Protein A/G resin. Flowthrough and elutions were collected to verify protein size via Western Blot.

Biotinylated HCDR3 constructs

HCDR3 peptides for injury and control groups were synthesized with N-terminus acetylation and C-terminus amidation for increased stability (WatsonBio, Houston, TX). Peptides were then cyclized using bromoacetamide scaffolding and biotinylated. Each reaction was analyzed by matrix assisted laser desorption/ionization to confirm presence

of peptide-scaffold conjugate. Constructs were purified via high performance liquid chromatography (HPLC) collection at 214 nm for downstream analyses.

Immunohistochemistry

Mice were subject to CCI or sham (n=3 per group/sex) as described previously and perfused with 0.1 M phosphate buffer and 4% paraformaldehyde at designated timepoints. Brains were fixed overnight in 4% paraformaldehyde at 4°C followed by immersion in 15% sucrose and then 30% sucrose. Brains were flash frozen on dry ice in optimal cutting temperature medium and stored at -80°C. Samples were sectioned coronally at 20 µm thickness. After incubation with excess streptavidin and biotin to block endogenous biotin (Endogenous Biotin Blocking Kit; Thermo Fisher Scientific, Waltham, MA), 5 µM of biotinylated HCDR3-construct or 5 µg/mL of dAb was incubated on tissue overnight at 4°C. Simultaneously, control sections were incubated with control HCDR3-construct or 1X PBS. Tissue sections were washed in 1X PBS, then HCDR3-construct samples were incubated with Alexa Fluor 555 streptavidin and dAb samples were incubated with 1:2000 dilution of biotinylated anti-6xhis antibody (Abcam; ab27025) at room temperature for 2 hours, followed by 1X PBS washes. dAb-incubated tissues were incubated with Alexa Fluor 555 streptavidin as a tertiary antibody. All tissue sections were subject to DAPI incubation for 5 minutes. Sections were visualized using fluorescence microscopy, and 20x magnification tile scans were prepared for processing using ImageJ software. Threshold values of control slices were used to quantify fraction of CDR3 construct positive staining. Analyzed area was approximately 1500 µm x 1500 µm.

Immunoprecipitation-mass spectrometry

CCI and sham surgeries were completed as described previously. Mice were sacrificed at 1 or 7 dpi (n=3/group) via transcardial perfusion with phosphate buffer, pH 7.4. The ipsilateral hemisphere of the brain was immediately dissected and homogenized in chilled lysis buffer (1X PBS, 1% Triton, protease inhibitor cocktail). Protein concentration was quantified with the Pierce BCA Protein Assay Kit (Thermo Fisher).

Streptavidin-coupled Dynabeads (Thermo Fisher) were washed with 0.1% Tween in 1X PBS and incubated with 1 mg/mL tissue lysate for 1 hour at room temperature. Pre-cleared lysate was collected after separation from magnetic beads and incubated with designated HCDR3-constructs rotating overnight at 4°C to form the immune complex. The immune complex was then incubated with streptavidin-coupled Dynabeads for 1 hour at room temperature before antigen was eluted from beads with 0.2% Rapigest. Eluate was processed by the ASU Biodesign Mass Spectrometry Facility for liquid chromatography-mass spectrometry (LC-MS) analysis using the Thermo Orbitrap Fusion Lumos (Thermo Fisher). Simultaneously, the same immunoprecipitation procedure was completed and antigen was eluted by heating sample at 95°C with SDS PAGE running buffer. Samples were run on a stain-free 12% SDS-PAGE gel and protein bands visualized with the Chemidoc following the manufacturer's protocol (Biorad, Hercules, CA) to confirm distinct proteins between injury and control groups.

UniProt IDs of identified proteins were uploaded to the PANTHER (Protein Analysis Through Evolutionary Relationships) classification system [190] and searched against the Mus musculus reference database. Ontological assessments to characterize cellular localization, molecular function, biological processes, and pathways were

conducted with PANTHER Overrepresentation test with the GO Ontology database (released 2019-10-08).

Statistics

For NGS analysis, raw counts were first normalized to reads per million (RPM) to account for library differences. A normalized z-score was then used as a threshold to identify dAbs that were highly represented and specific to their distinct injury timepoint. Selected dAbs were then screened for enrichment factor and individual frequency. Fluorescence percentage per area was conducted with ordinary one way ANOVA followed by Dunnett's test for multiple comparisons. Statistical significance was determined as $p < 0.05$. Identified proteins that met the false discovery rate (FDR) threshold of < 0.01 were used in all ontological assessments to categorize biological processes and candidate pathways.

3.3 Results

dAb phage bind to injured brain tissue *in vivo*

A dAb phage library was intravenously injected into CCI injured mice at 1, 7, and 21 dpi (Figure 3.1). Phage accumulation was analyzed through titer analysis to confirm that the phage library was given sufficient time to bind to target tissues. Titers determined that phage accumulated in all extracted tissues, with the spleen having the highest total CFU/g of 1.05×10^7 (Table 3.2). Up to 1.21×10^6 CFU/g were recovered from neural tissue of each cohort through trypsinization, including sham controls. An increase in ipsilateral hemisphere-binding phage was observed in the final biopanning round for both the acute and subacute timepoints (increases of 28 and 37% respectively), indicating

successful enrichment of affinity binders to target tissue (Figure 3.2b,c). CFU bound to chronic injured and sham tissue were similar between biopanning rounds (Figure 3.2a,d).

NGS analysis reveals HCDR3 sequences specific to distinct injury timepoints

Phage libraries were sequenced and the HCDR3 of each dAb was examined for all subsequent analyses. This region is the only HCDR within the dAb structure that differs in canonical composition and residue length, indicating that these characteristics promote unique antigen binding specificity [164, 165]. Injury libraries yielded thousands of HCDR3s for each biopanning round, with between 200,000 to 600,000 sequences in the final biopanning round (Figure 3.3a). This analysis yielded a small fraction of sequences similar between timepoints, suggesting that dAb phage interacted uniquely with the neural microenvironment dependent on the temporal condition. After the final biopanning round, less than 20% of sequences from each injury library were identical with the sham library, suggesting that injury libraries were specific to neural injury pathology (Figure 3.3b).

Biopanning increases frequency of neural injury-specific HCDR3s

Across conditions, libraries recovered from the ipsilateral hemisphere yielded substantially more sequences with higher expression (>200 reads) in the 2nd biopanning round than the first (Figure 3.4). This shift in frequency is representative of the biopanning process enriching the population of sequences that have preferential binding to injured neural tissue. Sequences that had an increased frequency in the final biopanning round than the first were categorized as “enriched” (Figure 3.5). Only 6.7% and 3.0% of sequences met this criterion for the acute and subacute libraries respectively,

which provided an opportunity to target HCDR3s that were highly expressed due to affinity selection (Table 3.3).

Phage display derived HCDR3s are temporally specific to distinct injury timepoints

Heatmaps of normalized sequence RPMS were constructed to visualize temporal relationships of the enriched HCDR3s for each timepoint. A majority of sequences with the highest RPMS in their respective groups were also observed in other timepoints post-injury (Figure 3.6a). In fact, several HCDR3s in the acute timepoint were most highly represented in the subacute and chronic timepoints, indicating temporally dependent expression. Nonetheless, creating a z-score matrix of the sequences provided an opportunity to develop stringent criteria for selecting timepoint-specific sequences for dAb or HCDR3-construct design. Z-scores were averaged for each timepoint and used as a threshold to identify HCDR3s with strong preference for their distinct timepoint. Of the enriched sequences, less than 2% met z-score criteria (Fig 3.6b,c; Table 3.3). This bioinformatic analysis narrowed the pool of candidate biological motifs to an exclusive and focused group. For final selection, HCDR3s were required to 1) be unique to a distinct temporal phase post-injury, as determined by z-score normalization and comparison against other injury libraries, 2) be enriched after biopanning, and 3) not be present in control libraries. In order to explore enriched sequences that relatively low frequency, we selected two HCDR3s for each injury group; one sequence with the highest frequency and another with the highest fold enrichment value (Table 3.4).

dAb production/purification

Two dAbs with the selected HCDR3 sequences for the acute timepoint were produced via recombinant protein techniques. A rigorous DoE analysis was applied to determine optimal conditions for time, media, IPTG concentration, and incubation time (Appendix, Table 1). Western blot analysis indicated that production and purification was successful (See Appendix B, Figure 1a,b).

Validation of spatiotemporal affinity

Immunohistochemistry (IHC) was used to evaluate the recognition of top dAb or HCDR3-constructs to CCI injury sections. dAbs designed from selected acute-targeting HCDR3s achieved bioreactivity on injured tissue (Appendix B, Figure 1). Acute-1 construct (A1) expressed the highest frequency after biopanning as determined by NGS analysis, yet the IHC analysis yielded no detectable signal on injured tissue. Acute-2 construct (A2) showed significant bioreactivity determined by the fluorescence on 1 dpi tissue in comparison to sham ($p= 0.0120$) and 7 dpi tissue ($p = 0.0221$). No significant differences were observed between 1 dpi and 21 dpi tissue ($p = 0.0658$). Positive stain with subacute-1 construct (SA1) was also observed in the peri-injury region of the 7 days post-injury tissue, while this localization was not observed in sham brain sections ($p = 0.0079$) (Figure 3.7). No significant differences were observed between SA1 bioreactivity on 7 dpi and 1 dpi tissue ($p = 0.0993$) or 21 dpi tissue ($p = 0.0780$).Control constructs (derived from spleen, heart, and propagation phage library, Table 3.5) showed no detectable signal on injured tissue at 1 or 7 days post-injury, demonstrating that the positive signal we observed from the A2 and SA1 were not due to non-specific artifact derived from construct structure (Figure 3.8).

Targets identified by immunoprecipitation-mass spectrometry

IP-MS analysis identified 18 and 20 proteins specific to injury when using A2 and SA1 as capture antibodies respectively (FDR <0.01) (Table 3.6, 3.7). Ontological analysis of candidate proteins revealed several biological processes that were similarly represented across groups, such as metabolic process and cellular processes (Figure 3.9). SA1 isolated proteins involved in behavioral and developmental processes (5.6%), which were not represented in the A2 condition (Figure 3.9). Pathway analysis of A2-specific proteins identified the TCA cycle and pyruvate metabolism pathway as highly represented processes (20% and 13% respectively) (Figure 3.10). Comparatively, proteins implicated in Parkinson's disease and apoptosis signaling pathways were highly represented for SA1-specific proteins (both 11%) (Figure3.10).

Interestingly, specific proteins identified as components of these pathways also had the highest number of identified peptides from their respective HCDR3-construct groups (Table 3.8). Citrate synthase (CS), and succinyl CoA synthetase subunit β were identified as prominent components of the TCA cycle, while CS was also represented in the pyruvate metabolism pathway. Heat shock cognate 71 kDa and endoplasmic reticulum chaperone binding immunoglobulin protein (ER chaperone BiP) were identified as components of both the Parkinson's disease and apoptosis signaling pathways. The high volume of peptides recovered by MS and their involvement in highly represented pathways suggest that they are the most probable targets of the A2 and SA1.

3.4 DISCUSSSION

A confounding factor in the diagnosis and treatment of TBI is temporal complexity of pathological progression. Analysis of temporal biomolecular mechanisms provide insight on injury progression that may better inform the development of theranostic tools. In this study, we leveraged the power of unbiased phage display to identify and develop novel biomolecular motifs that specifically recognize elements of acute and subacute TBI pathology. *In vivo* phage biopanning was conducted in a CCI rodent model at three distinct time points following injury (1, 7, and 21 dpi) to perform a robust bioinformatics driven assessment of enriched phage populations for each timepoint. The spatiotemporal specificity of HDCR3-constructs based on the NGS data were validated first with IHC analysis, demonstrating the strength of this high throughput screening and sequencing methodology. Using IP-MS, we positively identified several candidate proteins involved in metabolic and neurodegenerative processes as potential targets for A2 and SA1, respectively. The elegance of phage-based approach in contrast to traditional neuroproteomics (i.e., whole brain tissue analysis to identify differentially expressed proteins via mass spectrometry [70]), is that phage biopanning leverages molecular evolution to narrow the molecular pool for biomarker candidate selection.

dAb libraries are advantageous to screening against neural tissue *in vivo* due to their small size (12-15 kDa), high affinity, and ability to effectively bind to brain vasculature [98, 162]. Interestingly, dAb phage accumulation in naïve and chronic injury neural tissue was comparable across biopanning rounds while accumulation within acute and subacute injury groups drastically increased. BBB disruption permits intravenously

injected phage with accessibility to extravascular targets, which corroborates the study's findings of relatively lower percentage of phage accumulation in sham and chronic injury cohorts (Figure 3.2) [185, 191].

Recent sequencing advancements in NGS capabilities are instrumental to the identification of candidate biological motifs in phage display libraries. High-throughput sequence analysis provides an opportunity to uncover the entire population of phage display libraries at a sequencing space of 10^5-10^7 in comparison to 20-100 for traditional Sanger sequencing methods [106]. High-throughput sequence analysis also minimizes the probability of selecting false positive clones that may be overrepresented in the library due to propagation advantages, thereby overcoming a large drawback of utilizing phage display technology [172, 192]. Both of these advantages are critical for the analysis of a library derived from *in vivo* biopanning of the neural injury microenvironment.

Although dAb production and purification were successful for two 1dpi dAbs as measured by positive histine-tag Western blots, they failed to show bioreactivity to injured tissue via immunohistochemistry. These results were prime examples of the complications with traditional recombinant protein production for in vivo phage since the antigen(s) are also unknown and present a tremendous barrier to validation and characterization of the selected motifs [178, 187]. We directly addressed this challenge by designing novel peptide-based HCDR3 constructs that mimic the constrained HCDR loop structure, motivated by prior studies [181], thereby enabling high-throughput production via direct peptide synthesis and facile biochemical modifications to fabricate the constrained cyclic HCDR3 loop structure. The HCDR3 has been identified as the main contributor to binding specificity of antibodies and truncated antibody fragments.

Prior studies have highlighted the utility of generating HCDR3 peptide variants as a "synthetic antibody" with comparable binding efficiency to full length antibodies [181, 193]. Our data further supports this reductionist approach and future studies will focus on potential mechanisms and molecular tuning to optimize the HCDR loop structure.

Our validation results readily demonstrated the critical need for thorough testing of each phage identified candidate motif. Most prominent, A1 was identified based on our selection criteria for the acute timepoint, namely high frequency in biopanning round 2, yet IHC assessment did not show detectable bioreactivity with fixed mouse brain tissue at 1 dpi. In contrast, A2, selected namely for the high fold enrichment value from biopanning round 1 to round 2, showed high sensitivity and affinity to the peri-injury region at 1dpi compared to sham, subacute, and chronic tissue sections (Figure 3.7). For the subacute constructs, the opposite effect was observed with constructs targeting subacute injury, with SA1 positively binding to injured neural tissue. A1 had the highest observed frequency for its timepoint, yet it only exhibited a fold-enrichment value of 2.47; much lower than A2's value of 22. Furthermore, SA2's enrichment value of 17.57 dwarfed in comparison to SA1's value of 49 (Table 3.4). These results may suggest that enrichment facilitated by biopanning plays a critical role in the ability of the HCDR3 to bind successfully to its target. However, more testing is required to fully understand the factors that influence bioreactivity of a phage-selected motif. SA1 also exhibited bioreactivity on 1 dpi tissue sections in the injury region, even though bioinformatic analysis suggested this construct was specific to subacute injury alone. This may indicate targeting of antigens that are expressed at a minimal level acutely after injury but increase in expression over time.

Further validation of our HCDR3 constructs was performed by IP-MS analysis. We identified potential acute TBI pathology targets of A2 as critical metabolic processes mediators. Pyruvate metabolism and TCA cycle, two pathways revealed by subsequent A2 target pathway analysis, work in tandem to regulate cerebral metabolism [194]. After TBI, these pathways are inhibited due to oxidative stress damage caused by mitochondrial dysfunction [195]. Ontological analysis revealed two individual components targeted by A2 that are implicated in these pathways and highly represented in the mass spectrometry data; succinate CoA ligase β and citrate synthase (CS) (Table 3.8). Deficiencies in succinate-CoA ligase β cause mitochondrial dysfunction and negatively impacts the central nervous system with disorders such as encephalomyopathy [196, 197]. This subunit is increased in the rat brain proteome three hours after hemorrhagic stroke in comparison to naïve controls, providing evidence for time-dependent upregulation after neural injury [184]. Succinate-CoA β was also identified in a similar study analyzing differential expression of proteins following induction of experimental epilepsy [198]. Interestingly, CS is significantly downregulated in comparison to controls acutely after diffuse axonal injury and CCI [63, 199]. However, CS expression may be dependent on both severity and time, with significantly decreased expression of CS in severe weight drop models at 6, 24, 48, and 120 hours post-injury in comparison to mild TBI conditions [200].

SA1 isolated proteins strongly associated with neurodegenerative processes such as Huntington's, Alzheimer's, and Parkinson's disease. (Fig 7). Heat shock cognate 71 kDa and ER chaperone BiP, members of the heat shock protein 70 family, were both identified as components of Parkinson's disease and the apoptosis signaling pathway. ER

chaperone BiP, a monitor of endoplasmic reticulum stress is induced in Alzheimer's disease in response to protein misfolding and cell death [201, 202]. Additionally, a reduction in ER chaperone BiP expression leads to the acceleration of prion disease pathology [203]. Comparatively, an increase in ER chaperone BIP expression is suggested to be neuroprotective in models of brain ischemia [204, 205]. Recent studies suggest that heat shock cognate 71 kDa, a cytosolic facilitator of protein folding and degradation, may have a strong interaction with Tau protein, a hallmark of Alzheimer's disease [206]. This protein has been suggested as a possible therapeutic target for stroke and TBI as well, as its overexpression may reduce apoptosis and inflammation [207]. TBI is a risk factor for neurodegenerative diseases, and many factors in the secondary injury cascade run parallel to degenerative pathology such as neuronal cell death [208, 209]. However, this connection is not fully elucidated and potential therapeutic targets are still in the early stages of characterization. The unbiased identification of the heat shock proteins subacutely in TBI through phage display therefore provides insightful perspective on the link between brain injury and acquisition of neurodegenerative diseases

The current study not only identified proteins specific to temporal brain injury phases, but simultaneously developed targeting constructs for these candidates. The design of HCDR3 constructs that specifically bind to acute and subacute injury provides a foundation for the development of theranostic tools. This discovery will allow for future characterization of the candidate targets through several conditions within the neural injury microenvironment, in addition to the refinement of HCDR3-constructs as a targeting modality to detect and treat TBI

3.5 FIGURES

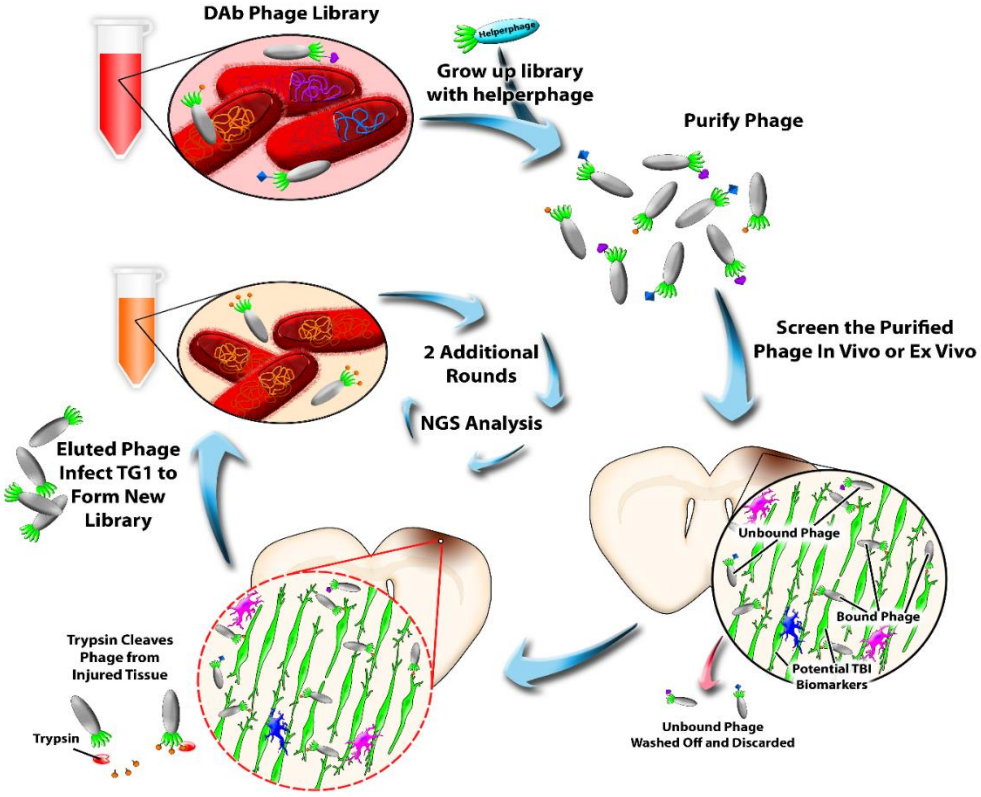

Figure 3.1: Schematic of phage display biopanning. A dAb phage parent library is produced and purified, then intravenously injected into a mouse that has either had a controlled cortical impact (CCI) at a distinct timepoint (1, 7, or 21 dpi) or a sham injury (sacrificed 1 day post procedure). Tissue are extracted, lysed, and trypsinized to cleave phage from tissue. The phage library from the ipsilateral hemisphere is then amplified with TG1 E. coli and applied in the final round of biopanning. Recovered phage are then analyzed using NGS.

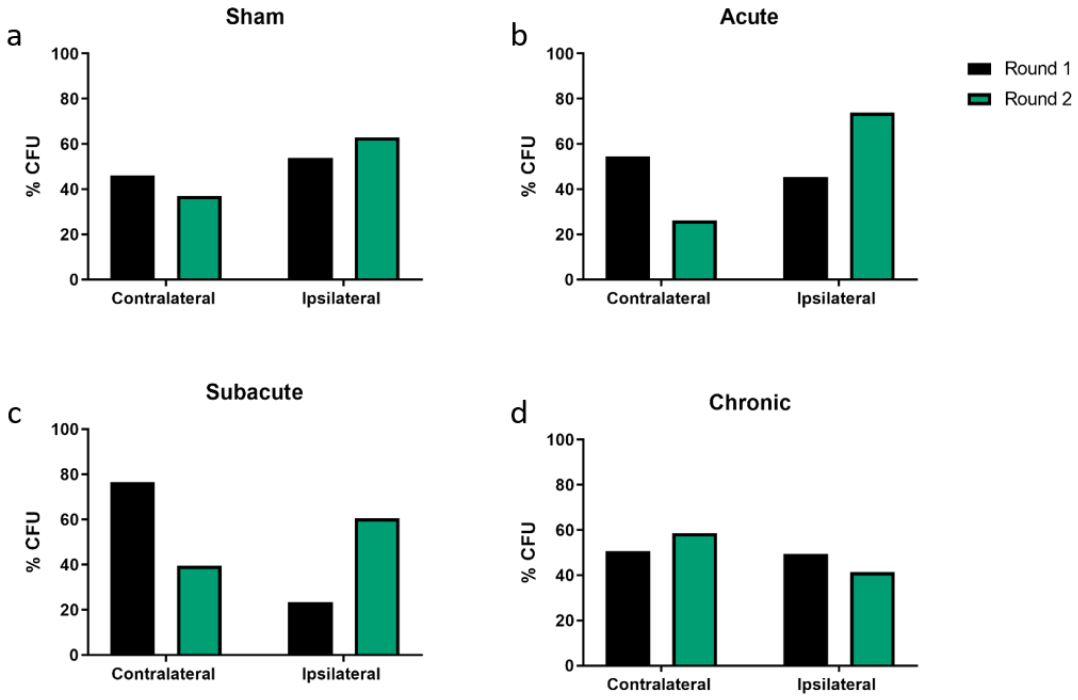

Figure 3.2: Hemisphere distribution of phage (CFU%). Recovery is quantified by % CFU for a) sham, b) acute (1dpi), c) subacute (7dpi), and d) chronic timepoints (21 dpi). Phage accumulation to the ipsilateral hemisphere increased after biopanning for both the acute and subacute timepoints. Phage distribution between hemispheres for the sham and chronic cohorts remained similar across biopanning rounds.

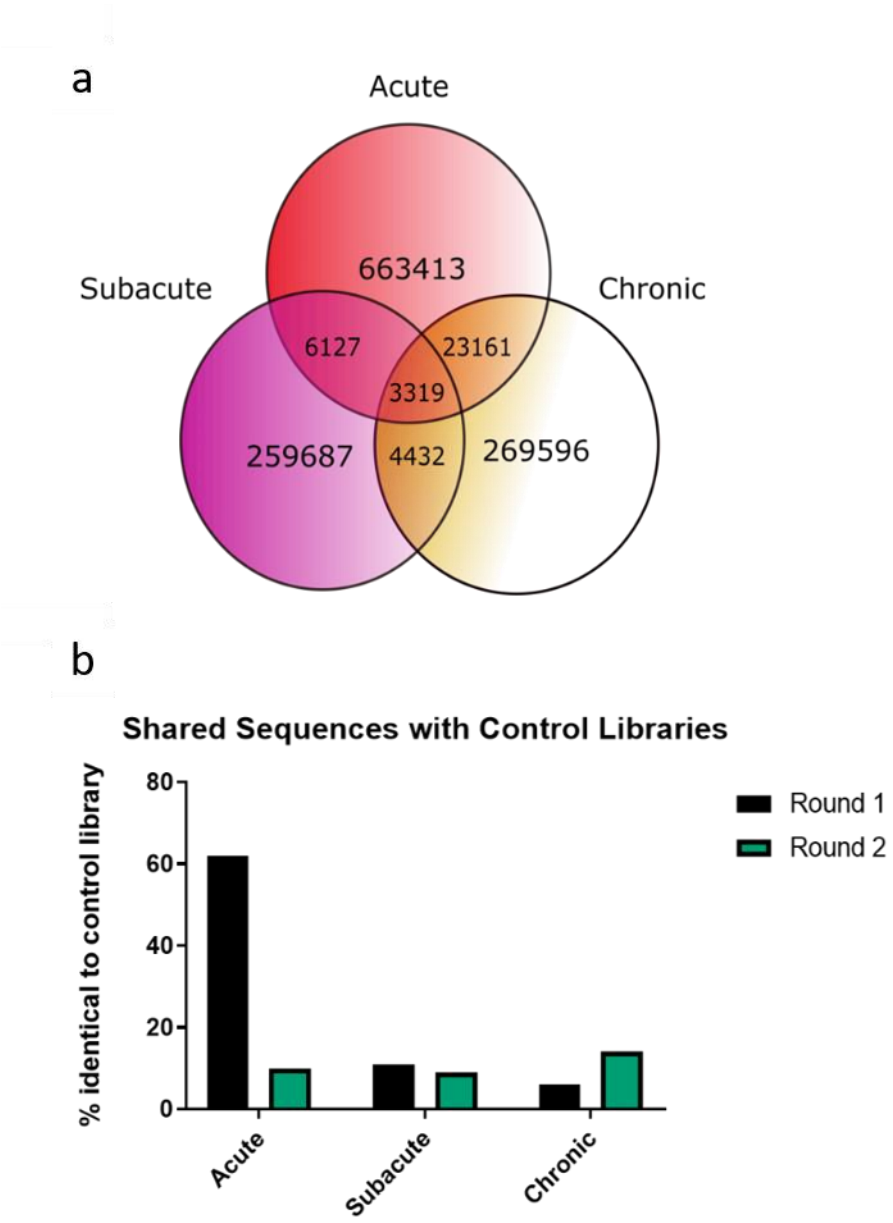

Figure 3.3: Sequence population diversity. (a) Comparison of recovered HCDR3s across injury timepoints represented by a Venn diagram. A majority of the recovered sequences were unique to their distinct timepoint, while a small fraction was found in multiple injury libraries simultaneously. (b) Comparison of recovered injury library HCDR3s against control propagation library. For the acute injury library, the percentage of sequences found in the control propagation library drastically decreased after biopanning. Both the subacute and chronic injury libraries yielded less than 20% similarity with controls across biopanning rounds.

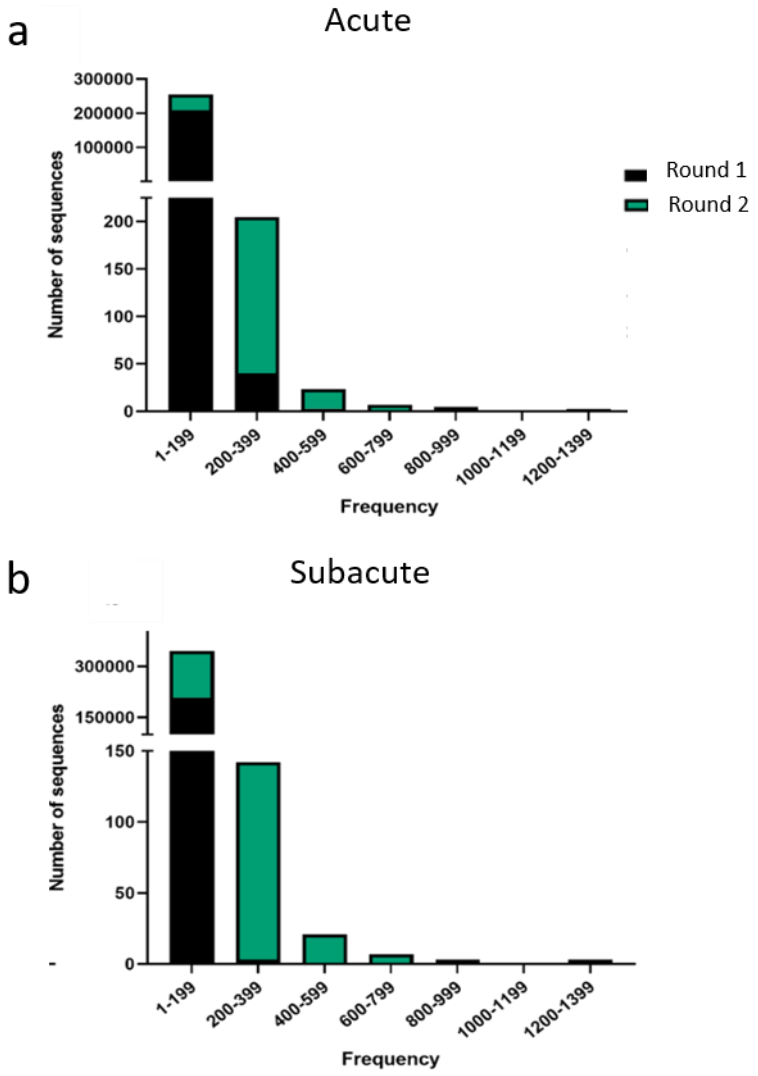

Figure 3.4: Frequency distribution of recovered HCDR3s within injury libraries. Round 2 yielded more sequences in higher ranges (>200 reads) than after round 1 of biopanning. This shift in frequency is representative of the biopanning process enriching the population of ipsilateral-specific sequences.

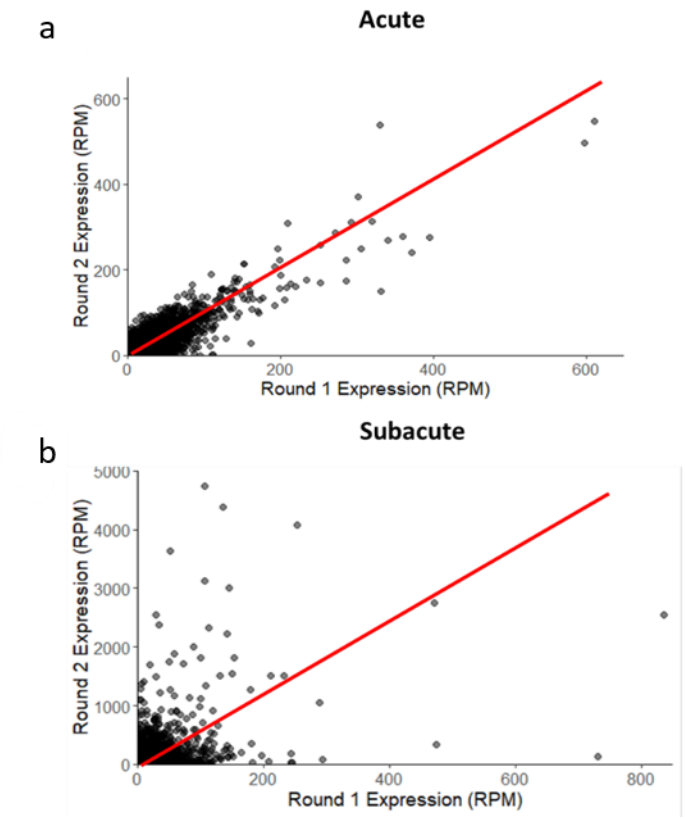

Figure 3.5: Reads per million (RPM) of sequences increased after biopanning. Relationship between individual sequence RPMs after the biopanning rounds are visualized with scatterplots for a) acute and b) subacute injury libraries. Data points above the diagonal red line represent sequences that were enriched through biopanning.

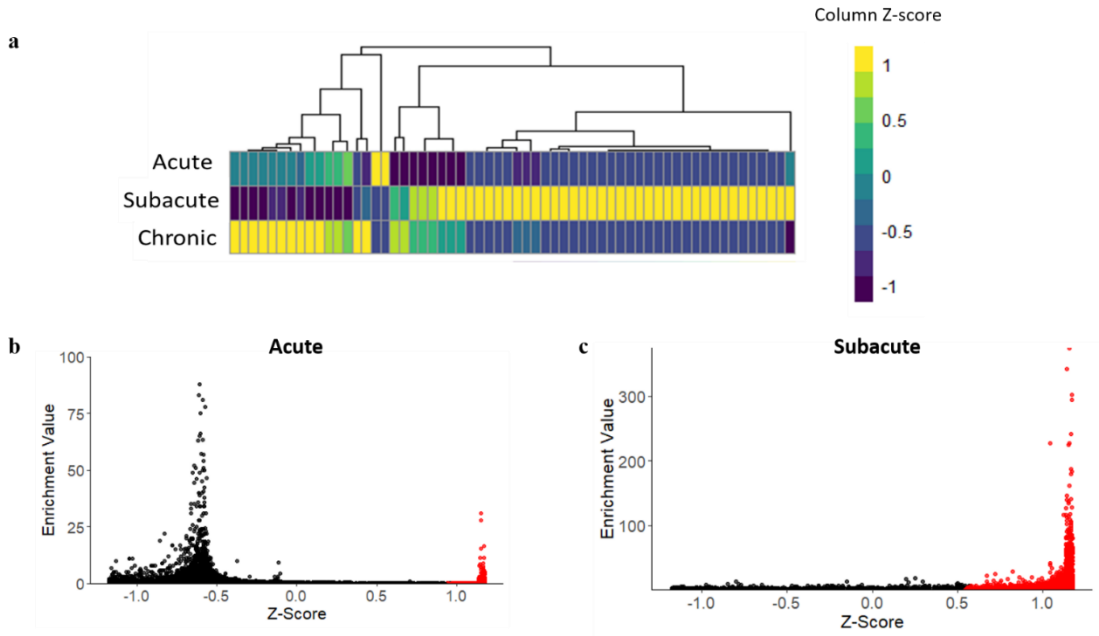

Figure 3.6: Analysis of HCDR3 temporal specificity a) representative heatmap of the top 20 highest frequency HCDR3s identified in each injury timepoint and their expression in adjacent timepoints. Z-scores are calculated by column (individual sequences). Scatter plots were generated to visualize the relationship between enrichment value (defined as Round 2 reads/Round 1 reads) and z-score for b) acute and c) subacute injuryHCDR3s. Red data points represent sequences that met z-score threshold criteria.

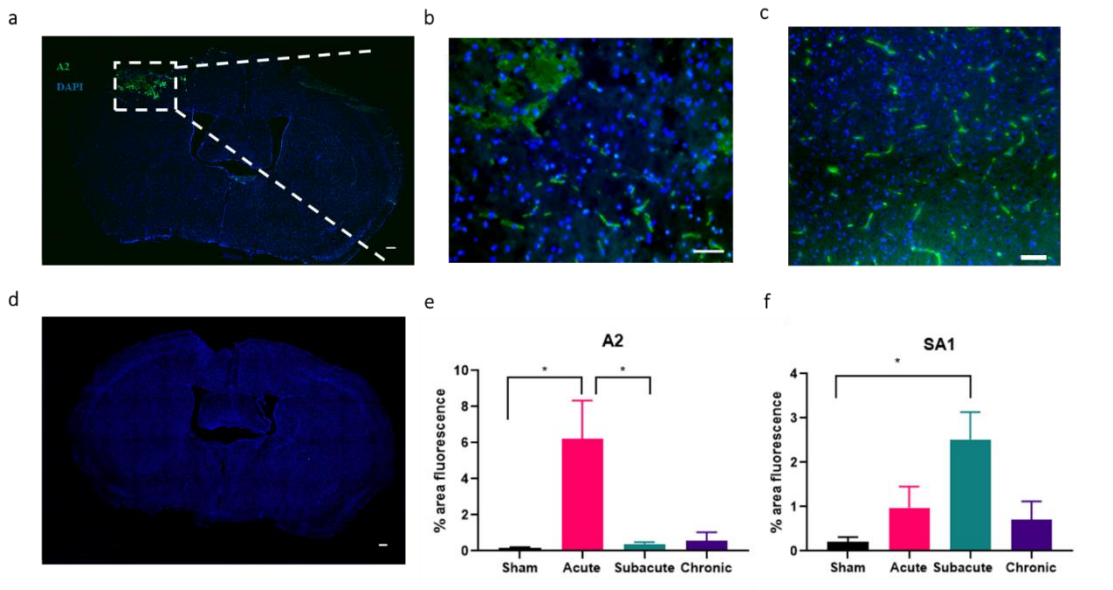

Figure 3.7: HCDR3 constructs show selectivity to injured tissue. a) Qualitative representation of injury-specific HCDR3 (green) and cell nuclei (blue) in 1 dpi tissue. ROI represented in white box. b) 20x magnification of A2 construct staining on 1 dpi tissue. c) 20x magnification of SA1 construct staining on 7 dpi tissue. d) qualitative representation of sham control. e and f) Quantification of % area fluorescence in 1500 µm x 1500 µm ROI (n=5-6). Data expressed in mean + SEM. * $p < 0.05$. Scale bar = 100 µm.

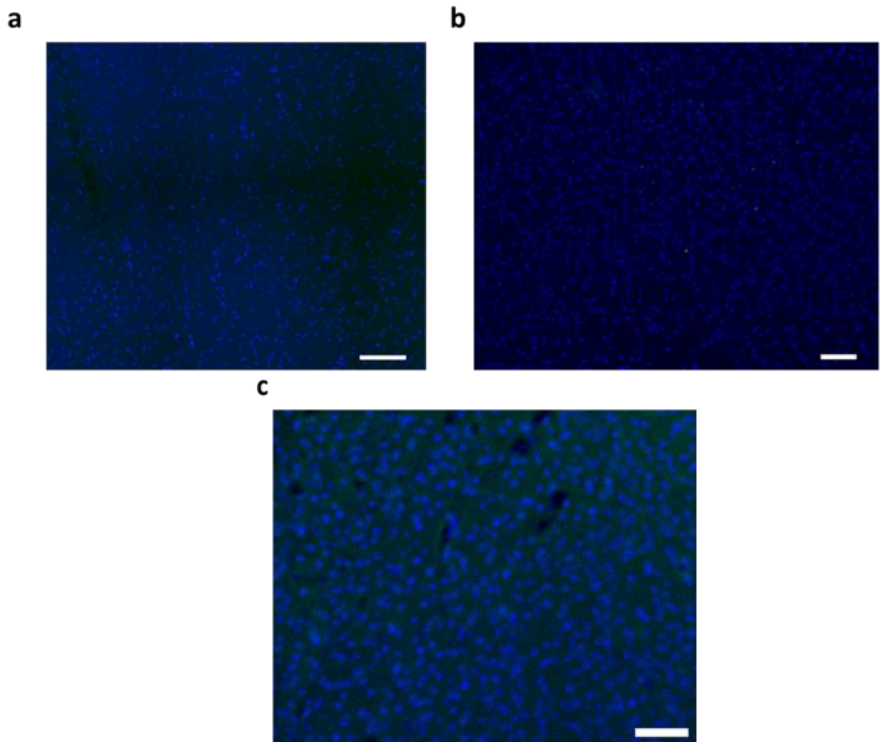

Figure 3.8: Control constructs show no detectable bioreactivity on injured neural tissue. Constructs were designed based on sequences highly expressed in control libraries. a) Spleen, b) dAb propagation and c) heart HCDR3 constructs showed no detectable bioreactivity with injured neural tissue. Scale bar = 100 µm.

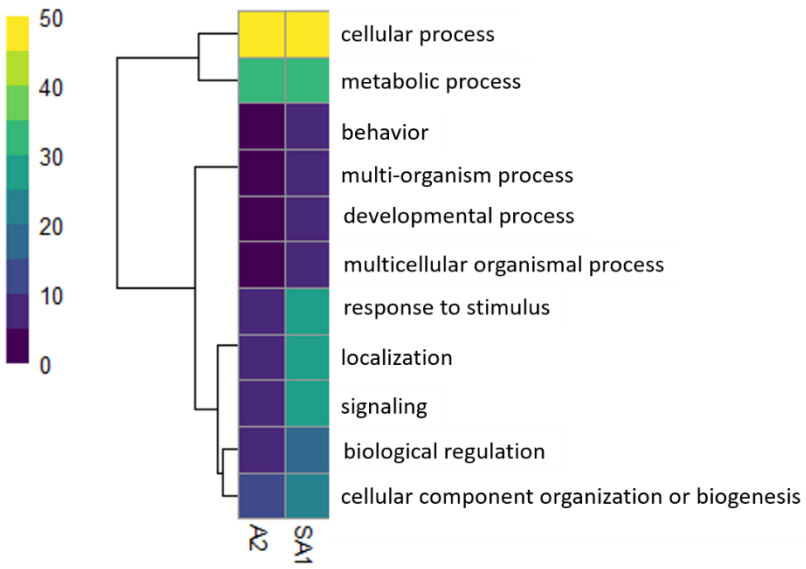

Figure 3.9: Biological process categorization of identified proteins isolated by A2 and SA1. Categories hierarchically clustered by percent of proteins identified in biological processes. A2 and SA1 had similar distribution of proteins involved in cellular and metabolic processes. Comparatively, more proteins isolated by SA1 were involved in localization, response to stimulus, and localization that proteins identified in the A2 condition.

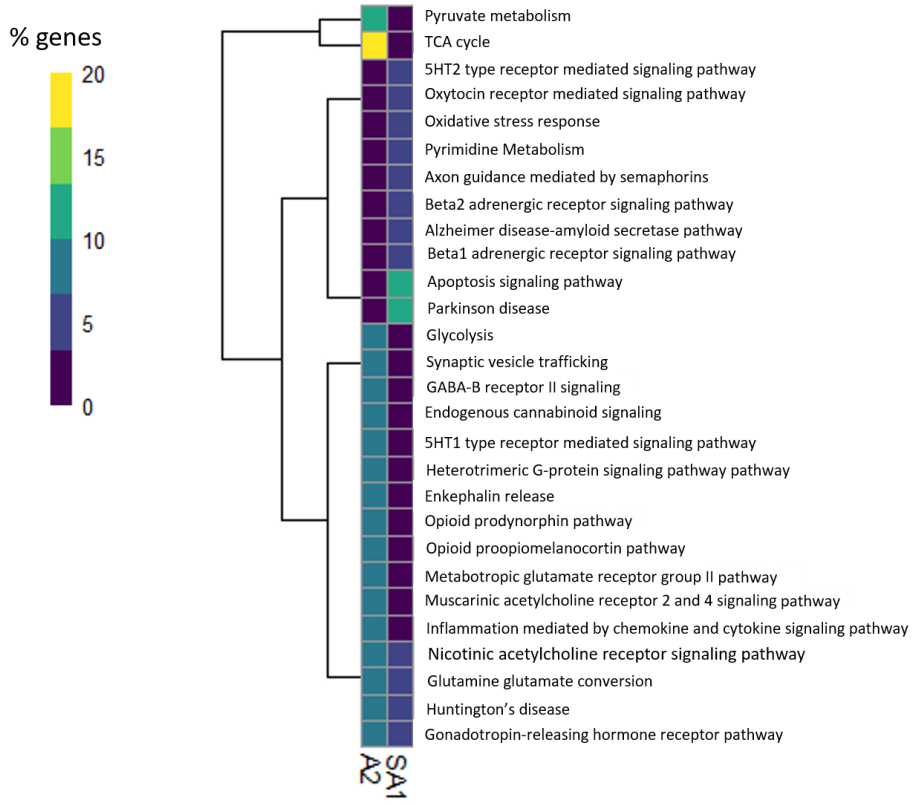

Figure 3.10: Pathway categorization of identified proteins isolated by A2 and SA1. Categories hierarchically clustered by percentage of proteins identified in pathway analysis. Proteins identified in the A2 condition were highly expressed in the TCA cycle and pyruvate metabolism in comparison to other pathway analysis categories. Proteins identified in the SA1 condition were highly expressed in Parkinson's disease and apoptotic signaling pathways by comparison.

Table 3.1: dAb sequencing primers for MiSeq 2 x 300 bp module. Underlined portion indicates Illumina overhang adapter sequence.

Primer Name	Sequence
dAb For	5’ TCGTCGGCAGCGTCAGATGTGTATAAGAGACAGCAGC TGTTGGAGTCTGGGG 3’
dAb rev	5’ GTCTCGTGGGCTCGGAGATGTGTATAAGAGACAGGAGA CGGTGACCAGGGTTC 3’

Table 3.2: Phage accumulation in ipsilateral and contralateral hemispheres determined by CFU/g

		Sham	Acute	Subacute	Chronic
Round 1 (CFU/g)	Heart	5.54×10^5	4.54×10^4	5.54×10^5	1.68×10^6
	Spleen	9.50×10^6	1.05×10^7	3.83×10^6	3.57×10^6
	Contralateral	1.08×10^5	3.92×10^3	1.21×10^6	5.69×10^4
	Ipsilateral	9.87×10^4	1.73×10^3	5.13×10^5	7.94×10^4
Round 2 (CFU/g)	Heart	1.90×10^6	4.79×10^6	1.17×10^4	8.72×10^6
	Spleen	3.11×10^6	1.77×10^7	1.867×10^7	9.20×10^7
	Contralateral	7.07×10^3	3.92×10^3	1.15×10^4	3.58×10^4
	Ipsilateral	1.54×10^4	7.69×10^5	2.26×10^4	2.52×10^4

Table 3.3: Percentage of HCDR3s meeting selection criteria. Enrichment is defined as an HCDR3 with increased frequency after biopanning. The z-score thresholds were 0.955 and 0.566 for acute and subacute libraries respectively, determined by the average for each injury group.

	Selection Criteria		
	Recovered	Enriched	Z-score
Acute	663413	44680 (6.73%)	500 (0.08%)
Subacute	259687	7945 (3.06%)	3996 (1.54%)

Table 3.4: Selected HCDR3s

	Enrichment Value	Frequency	Z-score	Sequence
Acute-1 (A1)	2.47	111	1.154	TAERDARTFQY
Acute-2 (A2)	22	22	1.155	SLYGSSRHTAPISF
Subacute-1 (SA1)	49	638	1.155	TDLAVAHPVRY
Subacute-2 (SA2)	17.57	246	1.148	AAPSWNNHVSY

Table 3.5: HCDR3 control constructs. HE-CDR3 = heart, SP-CDR3 = spleen, dAb-CDR3 = dAb propagation.

HCDR3-Construct	Sequence
HE-CDR3	TGHEGENEMAS
SP-CDR3	GPLDGKEEELRF
dAb-CDR3	GPLDGKEEELRF

Table 3.6: A2 isolated proteins determined by mass spectrometry (FDR<0.01)

Accession	Description
P18872	Guanine nucleotide-binding protein G(O) subunit alpha
P51863	V-type proton ATPase subunit d
Q62277	Synaptophysin
Q8BG05	Heterogeneous nuclear ribonucleoprotein A3
Q8R010	aminoacyl tRNA synthase complex-interacting multifunctional protein 2
P15105	Glutamine synthetase
P35486	Pyruvate dehydrogenase E1 component subunit alpha, somatic form, mitochondrial
P42669	Transcriptional activator protein Pur-alpha
P61164	Alpha-centractin
Q6ZQ38	cullin-associated nedd8-dissociated protein 1
Q8BG05	Heterogeneous nuclear ribonucleoprotein A3
Q8VHF2-1	Cadherin-related family member 5
Q9WV02-1	RNA-binding motif protein, X chromosome
Q9Z2I9	Succinate--CoA ligase [ADP-forming] subunit beta, mitochondrial
Q9WUM5	Succinate--CoA ligase [ADP/GDP-forming] subunit alpha, mitochondrial
Q9CZU6	citrate synthase, mitochondrial
P16330	2',3'-cyclic-nucleotide 3'-phosphodiesterase

Table 3.7: SA1 isolated proteins determined by mass spectrometry (FDR<0.01)

Accession	Description
Q8C0N1	Kinesin-like protein KIF2B
Q3U6U5	Putative GTP-binding protein 6
P62918	60S ribosomal protein L8
P63017	Heat shock cognate 71 kDa protein
P20029	78 kDa glucose-regulated protein
P19246	Neurofilament heavy polypeptide
P15105	Glutamine synthetase
Q6P5F9	Exportin-1
P62754	40S Ribosomal Protein S6
P04370-4	Isoform 4 of Myelin basic protein
O08553	Dihydropyrimidinase-related protein 2
Q9CXW4	60S ribosomal protein L11
P68254-1	14-3-3 protein theta
Q8BZ36	RAD50-interacting protein 1
Q7TQH7	Low-density lipoprotein receptor-related protein 10
Q99246	Voltage-dependent L-type calcium channel subunit alpha-1D
Q9DBB1	Dual specificity protein phosphatase 6
Q8CHC4	Synaptojanin-1

Table 3.8: Candidate proteins isolated by HCDR3 constructs

Targeting construct	Description	Accession	# Peptides
A2	Succinate--CoA ligase [ADP-forming] subunit beta, mitochondrial	Q9Z2I9	4
	citrate synthase, mitochondrial	Q9CZU6	3
SA1	Heat shock cognate 71 kDa protein	P63017	6
	Endoplasmic reticulum chaperone BiP	P20029	6

CHAPTER 4

CONCLUSION

4.1 SUMMARY OF FINDINGS

Traumatic brain injury (TBI) biomarkers have been identified previously through various avenues of discovery research, ranging from microRNA analysis to neuroimaging [210]. Current methods of biomarker discovery rely heavily on prior knowledge of injury pathology to determine candidate molecular biomarkers appropriate for further development. However, the heterogeneous pathophysiology of TBI has yet to be fully elucidated, leaving these narrowly focused techniques to possibly neglect unique features that are specific to TBI pathology. The work described in this dissertation addressed these limitations by applying domain antibody fragment (dAb) phage display to an *in vivo* screening pipeline for TBI biomarkers at 1, 7, and 21 days post-injury (dpi) in a controlled cortical impact (CCI) model of injury. To our knowledge, these are the first studies to apply *in vivo* dAb phage screening to an *in vivo* model of TBI.

First, we verified that dAb phage had the capacity to bind to injured neural tissue following intravenous injection. For both 1 and 7 dpi time points, phage titer quantification showed an increase in phage accumulation within the injured ipsilateral hemisphere of the brain following population enrichment from biopanning round one to round two. In contrast, minimal phage enrichment/accumulation was observed in both the sham and chronic timepoint (21 dpi) comparing phage titers from round one to two of biopanning. Nonetheless, this analysis confirmed that intravenously injected dAb phage were suitable for targeting brain tissue at various timepoints post-injury in the mouse CCI model. NGS analysis of the eluted libraries revealed that sequences were largely unique

to each injury cohort, with limited overlap among injury timepoint conditions or control libraries. The sequence exclusivity in the recovered libraries reflected the complexity of each stage of brain injury progression, demonstrating with bioinformatic evidence that this method is capable of capturing temporal complexity *in vivo*.

NGS data collection enabled bioinformatic analysis of dAb population across temporal and control biopanning screens to select appropriate candidates for targeting distinct temporal phases of TBI. We first focused on the heavy complementarity determining region 3 (HCDR3) due to its critical role in the antigen binding process [164, 165]. Although this approach effectively eliminated the remainder of the dAb sequence, recent studies have postulated that the primary role of HCDR1 and HCDR2 is to facilitate stable presentation of the HCDR3 domain in a loop conformation, while the HCDR3 is the primary antigen-binding region [179, 211]. Focusing on HCDR3 allowed for less computationally demanding processing and streamlined the examination of the recovered dAb libraries. The analysis was optimized to assess the following characteristics: 1) frequency after biopanning (i.e. frequency in eluted round 2 phage population), 2) fold enrichment change after biopanning (i.e. fold change from round 1 to round 2), and 3) specificity to timepoint post-injury (i.e. exclusivity of sequence for specific time point). From these methods and strict selection criteria, two potential candidates were identified for each timepoint; one based on fold-enrichment and the other based on frequency. The decision to select two candidates per timepoint was to include sequences that were substantially enriched, but had low frequency relative to other sequences that met criteria. The remainder of the dAb framework and HCDRs were then recovered from the source file by creating a query for the selected HCDR3.

We first attempted to produce the selected candidates via recombinant protein production methods (Appendix B). Selected dAbs were ligated into pET-22b(+) vectors with a C-terminus 6xhis tag. dAb production was subject to rigorous design of experiments (DoE) testing to assure optimized production standards. Although production and purification were successful determined by Western Blot and fast protein liquid chromatography (FPLC) analysis, these dAbs failed to show bioreactivity to injured tissue at their respective timepoints via immunohistochemistry (IHC). Recombinant protein production is understood to be a bottleneck of validation studies, and is often a time consuming, herculean effort. While dAb production and purification may be successful, affinity tags unfortunately tend to degrade completely and purification methods can also negatively affect stability due to high acidic elution buffers [178]. Due to the high volume of bioreactivity testing that needed to be completed, we decided to instead pursue an approach to evaluate HCDR3 constructs directly to test bioreactivity.

The HCDR3 constructs, cyclic peptides based solely on the HCDR3 region of the dAb, were biotinylated and used as primary antibodies in IHC experiments. Analysis revealed that the A2 (acute, 1dpi) and SA1 (subacute, 7 dpi) HCDR3 constructs showed significant specificity to their respective timepoints in comparison to sham controls (See Chapter 3 Figure 5). Notably, SA1 showed reactivity to 1 dpi and 21 dpi tissue sections. Additionally, control HCDR3s designed based on sequences heavily expressed in peripheral tissue did not show bioreactivity, demonstrating that the spatiotemporal specificity observed previous was not due to inherent characteristics of the constructs themselves. Unfortunately, neither candidate selected from the chronic injury (21 dpi) libraries showed measurable bioreactivity to injured tissue using IHC. There are a

number of reasons why a selected HCDR3 sequence could have been unsuitable even after stringent sequence selection criteria, such as a library losing a percentage of antigen-specific dAbs during screening due to misfolding in *E. coli* [182, 212]. Nonetheless, this streamlined analysis pipeline (phage display to NGS to HCDR3 bioinformatic selection) was established and refined to assist in selection of candidate biomotifs from large, diverse populations and this bioreactivity is evidence of its success.

Through a rigorously designed immunoprecipitation-mass spectrometry protocol, we identified candidate proteins for both HCDR3 construct-antigen pairs. Most importantly, these discovered candidate antigens/proteins are possible temporal biomarkers of focal brain injury. For A2, the proteins identified were highly implicated in metabolic dysfunction, but overall citrate synthase and succinate-CoA ligase β were determined to be most prevalent due to their involvement in the processes identified from pathway analysis and number of peptides recovered via mass spectrometry. Both proteins are highly involved in the pyruvate metabolism and TCA cycle, and consistent with previous reports in the literature, their expression is altered in response to mitochondrial and metabolic dysfunction after TBI [194, 195]. SA1 isolated heat shock cognate 71 kDa and endoplasmic reticulum chaperone binding immunoglobulin protein (ER BiP). The role these proteins hold in TBI pathology have not been fully explored, but have strong connections to neurodegenerative diseases such as Parkinson's disease and Alzheimer's disease [201, 206].

This work achieved two goals: 1) further elucidation of temporal mechanisms of TBI and 2) the design of a motif capable of targeting candidate biomarkers of said temporal mechanisms. The identification of distinct proteins from 1 and 7 dpi is reflective

of the elegance of *in vivo* dAb phage display and next generation sequencing. This approach demonstrated that dAb phage could interact with the heterogeneous injured neural microenvironment. More importantly, these findings captured complex TBI pathology as it unfolded, emphasizing the important role time plays in the advancement of injury. Identifying proteins that are critical in metabolic dysfunction and neurodegeneration at acute and subacute timepoints respectively provides a foundation for exploration of these processes to further elucidate how they contribute to injury. The candidate proteins identified may also serve as therapeutic targets, with the design of our HCDR3 constructs already providing the foundation to modify motifs that can modulate the expression of these proteins. Overall, the simultaneous task of discovery and design undertaken with this dissertation has the potential to be foundational for application of phage display to uncover the intricacies of neurotrauma.

4.2 FUTURE WORK

Validation of candidate dAb construct protein targets

The work described in this dissertation identified and designed HCDR3 constructs that target distinct temporal phases of injury and applies mass spectrometry analysis to identify accompanying ligands/potential biomarkers of injury. To further elucidate the mechanisms of injury progress and the utility of these constructs, validation of the candidate biomarkers is critical. Each of the identified proteins can be assessed using commercial antibodies and Western Blot analysis to compare expression with the HCDR3 constructs. Similarly, immunohistochemical experiments with these antibodies can be used to visualize localization of the constructs to the candidate biomarker, providing spatiotemporal characterization of how A2 and SA1 selectively bind to these

proteins. For A2, citrate synthase, for example, is ideal for this type of validation as it's been explored in animal models of TBI previously (downregulated acutely post-CCI and upregulated after acceleration injury) and commercial antibodies/reagents are readily available [200, 213, 214]. Similarly assessing the homing of SA1 to Heat shock cognate 71 kDa is feasible as this protein is currently investigated as therapeutic target for ischemic brain injury [207, 215].

Following protein target verification, the discovered dAb constructs may be used to further develop companion therapeutic intervention. For example, BIP protein inducer X (BIX) is a drug that increases expression of ER BiP and has been shown to promote neuroprotection in models of brain ischemia [204, 205]. A future study evaluating BIX treatment in CCI mouse model in combination with SA1 construct to monitor ER BiP levels demonstrate the potential to not only track injury progression, but also treatment efficacy.

Transgenic mouse models may also be used to further validate protein targets. For example, a transgenic knock down of specific succinate CoA ligase β subunits is readily available, mainly for to study mitochondrial encephalomyopathy [216]. Currently, there is little research conducted to address comparisons between mitochondrial encephalomyopathy and TBI. Thus, utilizing this transgenic knockout model with CCI model would introduce a rare perspective on the role succinate CoA ligase plays in these two conditions as well as further validation for the targeting dAb construct.

In Vivo Targeting

The specificity of the HCDR3 constructs for acute and subacute injury was measured by immunohistochemistry (IHC) and immunoprecipitation as bioreactivity

metrics. While optimization of the constructs as “antibodies” is vital for utility in immunoassays, their full potential for *in vivo* targeting motifs has yet to be explored. To our knowledge, HCDR3 constructs have not yet been applied to *in vivo* targeting. Rigorous dose testing is required to understand the feasibility of intravenous injection of the HCDR3 constructs for *in vivo* distribution studies. Our initial dose studies indicate no detectable toxicity up to 2000 µg/kg for up to 24 hours after intravenous injection. However, additional critical experiments to be conducted include a maximal tolerable dose studies followed by biodistribution and circulation time studies. Our phage biopanning circulation time was informed by previous literature, however, we cannot assume that HCDR3 constructs will have the same clearance and binding mechanisms as a phage-displayed dAb. Therefore, determining optimal amount of circulation and dose will be a necessary, although arduous, first step towards efficient analysis *in vivo*.

Testing the distribution of these constructs *in vivo* has tremendous potential for the advancement of pre-clinical biomarker research. For example, comparing the accumulation of A2 to the injured brain at several timepoints post-injury could provide a time course analysis of target ligand expression and also informs the design of imaging probes, sensors, or nanoparticle-based treatments that could utilize this technology. To achieve this, taking advantage of novel multiplex tracking technology, such as barcoded DNA tags, would provide a great opportunity for high-throughput analyses [217, 218]. Using these techniques, individual HCDR3 constructs can be conjugated with a unique barcode that can be detected via RT-qPCR primers. This approach will allow multiple constructs to be injected and quantified simultaneously. This multiplexed approach would

be paramount in determining the accumulation of the HCDR3s to various tissues at distinct timepoints using less animals.

An addition to these *in vivo* distribution studies is the incorporation of non-neural injuries during validation. Lack of specificity for neural injury is one of the problems plaguing biomarker-based therapeutics in TBI [28, 29]. Non-neural injuries such as skin or liver injuries should be included as controls for the *in vivo* distribution studies to assess both sensitivity and specificity. Overall, these experiments could provide a more comprehensive perspective on the complexities of the heterogeneous injury environment that would otherwise remain unknown.

Expansion to other injury models

It is important to note that the studies described in this dissertation solely focus on focal TBI, the CCI rodent model of TBI. One of the main contributors to TBI pathology is the phenotype of injury (e.g., closed head injury vs. penetrating brain injury), which can be caused by a myriad of events resulting in variable pathophysiological effects due to the difference in physical force and injury location [12, 219, 220]. For example, the candidate temporal biomarkers identified using the CCI model may not correlate as closely with progression mechanisms in the fluid percussion injury (FPI) or blast injury models. Expansion of this biomarker discovery pipeline to various injury models can illuminate the molecular differences between these injury models using a time course-focused perspective. Similarly, this work can be expanded to include various factors of injury beyond time and phenotype, such as severity, age, and comorbidity with other diseases such as anxiety and depression.

Implementation of the phage-HCDR3 construct pipeline described in this dissertation is instrumental in identifying a panel of biomarkers associated with very distinct injury characteristics that advances the field towards a more personalized approach to therapeutics. This panel would address factors such as phenotype, age, sex, and pre-existing conditions, and how these factors affect the neural injury microenvironment. Evaluating TBI pathology from multiple perspectives will also provide an array of HCDR3 constructs based on candidate biomarkers identified in these conditions, setting the foundation for designs that could modulate the expression of these potential therapeutic targets. Thus, the simultaneous act of biomarker discovery and HCDR3 construct design has the potential of significantly influencing the integration of biomarker-based therapeutics for neurotrauma.

REFERENCES

1. Faul M, Xu L, Wald MM, Coronado VG. Traumatic brain injury in the United States. Atlanta, GA Centers Dis Control Prev Natl Cent Inj Prev Control. 2010.

2. Maegele M, Engel D, Bouillon B, Lefering R, Fach H, Raum M, et al. Incidence and outcome of traumatic brain injury in an urban area in western Europe over 10 years. Eur Surg Res. 2007;39:372–9.

3. Langlois JA, Rutland-Brown W, Wald MM. The Epidemiology and Impact of Traumatic Brain Injury: A Brief Overview. J Head Trauma Rehabil. 2006;21. http://journals.lww.com/headtraumarehab/Fulltext/2006/09000/The_Epidemiology_and_Impact_of_Traumatic_Brain.1.aspx.

4. Bruns J, Hauser WA. The epidemiology of traumatic brain injury: a review. Epilepsia. 2003;44:2–10.

5. Ashman TA, Cantor JB, Gordon WA, Sacks A, Spielman L, Egan M, et al. A comparison of cognitive functioning in older adults with and without traumatic brain injury. J Head Trauma Rehabil. 2008;23:139–48.

6. Ruttan L, Martin K, Liu A, Colella B, Green RE. Long-term cognitive outcome in moderate to severe traumatic brain injury: a meta-analysis examining timed and untimed tests at 1 and 4.5 or more years after injury. Arch Phys Med Rehabil. 2008;89:S69–76.

7. Mioni G, Grondin S, Stablum F. Temporal dysfunction in traumatic brain injury patients: primary or secondary impairment? Front Hum Neurosci. 2014;8 April:269. doi:10.3389/fnhum.2014.00269.

8. Acosta SA, Tajiri N, de la Pena I, Bastawrous M, Sanberg PR, Kaneko Y, et al. Alpha-Synuclein as a pathological link between chronic traumatic brain injury and parkinson's disease. J Cell Physiol. 2015;230:1024–32.

9. Emmerling MR, Morganti-Kossmann MC, Kossmann T, Stahel PF, Watson MD, Evans LM, et al. Traumatic brain injury elevates the Alzheimer's amyloid peptide A beta 42 in human CSF. A possible role for nerve cell injury. Ann N Y Acad Sci. 2000;903:118–22.

10. Sivanandam TM, Thakur MK. Traumatic brain injury: A risk factor for Alzheimer's disease. Neurosci Biobehav Rev. 2012;36:1376–81. doi:10.1016/j.neubiorev.2012.02.013.

11. (CDC C for DC and P. CDC grand rounds: reducing severe traumatic brain injury in the United States. MMWR Morb Mortal Wkly Rep. 2013;62:549.

12. Xiong Y, Mahmood A, Chopp M. Animal models of traumatic brain injury. Nat Rev Neurosci. 2013;14:128–42. doi:10.1038/nrn3407.

13. Alluri H, Wiggins-Dohlvik K, Davis ML, Huang JH, Tharakan B. Blood–brain barrier dysfunction following traumatic brain injury. Metabolic Brain Disease. 2015;30:1093–104.

14. Shlosberrg D, Benifla M, Kaufer D, Friedman A. Blood-brain barrier breakdown as a therapeutic target in traumatic brain inury. Nat Rev Neurosci. 2010;6:393–403.

15. Greve MW, Zink BJ. Pathophysiology of traumatic brain injury. Mt Sinai J Med A J Transl Pers Med A J Transl Pers Med. 2009;76:97–104.

16. Xiong Y, Mahmood A, Chopp M. Emerging treatments for traumatic brain injury. Science (80-). 2009;14:67–84. doi:10.1517/14728210902769601.

17. Ottens AK, Kobeissy FH, Golden EC, Zhang Z, Haskins WE, Chen SS, et al. Neuroproteomics in neurotrauma. Mass Spectrom Rev. 2006;25:380–408.

18. Sharma R, Laskowitz DT. Biomarkers in traumatic brain injury. Curr Neurol Neurosci Rep. 2012;12:560–9.

19. Crash MRC, Collaborators T. Predicting outcome after traumatic brain injury: practical prognostic models based on large cohort of international patients. Bmj. 2008;336:425–9. doi:10.1136/bmj.39461.643438.25.

20. Hukkelhoven CWPM, Steyerberg EW, Rampen AJJ, Farace E, Habbema JDF, Marshall LF, et al. Patient age and outcome following severe traumatic brain injury: an analysis of 5600 patients. J Neurosurg. 2003;99:666–73. doi:10.3171/jns.2003.99.4.0666.

21. McCullagh S, Ouchterlony D, Protzner A, Blair N, Feinstein A. Prediction of neuropsychiatric outcome following mild trauma brain injury: An examination of the Glasgow Coma Scale. Brain Inj. 2001;15:489–97.

22. Foreman BP, Caesar RR, Parks J, Madden C, Gentilello LM, Shafi S, et al. Usefulness of the abbreviated injury score and the injury severity score in comparison to the Glasgow Coma Scale in predicting outcome after traumatic brain injury. J Trauma - Inj Infect Crit Care. 2007;62:946–50.

23. Shenton ME, Hamoda HM, Schneiderman JS, Bouix S, Pasternak O, Rathi Y, et al. A review of magnetic resonance imaging and diffusion tensor imaging findings in mild traumatic brain injury. Brain Imaging Behav. 2012;6:137–92.

24. Dash PK, Zhao J, Hergenroeder G, Moore AN. Biomarkers for the diagnosis, prognosis, and evaluation of treatment efficacy for traumatic brain injury. Neurotherapeutics. 2010;7:100–14. doi:10.1016/j.nurt.2009.10.019.

25. Dadas A, Janigro D. The role and diagnostic significance of cellular barriers after concussive head trauma. Concussion. 2018;:CNC53.

26. Bogoslovsky T, Wilson D, Chen Y, Hanlon D, Gill J, Jeromin A, et al. Increases of plasma levels of glial fibrillary acidic protein, tau, and amyloid β up to 90 days after traumatic brain injury. J Neurotrauma. 2017;34:66–73.

27. Raheja A, Sinha S, Samson N, Bhoi S, Subramanian A, Sharma P, et al. Serum biomarkers as predictors of long-term outcome in severe traumatic brain injury: analysis from a randomized placebo-controlled Phase II clinical trial. J Neurosurg. 2016;125:631–41.

28. Hossain I, Liedes H, Newcombe V, Outtrim J, Katila AJ, Frantze J, et al. Glial Fibrillary Acidic Protein and Ubiquitin C-Terminal Hydrolase-L1 Are Not Specific Biomarkers. 2016;12:1–12.

29. Kobeissy FH, Wang KKW, Zhang Z. Neuro-proteomics and Neuro-systems Biology in the Quest of TBI Biomarker Discovery. In: Biomarkers of Brain Injury and Neurological Disorders. CRC Press; 2014. p. 18–56.

30. Albert-Weissenberger C, Sirén A-L. Experimental traumatic brain injury. Exp Transl Stroke Med. 2010;2:16. doi:10.1186/2040-7378-2-16.

31. Cao T, Thomas TC, Ziebell JM, Pauly JR, Lifshitz J. Morphological and genetic activation of microglia after diffuse traumatic brain injury in the rat. Neuroscience. 2012;225:65–75. doi:10.1016/j.neuroscience.2012.08.058.

32. Sajja VS, Hubbard WB, Hall CS, Ghoddoussi F, Galloway MP, VandeVord PJ. Enduring deficits in memory and neuronal pathology after blast-induced traumatic brain injury. Sci Rep. 2015;5:15075. doi:10.1038/srep15075.

33. Risling M, Davidsson J. Experimental animal models for studies on the mechanisms of blast-induced neurotrauma. Front Neurol. 2012;3:30.

34. Marmarou A, Foda MAA-E, Brink W van den, Campbell J, Kita H, Demetriadou K. A new model of diffuse brain injury in rats: Part I: Pathophysiology and biomechanics. J Neurosurg. 1994;80:291–300.

35. Flierl MA, Stahel PF, Beauchamp KM, Morgan SJ, Smith WR, Shohami E. Mouse closed head injury model induced by a weight-drop device. Nat Protoc. 2009;4:1328–37.

36. van Rooij E. The art of microRNA research. Circ Res. 2011;108:219–34.

37. Miñones-Moyano E, Porta S, Escaramís G, Rabionet R, Iraola S, Kagerbauer B, et al. MicroRNA profiling of Parkinson's disease brains identifies early downregulation of miR-34b/c which modulate mitochondrial function. Hum Mol Genet. 2011;20:3067–78.

38. Wang W-X, Huang Q, Hu Y, Stromberg AJ, Nelson PT. Patterns of microRNA expression in normal and early Alzheimer's disease human temporal cortex: white matter versus gray matter. Acta Neuropathol. 2011;121:193–205.

39. Liu XS, Chopp M, Zhang RL, Tao T, Wang XL, Kassis H, et al. MicroRNA profiling in subventricular zone after stroke: MiR-124a regulates proliferation of neural progenitor cells through Notch signaling pathway. PLoS One. 2011;6:e23461.

40. Qiu L, Tan EK, Zeng L. microRNAs and neurodegenerative diseases. In: microRNA: Medical Evidence. Springer; 2015. p. 85–105.

41. Munro KM, Perreau VM. Current and future applications of transcriptomics for discovery in CNS disease and injury. NeuroSignals. 2009;17:311–27.

42. Bhalala OG. The emerging impact of microRNAs in neurotrauma pathophysiology and therapy. 2015.

43. Pietro V Di, Yakoub KM, Scarpa U, Di Pietro C, Belli A. MicroRNA signature of traumatic brain injury: From the biomarker discovery to the point-of-care. Front Neurol. 2018;9 JUN:1–15.

44. Wanunu M, Dadosh T, Ray V, Jin J, McReynolds L, Drndić M. Rapid electronic detection of probe-specific microRNAs using thin nanopore sensors. Nat Nanotechnol. 2010;5:807.

45. Alhasan AH, Kim DY, Daniel WL, Watson E, Meeks JJ, Thaxton CS, et al. Scanometric microRNA array profiling of prostate cancer markers using spherical nucleic acid–gold nanoparticle conjugates. Anal Chem. 2012;84:4153–60.

46. Ding X, Yan Y, Li S, Zhang Y, Cheng W, Cheng Q, et al. Surface plasmon resonance biosensor for highly sensitive detection of microRNA based on DNA super-sandwich assemblies and streptavidin signal amplification. Anal Chim Acta. 2015;874:59–65.

47. Qin X, Li L, Lv Q, Shu Q, Zhang Y, Wang Y. Expression profile of plasma microRNAs and their roles in diagnosis of mild to severe traumatic brain injury. PLoS One. 2018;13:e0204051. doi:10.1371/journal.pone.0204051.

48. Yang T, Song J, Bu X, Wang C, Wu J, Cai J, et al. Elevated serum miR-93, miR-191, and miR-499 are noninvasive biomarkers for the presence and progression of traumatic brain injury. J Neurochem. 2016;137:122–9.

49. Lei P, Li Y, Chen X, Yang S, Zhang J. Microarray based analysis of microRNA expression in rat cerebral cortex after traumatic brain injury. Brain Res. 2009;1284:191–201. doi:10.1016/j.brainres.2009.05.074.

50. Hu Z, Yu D, Almeida-Suhett C, Tu K, Marini AM, Eiden L, et al. Expression of miRNAs and their cooperative regulation of the pathophysiology in traumatic brain injury. PLoS One. 2012;7:e39357.

51. Hicks SD, Johnson J, Carney MC, Bramley H, Olympia RP, Loeffert AC, et al. Overlapping microRNA expression in saliva and cerebrospinal fluid accurately identifies pediatric traumatic brain injury. J Neurotrauma. 2017; October:neu.2017.5111. doi:10.1089/neu.2017.5111.

52. Papa L, Ramia MM, Kelly JM, Burks SS, Pawlowicz A, Berger RP. Systematic review of clinical research on biomarkers for pediatric traumatic brain injury. J Neurotrauma. 2013;30:324–38.

53. Kövesdi E, Lückl J, Bukovics P, Farkas O, Pál J, Czeiter E, et al. Update on protein biomarkers in traumatic brain injury with emphasis on clinical use in adults and pediatrics. Acta Neurochir (Wien). 2010;152:1–17.

54. Di Pietro V, Porto E, Ragusa M, Barbagallo C, Davies D, Forcione M, et al. Salivary MicroRNAs: Diagnostic Markers of Mild Traumatic Brain Injury in Contact-Sport. Front Mol Neurosci. 2018;11 August:1–13. doi:10.3389/fnmol.2018.00290.

55. Balakathiresan N, Bhomia M, Chandran R, Chavko M, McCarron RM, Maheshwari RK. MicroRNA Let-7i Is a Promising Serum Biomarker for Blast-Induced Traumatic Brain Injury. J Neurotrauma. 2012;29:1379–87. doi:10.1089/neu.2011.2146.

56. Redell JB, Liu Y, Dash PK. Traumatic brain injury alters expression of hippocampal microRNAs: Potential regulators of multiple pathophysiological processes. J Neurosci Res. 2009;87:1435–48.

57. Sun T, Chen X, Liu Z, Zhao L, Jiang Y, Qu G, et al. Expression profiling of MicroRNAs in hippocampus of rats following traumatic brain injury. J Huazhong Univ Sci Technol [Medical Sci. 2014;34:548–53. doi:10.1007/s11596-014-1313-1.

58. Meissner L, Gallozzi M, Balbi M, Schwarzmaier S, Tiedt S, Terpolilli NA, et al. Temporal Profile of MicroRNA Expression in Contused Cortex after Traumatic Brain Injury in Mice. J Neurotrauma. 2016;33:713–20. doi:10.1089/neu.2015.4077.

59. Sandhir R, Gregory E, Berman NEJ. Differential response of miRNA-21 and its targets after traumatic brain injury in aging mice. Neurochem Int. 2014;78:117–21. doi:10.1016/j.neuint.2014.09.009.

60. Sharma A, Chandran R, Barry ES, Bhomia M, Hutchison MA, Balakathiresan NS, et al. Identification of serum MicroRNA signatures for diagnosis of mild traumatic brain injury in a closed head injury model. PLoS One. 2014;9:1–20.

61. Chandran R, Sharma A, Bhomia M, Balakathiresan NS, Knollmann-Ritschel BE, Maheshwari RK. Differential expression of microRNAs in the brains of mice subjected to increasing grade of mild traumatic brain injury. Brain Inj. 2017;31:106–19. doi:10.1080/02699052.2016.1213420.

62. Guingab-Cagmat JD, Cagmat EB, Hayes RL, Anagli J. Integration of proteomics, bioinformatics, and systems biology in traumatic brain injury biomarker discovery. Front Neurol. 2013;4 May:1–12.

63. Zhang P, Zhu S, Li Y, Zhao M, Liu M, Gao J, et al. Quantitative proteomics analysis to identify diffuse axonal injury biomarkers in rats using iTRAQ coupled LC–MS/MS. J Proteomics. 2016;133:93–9.

64. Calligaris D, Villard C, Lafitte D. Advances in top-down proteomics for disease biomarker discovery. J Proteomics. 2011;74:920–34. doi:10.1016/j.jprot.2011.03.030.

65. Choudhary J, Grant SGN. Proteomics in postgenomic neuroscience: the end of the beginning. Nat Neurosci. 2004;7:440.

66. Boutté AM, Yao C, Kobeissy F, May Lu XC, Zhang Z, Wang KK, et al. Proteomic analysis and brain-specific systems biology in a rodent model of penetrating ballistic-like brain injury. Electrophoresis. 2012;33:3693–704.

67. Kobeissy FH, Ottens AK, Zhang Z, Liu MC, Denslow ND, Dave JR, et al. Novel differential neuroproteomics analysis of traumatic brain injury in rats. Mol Cell Proteomics. 2006;5:1887–98.

68. Thelin EP, Just D, Frostell A, Häggmark-Månberg A, Risling M, Svensson M, et al. Protein profiling in serum after traumatic brain injury in rats reveals potential injury markers. Behav Brain Res. 2016.

69. Ahmed F, Gyorgy A, Kamnaksh A, Ling G, Tong L, Parks S, et al. Time-dependent changes of protein biomarker levels in the cerebrospinal fluid after blast traumatic brain injury. Electrophoresis. 2012;33:3705–11.

70. Kobeissy FH, Guingab-Cagmat JD, Zhang Z, Moghieb A, Glushakova OY, Mondello S, et al. Neuroproteomics and systems biology approach to identify temporal biomarker changes post experimental traumatic brain injury in rats. Front Neurol. 2016;7 NOV:1–16.

71. Halford J, Shen S, Itamura K, Levine J, Chong AC, Czerwieniec G, et al. New astroglial injury-defined biomarkers for neurotrauma assessment. J Cereb Blood Flow Metab. 2017;37:3278–99.

72. Markley JL, Brüschweiler R, Edison AS, Eghbalnia HR, Powers R, Raftery D, et al. The future of NMR-based metabolomics. Curr Opin Biotechnol. 2017;43:34–40.

73. Viant MR, Lyeth BG, Miller MG, Berman RF. An NMR metabolomic investigation of early metabolic disturbances following traumatic brain injury in a mammalian model. NMR Biomed An Int J Devoted to Dev Appl Magn Reson vivo. 2005;18:507–16.

74. Wolahan SM, Hirt D, Braas D, Glenn TC. Role of Metabolomics in Traumatic Brain Injury Research. Neurosurg Clin N Am. 2016;27:465–72.

75. Zheng F, Xia Z-A, Zeng Y-F, Luo J-K, Sun P, Cui H-J, et al. Plasma metabolomics profiles in rats with acute traumatic brain injury. PLoS One. 2017;12:e0182025. doi:10.1371/journal.pone.0182025.

76. Bahado-Singh RO, Graham SF, Turkoglu O, Beauchamp K, Bjorndahl TC, Han B, et al. Identification of candidate biomarkers of brain damage in a mouse model of closed head injury: a metabolomic pilot study. Metabolomics. 2016;12:42.

77. Bahado-Singh RO, Graham SF, Han B, Turkoglu O, Ziadeh J, Mandal R, et al. Serum metabolomic markers for traumatic brain injury: a mouse model. Metabolomics. 2016;12:100. doi:10.1007/s11306-016-1044-3.

78. Pardridge WM. The blood-brain barrier: bottleneck in brain drug development. NeuroRx. 2005;2:3–14. doi:10.1602/neurorx.2.1.3.

79. Hogan SR, Phan JH, Alvarado-Velez M, Wang MD, Bellamkonda R V., Fernandez FM, et al. Discovery of Lipidome Alterations Following Traumatic Brain Injury via High-Resolution Metabolomics. J Proteome Res. 2018.

80. Sparvero LJ, Amoscato AA, Kochanek PM, Pitt BR, Kagan VE, Bayär H. Mass-spectrometry based oxidative lipidomics and lipid imaging: Applications in traumatic brain injury. J Neurochem. 2010;115:1322–36.

81. Han X, Yang J, Yang K, Zhao Z, Abendschein DR, Gross RW. Alterations in myocardial cardiolipin content and composition occur at the very earliest stages of diabetes: a shotgun lipidomics study. Biochemistry. 2007;46:6417–28.

82. Sheth SA, Iavarone AT, Liebeskind DS, Won SJ, Swanson RA. Targeted lipid profiling discovers plasma biomarkers of acute brain injury. PLoS One. 2015;10:e0129735.

83. Abdullah L, Evans JE, Ferguson S, Mouzon B, Montague H, Reed J, et al. Lipidomic analyses identify injury-specific phospholipid changes 3 mo after traumatic brain injury. FASEB J. 2014;28:5311–21.

84. Bayir H, Tyurin VA, Tyurina YY, Viner R, Ritov V, Amoscato AA, et al. Selective early cardiolipin peroxidation after traumatic brain injury: An oxidative lipidomics analysis. Ann Neurol. 2007;62:154–69.

85. Tyurin VA, Tyurina YY, Borisenko GG, Sokolova T V, Ritov VB, Quinn PJ, et al. Oxidative stress following traumatic brain injury in rats: quantitation of biomarkers and detection of free radical intermediates. J Neurochem. 2000;75:2178–89.

86. Emmerich T, Abdullah L, Crynen G, Dretsch M, Evans J, Ait-Ghezala G, et al. Plasma Lipidomic Profiling in a Military Population of Mild Traumatic Brain Injury and Post-Traumatic Stress Disorder with Apolipoprotein E ε4–Dependent Effect. J Neurotrauma. 2016;33:1331–48.

87. Bábíčková J, Tóthová Ľ, Boor P, Celec P. In vivo phage display--a discovery tool in molecular biomedicine. Biotechnol Adv. 2013;31:1247–59. doi:10.1016/j.biotechadv.2013.04.004.

88. Tan Y, Tian T, Liu W, Zhu Z, Yang CJ. Advance in phage display technology for bioanalysis. Biotechnol J. 2015;:1–14.

89. Smith GP. Filamentous fusion phage: novel expression vectors that display cloned antigens on the virion surface. Science (80-). 1985;228:1315–7.

90. Schirrmann T, Meyer T, Schütte M, Frenzel A, Hust M. Phage display for the generation of antibodies for proteome research, diagnostics and therapy. Molecules. 2011;16:412–26.

91. Hoogenboom HR, de Bruïne AP, Hufton SE, Hoet RM, Arends J-W, Roovers RC. Antibody phage display technology and its applications. Immunotechnology. 1998;4:1–20. doi:10.1016/S1380-2933(98)00007-4.

92. Marsh W, Witten A, Stabenfeldt SE. Exploiting Phage Display for Development of Novel Cellular Targeting Strategies. In: Targeted Drug Delivery. Springer; 2018. p. 71–94.

93. Ma C, Yin G, Yan D, He X, Zhang L, Wei Y, et al. A novel peptide specifically targeting ovarian cancer identified by in vivo phage display. J Pept Sci. 2013;19:730–6.

94. Cooksley-Decasper S, Reiser H, Thommen DS, Biedermann B, Neidhart M, Gawinecka J, et al. Antibody phage display assisted identification of junction plakoglobin as a potential biomarker for atherosclerosis. PLoS One. 2012;7:e47985.

95. Ghoshal S, Bondada V, Saatman KE, Guttmann RP, Geddes JW. Phage display for identification of serum biomarkers of traumatic brain injury. J Neurosci Methods. 2016;:4–8. doi:10.1016/j.jneumeth.2016.04.026.

96. Pasqualini R, Ruoslahti E. Organ targeting in vivo using phage display peptide libraries. Nature. 1996;380:364–6.

97. Fan X, Venegas R, Fey R, Heyde H, Bernard M a., Lazarides E, et al. An In Vivo Approach to Structure Activity Relationship Analysis of Peptide Ligands. Pharm Res. 2007;24:868–79.

98. Muruganandam A, Tanha J, Narang S, Stanimirovic D. Selection of phage-displayed llama single-domain antibodies that transmigrate across human blood-brain barrier endothelium. FASEB J. 2002;16:240–2.

99. Jones AR, Stutz CC, Zhou Y, Marks JD, Shusta E V. Identifying blood-brain-barrier selective single-chain antibody fragments. Biotechnol J. 2014;9:664–74.

100. Toy R, Peiris PM, Ghaghada KB, Karathanasis E. Shaping cancer nanomedicine: The effect of particle shape on the in vivo journey of nanoparticles. Nanomedicine. 2014;9:121–34.

101. Bakhshinejad B, Karimi M, Khalaj-Kondori M. Phage display: development of nanocarriers for targeted drug delivery to the brain. Neural Regen Res. 2015;10:862–5. doi:10.4103/1673-5374.158330.

102. Mann AP, Scodeller P, Hussain S, Joo J, Kwon E, Braun GB, et al. A peptide for targeted, systemic delivery of imaging and therapeutic compounds into acute brain injuries. Nat Commun. 2016;7:1–11.

103. Wang J, Wang J, Li N, Ma J, Gu Z, Yu L, et al. Effects of an amyloid-beta 1-42 oligomers antibody screened from a phage display library in APP/PS1 transgenic mice. Brain Res. 2016;1635:169–79. doi:10.1016/j.brainres.2016.01.028.

104. Tian H, Davidowitz E, Lopez P, He P, Schulz P, Moe J, et al. Isolation and characterization of antibody fragments selective for toxic oligomeric tau. Neurobiol Aging. 2015;36:1342–55. doi:10.1016/j.neurobiolaging.2014.12.002.

105. Hong H-Y, Choi JS, Kim YJ, Lee HY, Kwak W, Yoo J, et al. Detection of apoptosis in a rat model of focal cerebral ischemia using a homing peptide selected from in vivo phage display. J Control Release. 2008;131:167–72. doi:10.1016/j.jconrel.2008.07.020.

106. Liu GW, Livesay BR, Kacherovsky NA, Cieslewicz M, Lutz E, Waalkes A, et al. Efficient Identification of Murine M2 Macrophage Peptide Targeting Ligands by Phage Display and Next-Generation Sequencing. Bioconjug Chem. 2015;26:1811–7.

107. Turner KB, Naciri J, Liu JL, Anderson GP, Goldman ER, Zabetakis D. Next-Generation Sequencing of a Single Domain Antibody Repertoire Reveals Quality of Phage Display Selected Candidates. PLoS One. 2016;11:e0149393. doi:10.1371/journal.pone.0149393.

108. Ravn U, Didelot G, Venet S, Ng KT, Gueneau F, Rousseau F, et al. Deep sequencing of phage display libraries to support antibody discovery. Methods. 2013;60:99–110. doi:10.1016/j.ymeth.2013.03.001.

109. Alam KK, Chang JL, Burke DH. FASTAptamer: A Bioinformatic Toolkit for High-throughput Sequence Analysis of Combinatorial Selections. Mol Ther Acids. 2015;4 August 2014:e230. doi:10.1038/mtna.2015.4.

110. D'Angelo S, Glanville J, Ferrara F, Naranjo L, Gleasner CD, Shen X, et al. The antibody mining toolbox. MAbs. 2013;6:160–72. doi:10.4161/mabs.27105.

111. Esposito D, Chatterjee DK. Enhancement of soluble protein expression through the use of fusion tags. Curr Opin Biotechnol. 2006;17:353–8.

112. Papaneophytou CP, Kontopidis G. Statistical approaches to maximize recombinant protein expression in Escherichia coli: A general review. Protein Expr Purif. 2014;94:22–32. doi:10.1016/j.pep.2013.10.016.

113. Lee B, Newberg A. Neuroimaging in traumatic brain imaging. NeuroRx. 2005;2:372–83.

114. Laalo JP, Kurki TJ, Sonninen PH, Tenovuo OS. Reliability of diagnosis of traumatic brain injury by computed tomography in the acute phase. J Neurotrauma. 2009;26:2169–78.

115. Kraus MF, Susmaras T, Caughlin BP, Walker CJ, Sweeney JA, Little DM. White matter integrity and cognition in chronic traumatic brain injury: A diffusion tensor imaging study. Brain. 2007;130:2508–19.

116. Scheid R, Walther K, Guthke T, Preul C, von Cramon DY. Cognitive sequelae of diffuse axonal injury. Arch Neurol. 2006;63:418–24.

117. Mac Donald CL, Dikranian K, Song SK, Bayly P V., Holtzman DM, Brody DL. Detection of traumatic axonal injury with diffusion tensor imaging in a mouse model of traumatic brain injury. Exp Neurol. 2007;205:116–31.

118. Kikinis Z, Muehlmann M, Pasternak O, Peled S, Kulkarni P, Ferris C, et al. Diffusion imaging of mild traumatic brain injury in the impact accelerated rodent model: A pilot study. Brain Inj. 2017;31:1376–81. doi:10.1080/02699052.2017.1318450.

119. Li J, Li X-Y, Feng D-F, Gu L. Quantitative evaluation of microscopic injury with diffusion tensor imaging in a rat model of diffuse axonal injury. Eur J Neurosci. 2011;33:933–45. doi:10.1111/j.1460-9568.2010.07573.x.

120. Bennett RE, Mac Donald CL, Brody DL. Diffusion tensor imaging detects axonal injury in a mouse model of repetitive closed-skull traumatic brain injury. Neurosci Lett. 2012;513:160–5. doi:10.1016/j.neulet.2012.02.024.

121. Rangaprakash D, Deshpande G, Daniel TA, Goodman AM, Robinson JL, Salibi N, et al. Compromised hippocampus-striatum pathway as a potential imaging biomarker of mild-traumatic brain injury and posttraumatic stress disorder. Hum Brain Mapp. 2017;38:2843–64.

122. Kotapka MJ, Graham DI, Adams JH, Gennarelli TA. Hippocampal pathology in fatal non-missile human head injury. Acta Neuropathol. 1992;83:530–4.

123. Girgis F, Pace J, Sweet J, Miller JP. Hippocampal Neurophysiologic Changes after Mild Traumatic Brain Injury and Potential Neuromodulation Treatment Approaches. Front Syst Neurosci. 2016;10 February:1–10. doi:10.3389/fnsys.2016.00008.

124. Wallace EJ, Mathias JL, Ward L. The relationship between diffusion tensor imaging findings and cognitive outcomes following adult traumatic brain injury: A meta-analysis. Neurosci Biobehav Rev. 2018;92 August 2017:93–103.

125. Oehr L, Anderson J. Diffusion-Tensor Imaging Findings and Cognitive Function Following Hospitalized Mixed-Mechanism Mild Traumatic Brain Injury: A Systematic Review and Meta-Analysis. Arch Phys Med Rehabil. 2017;98:2308–19. doi:10.1016/j.apmr.2017.03.019.

126. Ryan NP, Genc S, Beauchamp MH, Yeates KO, Hearps S, Catroppa C, et al. White matter microstructure predicts longitudinal social cognitive outcomes after paediatric traumatic brain injury: a diffusion tensor imaging study. Psychol Med. 2017;:1–13.

127. Budde MD, Shah A, McCrea M, Cullinan WE, Pintar FA, Stemper BD. Primary Blast Traumatic Brain Injury in the Rat: Relating Diffusion Tensor Imaging and Behavior. Front Neurol. 2013;4 October:1–12. doi:10.3389/fneur.2013.00154.

128. Bazeed MF, El-Fatah Ghanem MA, Afif HFS, Sunbulli MHA, Abdelaal AME. Can diffusion tensor imaging predict motor power affection after moderate traumatic brain injury? Egypt J Radiol Nucl Med. 2013;44:879–83. doi:10.1016/j.ejrnm.2013.09.006.

129. Lee H Do, Jang SH. Injury of the corticoreticular pathway in patients with mild traumatic brain injury: A diffusion tensor tractography study. Brain Inj. 2015;29:1219–22.

130. Sener S, Van Hecke W, Feyen BFE, Van Der Steen G, Pullens P, Van De Hauwe L, et al. Diffusion Tensor Imaging: A Possible Biomarker in Severe Traumatic Brain Injury and Aneurysmal Subarachnoid Hemorrhage? Neurosurgery. 2016;79:786–93.

131. Davalos DB, Bennett TL. A review of the use of single-photon emission computerized tomography as a diagnostic tool in mild traumatic brain injury. Appl Neuropsychol. 2002;9:92–105.

132. Benamer HTS, Patterson J, Grosset DG, Booij J, De Bruin K, Van Royen E, et al. Accurate differentiation of Parkinsonism and essential tremor using visual assessment of [123I]-FP-CIT SPECT imaging: The [123I]-FP-CIT study group. Mov Disord Off J Mov Disord Soc. 2000;15:503–10.

133. Marshall VL, Reininger CB, Marquardt M, Patterson J, Hadley DM, Oertel WH, et al. Parkinson's disease is overdiagnosed clinically at baseline in diagnostically uncertain cases: a 3-year European multicenter study with repeat [123I] FP-CIT SPECT. Mov Disord. 2009;24:500–8.

134. Kinuya K, Kakuda K, Nobata K, Sakai S, Yamamoto K, Itoh S, et al. Role of brain perfusion single-photon emission tomography in traumatic head injury. Nucl Med Commun. 2004;25:333–7.

135. Raji CA, Tarzwell R, Pavel D, Schneider H, Uszler M, Thornton J, et al. Clinical utility of SPECT neuroimaging in the diagnosis and treatment of traumatic brain injury: A systematic review. PLoS One. 2014;9.

136. Newberg AB, Serruya M, Gepty A, Intenzo C, Lewis T, Amen D, et al. Clinical comparison of99mTc exametazime and123I ioflupane SPECT in patients with chronic mild traumatic brain injury. PLoS One. 2014;9.

137. Cruz JA, Wishart DS. Applications of machine learning in cancer prediction and prognosis. Cancer Inform. 2006;2:117693510600200030.

138. Sun D, van Erp TGM, Thompson PM, Bearden CE, Daley M, Kushan L, et al. Elucidating a magnetic resonance imaging-based neuroanatomic biomarker for psychosis: classification analysis using probabilistic brain atlas and machine learning algorithms. Biol Psychiatry. 2009;66:1055–60.

139. Moradi E, Pepe A, Gaser C, Huttunen H, Tohka J, Initiative ADN. Machine learning framework for early MRI-based Alzheimer's conversion prediction in MCI subjects. Neuroimage. 2015;104:398–412.

140. Rizk-Jackson A, Stoffers D, Sheldon S, Kuperman J, Dale A, Goldstein J, et al. Evaluating imaging biomarkers for neurodegeneration in pre-symptomatic Huntington's disease using machine learning techniques. Neuroimage. 2011;56:788–96.

141. Mitra J, Shen K kai, Ghose S, Bourgeat P, Fripp J, Salvado O, et al. Statistical machine learning to identify traumatic brain injury (TBI) from structural disconnections of white matter networks. Neuroimage. 2016;129:247–59. doi:10.1016/j.neuroimage.2016.01.056.

142. Vergara VM, Mayer AR, Kiehl KA, Calhoun VD. Dynamic functional network connectivity discriminates mild traumatic brain injury through machine learning. NeuroImage Clin. 2018;19 March:30–7. doi:10.1016/j.nicl.2018.03.017.

143. Hellyer PJ, Leech R, Ham TE, Bonnelle V, Sharp DJ. Individual prediction of white matter injury following traumatic brain injury. Ann Neurol. 2013;73:489–99.

144. Chen R, Herskovits EH. Graphical-model-based multivariate analysis of functional magnetic-resonance data. Neuroimage. 2007;35:635–47.

145. Liu Y, Wang T, Chen X, Zhang J, Zhou G, Wang Z, et al. Tract-based Bayesian multivariate analysis of mild traumatic brain injury. Comput Math Methods Med. 2014;2014.

146. Wang Z, Wu W, Liu Y, Wang T, Chen X, Zhang J, et al. Altered cerebellar white matter integrity in patients with mild traumatic brain injury in the acute stage. PLoS One. 2016;11:e0151489.

147. Shi J, Wang Y, Chen T, Xu D, Zhao H, Chen L, et al. Automatic evaluation of traumatic brain injury based on terahertz imaging with machine learning. Opt Express. 2018;26:6371–81.

148. Nielson JL, Cooper SR, Yue JK, Sorani MD, Inoue T, Yuh EL, et al. Uncovering precision phenotype-biomarker associations in traumatic brain injury using topological data analysis. PLoS One. 2017;12:1–19.

149. Nielson JL, Paquette J, Liu AW, Guandique CF, Tovar CA, Inoue T, et al. Topological data analysis for discovery in preclinical spinal cord injury and traumatic brain injury. Nat Commun. 2015;6:8581.

150. Peacock WF, Van Meter TE, Mirshahi N, Ferber K, Gerwien R, Rao V, et al. Derivation of a three biomarker panel to improve diagnosis in patients with mild traumatic brain injury. Front Neurol. 2017;8 NOV:1–12.

151. Cai Y, Wu S, Zhao W, Li Z, Wu Z, Ji S. Concussion classification via deep learning using whole-brain white matter fiber strains. PLoS One. 2018;13:e0197992.

152. Dimitriadis SI, Zouridakis G, Rezaie R, Babajani-Feremi A, Papanicolaou AC. Functional connectivity changes detected with magnetoencephalography after mild traumatic brain injury. NeuroImage Clin. 2015;9:519–31.

153. Chong S-L, Liu N, Barbier S, Ong MEH. Predictive modeling in pediatric traumatic brain injury using machine learning. BMC Med Res Methodol. 2015;15:22.

154. Karamzadeh N, Amyot F, Kenney K, Anderson A, Chowdhry F, Dashtestani H, et al. A machine learning approach to identify functional biomarkers in human prefrontal cortex for individuals with traumatic brain injury using functional near-infrared spectroscopy. Brain Behav. 2016;6:1–14.

155. Strimbu K, Tavel J. What are Biomarkers? Curr Opin HIV AIDS. 2010;5:463–6.
156. Pienaar IS, Daniels WMU, Götz J. Neuroproteomics as a promising tool in Parkinson's disease research. J Neural Transm. 2008;115:1413–30.

157. Lassen PS, Thygesen C, Larsen MR, Kempf SJ. Understanding Alzheimer's disease by global quantification of protein phosphorylation and sialylated N-linked glycosylation profiles: A chance for new biomarkers in neuroproteomics? J Proteomics. 2017;161:11–25.

158. Alawieh A, Zaraket FA, Li J-L, Mondello S, Nokkari A, Razafsha M, et al. Systems Biology, Bioinformatics, and Biomarkers in Neuropsychiatry. Front Neurosci. 2012;6 December:187. doi:10.3389/fnins.2012.00187.

159. Jiang Y, Zhao H, Lin Y, Zhu N, Ma Y, Mao L. Colorimetric detection of glucose in rat brain using gold nanoparticles. Angew Chemie Int Ed. 2010;49:4800–4.

160. Santos RM, Rodrigues MS, Laranjinha J, Barbosa RM. Biomimetic sensor based on hemin/carbon nanotubes/chitosan modified microelectrode for nitric oxide measurement in the brain. Biosens Bioelectron. 2013;44:152–9.

161. Maysinger D, Ji J, Hutter E, Cooper E. Nanoparticle-based and bioengineered probes and sensors to detect physiological and pathological biomarkers in neural cells. Front Neurosci. 2015;9:480.

162. Holt LJ, Herring C, Jespers LS, Woolven BP, Tomlinson IM. Domain antibodies: Proteins for therapy. Trends Biotechnol. 2003;21:484–90.

163. Bélanger K, Iqbal U, Tanha J, MacKenzie R, Moreno M, Stanimirovic D. Single-Domain Antibodies as Therapeutic and Imaging Agents for the Treatment of CNS Diseases. Antibodies. 2019;8:27.

164. Barrios Y, Jirholt P, Ohlin M. Length of the antibody heavy chain complementarity determining region 3 as a specificity-determining factor. J Mol Recognit. 2004;17:332–8.

165. Xu JL, Davis MM. Diversity in the CDR3 Region of V H Is Sufficient for Most Antibody Specificities. Immunity. 2000;13:37–45.

166. Bates A, Power CA. David vs. Goliath: The Structure, Function, and Clinical Prospects of Antibody Fragments. Antibodies. 2019;8:28.

167. Lee CMY, Iorno N, Sierro F, Christ D. Selection of human antibody fragments by phage display. Nat Protoc. 2007;2:3001–8.

168. Muruganandam A, Tanha J, Narang S, Stanimirovic D. Selection of phage-displayed llama single-domain antibodies that transmigrate across human blood-brain barrier endothelium. FASEB J. 2002;16:1805–7.

169. Habicht G, Haupt C, Friedrich RP, Hortschansky P, Sachse C, Meinhardt J, et al. Directed selection of a conformational antibody domain that prevents mature amyloid fibril formation by stabilizing Aβ protofibrils. Proc Natl Acad Sci. 2007;104:19232–7.

170. Matochko WL, Cory Li S, Tang SKY, Derda R. Prospective identification of parasitic sequences in phage display screens. Nucleic Acids Res. 2014;42:1784–98.

171. Liu GW, Livesay BR, Kacherovsky NA, Cieslewicz M, Lutz E, Waalkes A, et al. Efficient Identification of Murine M2 Macrophage Peptide Targeting Ligands by Phage Display and Next-Generation Sequencing. Bioconjug Chem. 2015;26:1811–7. doi:10.1021/acs.bioconjchem.5b00344.

172. Vodnik M, Zager U, Strukelj B, Lunder M. Phage display: Selecting straws instead of a needle from a haystack. Molecules. 2011;16:790–817.

173. Gentleman RC, Carey VJ, Bates DM, Bolstad B, Dettling M, Dudoit S, et al. Bioconductor: open software development for computational biology and bioinformatics. Genome Biol. 2004;5.

174. Davis MM, Bjorkman PJ. T-cell antigen receptor genes and T-cell recognition. Nature. 1988;334:395–402.

175. Afgan E, Baker D, Batut B, Van Den Beek M, Bouvier D, Čech M, et al. The Galaxy platform for accessible, reproducible and collaborative biomedical analyses: 2018 update. Nucleic Acids Res. 2018;46:W537–44.

176. Yardeni T, Eckhaus M, Morris HD, Huizing M, Hoogstraten-Miller S. Retro-orbital injections in mice. Lab Anim (NY). 2011;40:155–60. doi:10.1038/laban0511-155.

177. Magoč T, Salzberg SL. FLASH: Fast length adjustment of short reads to improve genome assemblies. Bioinformatics. 2011;27:2957–63.

178. Lykkemark S, Mandrup OA, Friis NA, Kristensen P. Degradation of C-terminal tag sequences on domain antibodies purified from E. coli supernatant. MAbs. 2014;6:1551–9.

179. Zimmermann I, Egloff P, Hutter CAJ, Arnold FM, Stohler P, Bocquet N, et al. Synthetic single domain antibodies for the conformational trapping of membrane proteins. Elife. 2018;7:1–32.

180. Chung J, Rader C, Popkov M, Hur YM, Kim HK, Lee YJ, et al. Integrin alphaIIbbeta3-specific synthetic human monoclonal antibodies and HCDR3 peptides that potently inhibit platelet aggregation. FASEB J. 2004;18:361–3.

181. Deng YJ, Notkins AL. Molecular determinants of polyreactive antibody binding: HCDR3 and cyclic peptides. Clin Exp Immunol. 2000;119:69–76.

182. Hammers CM, Stanley JR. Antibody Phage Display: Technique and Applications. J Invest Dermatol. 2014;134:e17. doi:10.1038/jid.2013.521.

183. Guingab-Cagmat JD, Newsom K, Vakulenko A, Cagmat EB, Kobeissy FH, Zoltewicz S, et al. In vitro MS-based proteomic analysis and absolute quantification of neuronal-glial injury biomarkers in cell culture system. Electrophoresis. 2012;33:3786–97.

184. Ren C, Guingab-Cagmat J, Kobeissy F, Zoltewicz S, Mondello S, Gao M, et al. A neuroproteomic and systems biology analysis of rat brain post intracerebral hemorrhagic stroke. Brain Res Bull. 2014;102:46–56.

185. Mann AP, Scodeller P, Hussain S, Joo J, Kwon E, Gary B. A peptide for targeted , systemic delivery of imaging and therapeutic compounds into acute brain injuries. 2016; May.

186. Frenkel D, Solomon B. Filamentous phage as vector-mediated antibody delivery to the brain. Proc Natl Acad Sci. 2002;99:5675–9. doi:10.1073/pnas.072027199.

187. Conley GP, Viswanathan M, Hou Y, Rank DL, Lindberg AP, Cramer SM, et al. Evaluation of protein engineering and process optimization approaches to enhance antibody drug manufacturability. Biotechnol Bioeng. 2011;108:2634–44.

188. Chothia C, Lesk AM, Tramontano A, Levitt M, Smith-Gill SJ, Air G, et al. Conformations of immunoglobulin hypervariable regions. Nature. 1989;342:877–83. doi:10.1038/342877a0.

189. O. B, F. B, S. D. Hyperphage. Improving antibody presentation in phage display. Methods Mol Biol. 2003;205:295-302.

190. Mi H, Muruganujan A, Ebert D, Huang X, Thomas PD. PANTHER version 14: more genomes, a new PANTHER GO-slim and improvements in enrichment analysis tools. Nucleic Acids Res. 2018;47:D419–26.

191. Başkaya MK, Rao AM, Doğan A, Donaldson D, Dempsey RJ. The biphasic opening of the blood–brain barrier in the cortex and hippocampus after traumatic brain injury in rats. Neurosci Lett. 1997;226:33–6.

192. 'T Hoen PAC, Jirka SMG, Ten Broeke BR, Schultes EA, Aguilera B, Pang KH, et al. Phage display screening without repetitious selection rounds. Anal Biochem. 2012;421:622–31. doi:10.1016/j.ab.2011.11.005.

193. Takahashi M, Ueno A, Mihara H. Peptide design based on an antibody complementarity-determining region (CDR): Construction of porphyrin-binding peptides and their affinity maturation by a combinatorial method. Chem - A Eur J. 2000;6:3196–203.

194. Mishkovsky M, Comment A, Gruetter R. In vivo detection of brain Krebs cycle intermediate by hyperpolarized magnetic resonance. J Cereb Blood Flow Metab. 2012;32:2108–13.

195. Shijo K, Sutton RL, Ghavim SS, Harris NG, Bartnik-Olson BL. Metabolic fate of glucose in rats with traumatic brain injury and pyruvate or glucose treatments: a NMR spectroscopy study. Neurochem Int. 2017;102:66–78.

196. Elpeleg O, Miller C, Hershkovitz E, Bitner-Glindzicz M, Bondi-Rubinstein G, Rahman S, et al. Deficiency of the ADP-forming succinyl-CoA synthase activity is associated with encephalomyopathy and mitochondrial DNA depletion. Am J Hum Genet. 2005;76:1081–6.

197. Pinto M, Moraes CT. Mitochondrial genome changes and neurodegenerative diseases. Biochim Biophys Acta (BBA)-Molecular Basis Dis. 2014;1842:1198–207.

198. Araujo B, Torres L, Stein M, Cabral FR, Herai R, Okamoto O, et al. Decreased expression of proteins involved in energy metabolism in the hippocampal granular layer of rats submitted to the pilocarpine epilepsy model. Neurosci Lett. 2014;561:46–51.

199. Kilbaugh TJ, Karlsson M, Byro M, Bebee A, Ralston J, Sullivan S, et al. Mitochondrial bioenergetic alterations after focal traumatic brain injury in the immature brain. Exp Neurol. 2015;271:136–44.

200. Di Pietro V, Lazzarino G, Amorini AM, Signoretti S, Hill LJ, Porto E, et al. Fusion or fission: the destiny of mitochondria in traumatic brain injury of different severities. Sci Rep. 2017;7:9189.

201. Hoozemans JJM, Veerhuis R, Van Haastert ES, Rozemuller JM, Baas F, Eikelenboom P, et al. The unfolded protein response is activated in Alzheimer's disease. Acta Neuropathol. 2005;110:165–72.

202. Lee AS. The ER chaperone and signaling regulator GRP78/BiP as a monitor of endoplasmic reticulum stress. Methods. 2005;35:373–81.

203. Park K-W, Kim GE, Morales R, Moda F, Moreno-Gonzalez I, Concha-Marambio L, et al. The endoplasmic reticulum chaperone GRP78/BiP modulates prion propagation in vitro and in vivo. Sci Rep. 2017;7:44723.

204. Kudo T, Kanemoto S, Hara H, Morimoto N, Morihara T, Kimura R, et al. A molecular chaperone inducer protects neurons from ER stress. Cell Death Differ. 2008;15:364–75.

205. Oida Y, Izuta H, Oyagi A, Shimazawa M, Kudo T, Imaizumi K, et al. Induction of BiP, an ER-resident protein, prevents the neuronal death induced by transient forebrain ischemia in gerbil. Brain Res. 2008;1208:217–24.

206. Taylor IR, Ahmad A, Wu T, Nordhues BA, Bhullar A, Gestwicki JE, et al. The disorderly conduct of Hsc70 and its interaction with the Alzheimer's-related Tau protein. J Biol Chem. 2018;293:10796–809.

207. Giffard RG, Xu L, Zhao H, Carrico W, Ouyang Y, Qiao Y, et al. Chaperones, protein aggregation, and brain protection from hypoxic/ischemic injury. J Exp Biol. 2004;207:3213–20.

208. Becker RE, Kapogiannis D, Greig NH. Does traumatic brain injury hold the key to the Alzheimer's disease puzzle? Alzheimer's Dement. 2018;14:431–43.

209. Ramos-Cejudo J, Wisniewski T, Marmar C, Zetterberg H, Blennow K, de Leon MJ, et al. Traumatic Brain Injury and Alzheimer's Disease: The Cerebrovascular Link. EBioMedicine. 2018;28:21–30. doi:10.1016/j.ebiom.2018.01.021.

210. Martinez BI, Stabenfeldt SE. Current trends in biomarker discovery and analysis tools for traumatic brain injury. J Biol Eng. 2019;13.

211. Bekker G, Ma B, Kamiya N. Thermal stability of single-domain antibodies estimated by molecular dynamics simulations. Protein Sci. 2019;28:429–38.

212. Turner KB, Zabetakis D, Legler P, Goldman ER, Anderson GP. Isolation and epitope mapping of staphylococcal enterotoxin B single-domain antibodies. Sensors (Switzerland). 2014;14:10846–63.

213. Kilbaugh TJ, Karlsson M, Byro M, Bebee A, Ralston J, Sullivan S, et al. Mitochondrial bioenergetic alterations after focal traumatic brain injury in the immature brain. Exp Neurol. 2015;271:136–44.

214. Lazzarino G, Amorini AM, Signoretti S, Musumeci G, Lazzarino G, Caruso G, et al. Pyruvate dehydrogenase and tricarboxylic acid cycle enzymes are sensitive targets of traumatic brain injury induced metabolic derangement. Int J Mol Sci. 2019;20.

215. Kim JY, Han Y, Lee JE, Yenari MA. The 70-kDa heat shock protein (Hsp70) as a therapeutic target for stroke. Expert Opin Ther Targets. 2018;22:191–9.

216. Kacso G, Ravasz D, Doczi J, Németh B, Madgar O, Saada A, et al. Two transgenic mouse models for β-subunit components of succinate-CoA ligase yielding pleiotropic metabolic alterations. Biochem J. 2016;473:3463–85.

217. Paunovska K, Sago CD, Monaco CM, Hudson WH, Castro MG, Rudoltz TG, et al. A Direct Comparison of in Vitro and in Vivo Nucleic Acid Delivery Mediated by Hundreds of Nanoparticles Reveals a Weak Correlation. Nano Lett. 2018;18:2148–57.

218. Dahlman JE, Kauffman KJ, Xing Y, Shaw TE, Mir FF, Dlott CC, et al. Barcoded nanoparticles for high throughput in vivo discovery of targeted therapeutics. Proc Natl Acad Sci U S A. 2017;:201620874. doi:10.1073/pnas.1620874114.

219. Peterson TC, Maass WR, Anderson JR, Anderson GD, Hoane MR. A behavioral and histological comparison of fluid percussion injury and controlled cortical impact injury to the rat sensorimotor cortex. Behav Brain Res. 2015;294:254–63. doi:10.1016/j.bbr.2015.08.007.

220. Clausen F, Hillered L. Intracranial pressure changes during fluid percussion, controlled cortical impact and weight drop injury in rats. Acta Neurochir (Wien). 2005;147:775–80.

APPENDIX A

ANIMAL SUBECTS

Research involving the use of animals conducted under the auspices of Arizona State University is reviewed by the University Institutional Animal Care & Use Committee (IACUC, approval #17-1590R), Institutional Biosafety Committee (IBC, approval #15-570), and in compliance with federal regulations.

APPENDIX B

DOMAIN ANTIBODY FRAGMENT BIOREACTIVITY

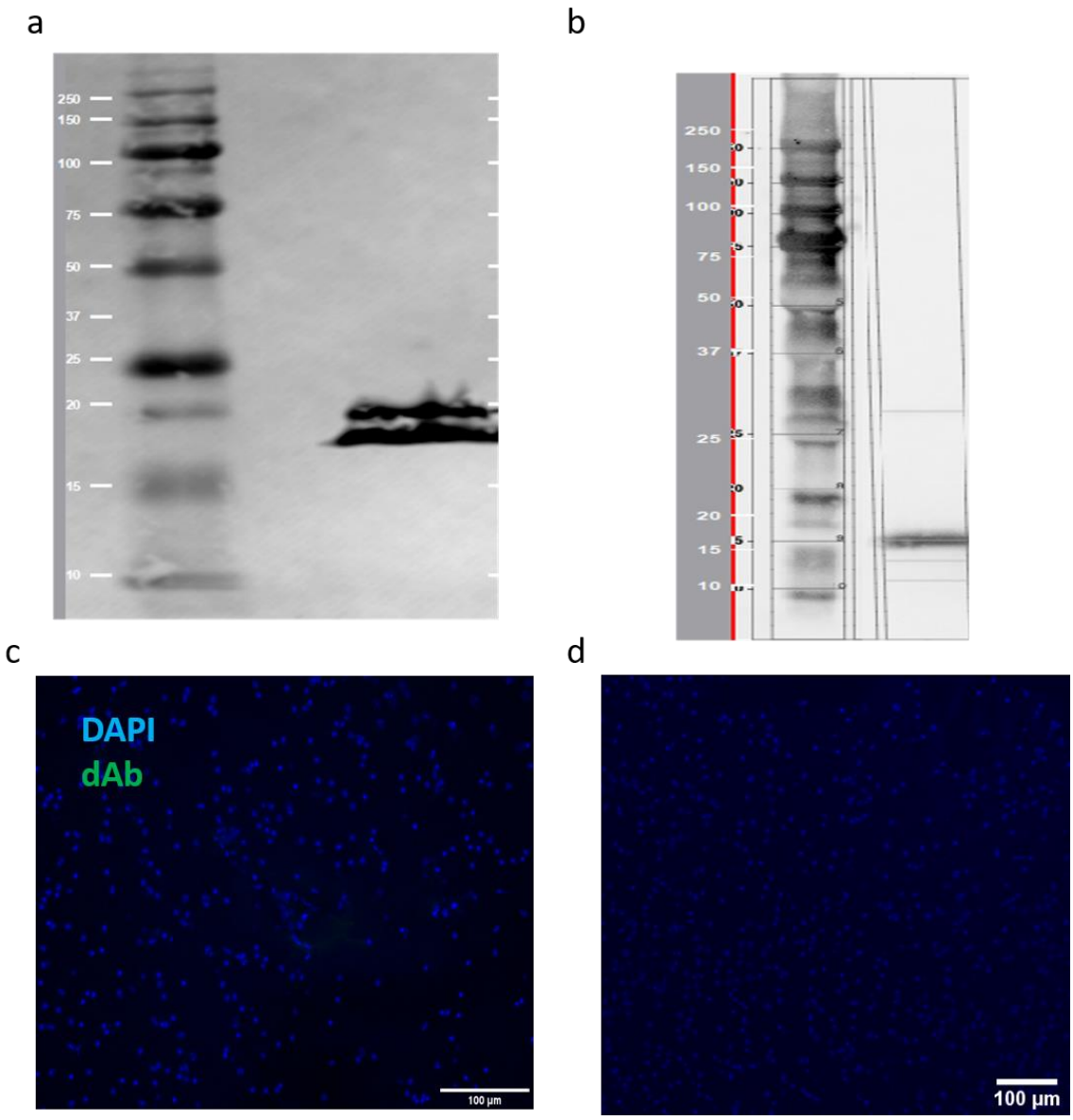

Appendix B Figure 1: Produced dAbs have no detectable reactivity to injured tissue. Visualization of purified a) dAb-A1 and b) dAb-A2 recombinant proteins via Western Blot after DoE optimization (rabbit anti-His-Biotin, abcam #ab27025). c) Representative image of c) dAb-A1 and d) dAb-A2 binding to 1dpi tissue with no detectable signal. (rabbit anti-His-Biotin, abcam #ab27025; streptavidin Alexa Fluor 555, ThermoFisher #S21381).

Appendix B Table 1: Design of experiments (DoE) factors and levels. Media levels were determined by concentration of tryptone and yeast extract.

Factor	Inferior level (-1)	Central level (0)	Superior level (+)
IPTG (mM)	0.1	0.2	1.0
Temperature (°C)	25	30	37
Media	LB	2xTY	Terrific Broth
Time post-induction	3h	6h	16 hours

Appendix Table 2: dAb-A1 DoE ANOVA. Optimal production conditions are LB media, 0.5 mM IPTG, 1 hour incubation and 25°C.

Source	Adj SS	Adj MS	F-Value	P-Value
IPTG	0.0015	0.0015	1.25	0.345
Temp	0.0386	0.0386	31.98	0.011
Media	0.3570	0.3570	295.46	0.000
Time	0.0001	0.0001	0.12	0.756
2-Way Interactions	0.0680	0.0226	18.77	0.019
IPTG*Temp	0.0033	0.0033	2.78	0.194
IPTG*Media	0.0006	0.0006	0.51	0.528
IPTG*Time	0.0640	0.0640	53.03	0.005

Appendix B Table 3: dAb-A2 DoE ANOVA Analysis of Variance. Optimal production conditions are Terrific Broth, 0.1 mM IPTG, 3 hour incubation, and 25°C.

Source	Adj SS	Adj MS	F-Value	P-Value
IPTG	0.0109	0.0109	11.76	0.042
Temp	0.0154	0.0154	16.62	0.027
Media	0.0792	0.0792	85.01	0.003
Time	0.0994	0.0994	106.75	0.002
2-way Interactions	0.1145	0.3819	40.99	0.006
IPTG*Temp	0.0512	0.0512	54.96	0.005
IPTG*Media	0.0165	0.0165	17.78	0.024
IPTG*Time	0.0468	0.0468	50.25	0.006

APPENDIX C

CHRONIC INJURY-TARGETING HCDR3 CONSTRUCTS

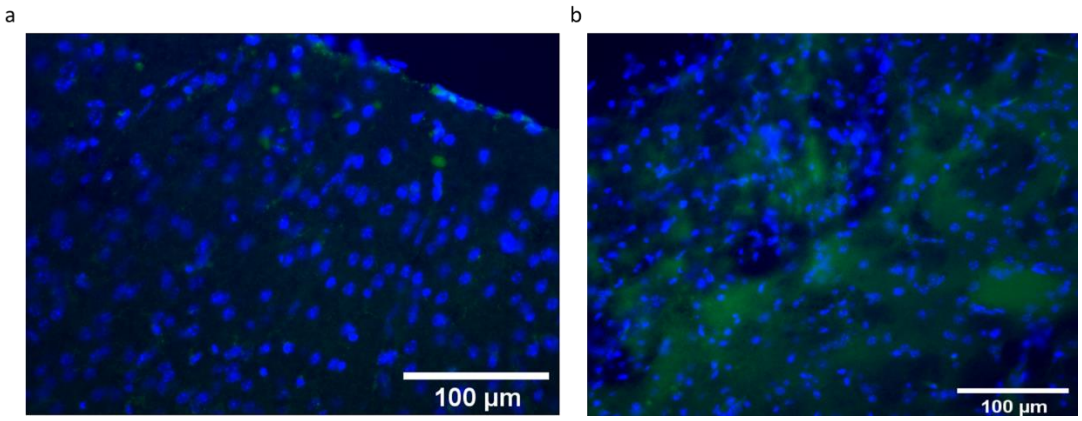

Appendix C Figure 1: Chronic injury targeting HCDR3 constructs. a) CH1 showed negligible bioreactivity to 21 dpi tissue sections. b) CH2 showed non-specific staining consistent with secondary-only control background. Both images representative of 5 µM construct concentration with Triton-X permeabilization.

Appendix C Table 1: Selected HCDR3s. Selection of sequences and HCDR3-constructs design was as described in Chapter 3.

	Sequence
CH1	RLVRESSQEHTLSS
CH2	TDCQETPYELKS

APPENDIX D

INDIRECT IMMUNOPRECIPITATION

Protocol

This protocol describes an immunoprecipitation procedure for immobilizing biotinylated HCDR3- constructs to streptavidin-coated magnetic beads and incubating with tissue lysate. The resulting elution can then be analyzed by SDS-PAGE or submitted for liquid chromatography-mass spectrometry analysis (LC-MS).

Materials:

- Streptavidin Dynabeads Myone C1 (Thermo Fisher Scientific #65-001).
- Biotinylated HCDR3 constructs
- 1X PBST
- 1X PBS
- Lysis Buffer
- Tissue lysates (1 mg/mL)
- Magnetic stand (recommend DynaMag-2, Thermo Fisher Scientific # 12321D)
- 1.5 mL microcentrifuge tubes

Pre-clearing lysates

1. Resuspend beads by vortexing in container
2. Add 25 µl of beads to each sample tube
3. Wash once with 1 mL 1x PBST. Place tube on stand for 1 minute to separate beads from solution.
4. Discard supernatant, and wash beads with bead volume 1x PBST twice for 1 minute each.

5. Add tissue lysate to tubes, incubate at room temperature for 1 hour rotating
6. Place tubes on magnetic rack to separate beads from lysate solution

Forming immune complex

7. Mix pre-cleared lysate (supernatant from previous step) with 150 µl HCDR3 construct solution (75 pmol).
    a. Note: Binding capacity for the streptavidin-coupled beads is 600 pmol and it is intuitive to maximize the concentration of the biotinylated peptide-solution to match the capacity. However, excess biotinylated peptide binds more easily to the streptavidin coupled beads than biotinylated constructs that are bound to an antigen from the tissue lysate. It is recommended to start with a low concentration of solution (75 pmol) and adjust as needed , determined by SDS-PAGE results.
8. Incubate samples at 4°C overnight, rotating.

Immobilization of HCDR3 construct-antigen complex

9. Add 50 µl beads to clean 1.5 mL tubes, wash as described previously
10. Retrieve overnight samples from 4°C, add lysates to washed beads
11. Incubate at room temperature rotating for 1 hour

Wash and Elution

12. Place samples on stand for 1 minute, remove supernatant
13. Wash three times with 100 µl lysis buffer
14. Elution for mass spectrometry analysis:
    a. Elute with 0.2% RapiGest

15. Elution for SDS-PAGE analysis:

- **a.** Add 25-30 µL 2X SDS-PAGE sample buffer to sample, vortex briefly to mix
- **b.** Heat samples for 5 minutes at 95°C
- **c.** Place tubes on magnetic rack to separate elution from beads. Collect supernatant and place into clean tube.
    - **i.** Note: It is best to conduct SDS-PAGE experiment on the same day as the elution step.

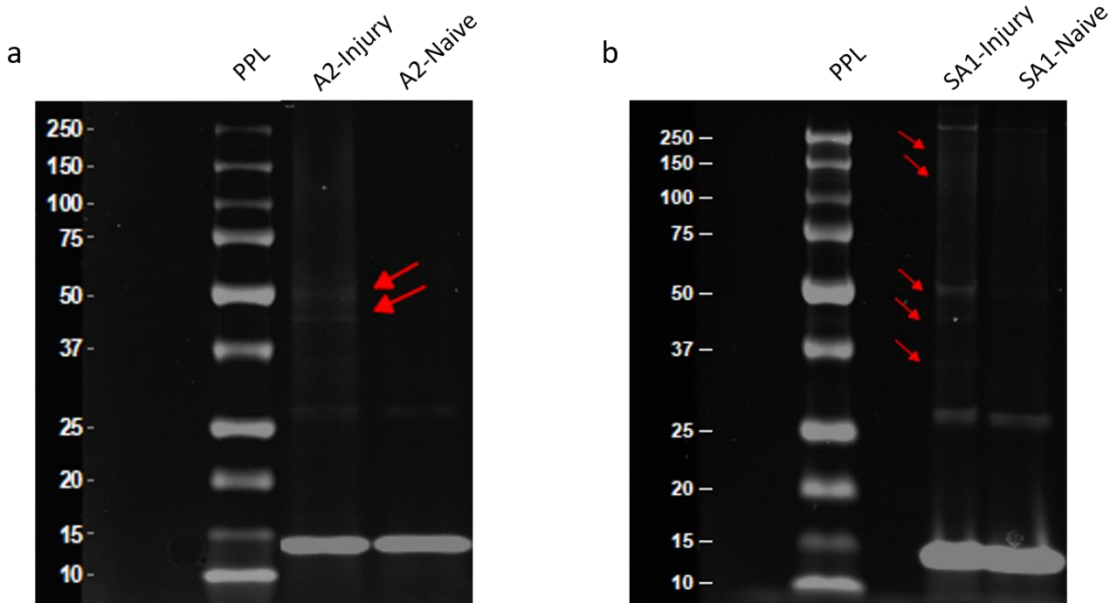

Appendix D Figure 1: Immunoprecipitation eluate separated by SDS-PAGE.

a) A2 incubation with 1 dpi tissue lysates and b) SA1 incubation with 7 dpi tissue lysates. Both constructs isolated proteins unique to the injury condition, indicated above with red arrows. Streptavidin subunits (~13 kDa) are preset in each condition, indicating that the streptavidin from the magnetic beads was stripped during the harsh elution process.